5-2017

PARTICLE MORPHOLOGY AND ITS INFLUENCE ON FRICTION AND DILATANCY OF SANDS

Karen Carmen Lee
University of Tennessee, Knoxville, klee50@vols.utk.edu

To the Graduate Council:

I am submitting herewith a thesis written by Karen Carmen Lee entitled "PARTICLE MORPHOLOGY AND ITS INFLUENCE ON FRICTION AND DILATANCY OF SANDS." I have examined the final electronic copy of this thesis for form and content and recommend that it be accepted in partial fulfillment of the requirements for the degree of Master of Science, with a major in Civil Engineering.

Khalid Alshibli, Major Professor

We have read this thesis and recommend its acceptance:

Angel Palomino, Mingzhou Jin

Accepted for the Council:
Dixie L. Thompson

Vice Provost and Dean of the Graduate School

(Original signatures are on file with official student records.)

PARTICLE MORPHOLOGY AND ITS INFLUENCE ON FRICTION AND DILATANCY OF SANDS

A Thesis Presented for the
Master of Science
Degree
The University of Tennessee, Knoxville

Karen Carmen Lee
May 2017

ACKNOWLEDGMENTS

I greatly thank and give my sincere appreciation to Dr. Khalid Alshibli for his guidance, knowledge, and encouragements throughout my entire undergraduate and graduate career. I also would like to acknowledge my committee members Dr. Angel Palomino and Dr. Mingzhou Jin for their cooperation and support. For statistical analysis recommendations, I would like to recognize Dr. Xiaojuan Zhu for her generous time and assistance. I am very thankful for my parents Kiento and Steve Lanter for their love, support, and inspirations. Lastly, I would like to extend appreciation to my fiancé Curtis Hughes for all of his love and encouragements throughout the many years. This thesis is partially funded by the National Science Foundation under Grant No. CMMI-1266230.

ABSTRACT

Particle morphology outlines the general analytical method used to describe soil particles' structure and shape. The characteristics defining this term include sphericity, roundness, and surface texture. Particle morphology has a significant influence on sand behavior and consequently affects dilatancy and friction. Understanding the relationship between shear strength parameters and particle morphology answers fundamental questions about the mechanics of granular materials in general and has the potential to enhance the development of advanced constitutive models that describe granular materials' behavior.

Many researchers have reported measurements for sphericity, roundness, and surface texture using both two-dimensional (2D) and three-dimensional (3D) images to analyze the effects on granular materials' friction and dilatancy angles. This thesis investigates the influence of morphology measurements from 3D images on friction and dilatancy of three types of sands (#1 Dry Glass, GS#40 Columbia, and F-35 Ottawa Sand) and on glass beads. A series of direct shear experiments were conducted at various normal stresses and densities to achieve this goal.

Experimental measurements of friction and dilatancy angles were compared to findings in a previous study. A stepwise regression analysis was performed to develop statistical models predicting friction and dilatancy using the specimen's relative density, normal stress, and particle morphology as input parameters. This thesis discusses how these explanatory variables affect the model and compares the experimental results with the predicted values. A reasonable agreement is found between the model's predictions and the experimental results.

The development of simple statistical models capable of accurately predicting friction and dilatancy values has a major impact on many field applications (e.g., processing granular materials for industrial and engineering purposes, foundation design, landslides, agricultural and

pharmaceutical products, and future research on granular materials' behavior). This study contributes to further advancements in theories predicting granular materials' behavior and provides experimental evidence to support improvements of constitutive models that describe the behavior of sands.

TABLE OF CONTENTS

LIST OF TABLES

LIST OF FIGURES

CHAPTER 1

INTRODUCTION

1.1 Motivation

Morphology refers to soil particles' shape and structure. Particle morphology influences particle sliding, rolling, interlocking, bending, and breaking. Moreover, it affects particle contacts, which in turn influence the particulate system's friction and dilatancy. The nature and number of particle contacts with neighboring particles play a major role in granular materials' shearing resistance. Few studies have been reported in the literature investigating the relationship between sand's particle morphology and shear strength. For example, Dodds (2004) and Edil and Benson (2007) studied particle morphology, but only related roundness to friction as opposed to considering multiple explanatory variables. Alshibli and Alsaleh (2004) related surface texture to friction and dilatancy; however, the results were based on limited experimental measurements and were inconclusive because particle sphericity and roundness were not quantified from 3D images. In contrast, this thesis investigates the influence of multiple particle morphology parameters from 3D imaging, as well as normal stress and relative density, on friction and dilatancy of sand systems.

Silica sands with different morphologies and glass beads were tested in direct shear at multiple densities and normal stresses to bridge the knowledge gap by developing simple statistical models relating shear strength parameters to morphology. The direct shear test has proved to be a simple, inexpensive, and common test for sands and therefore has been used extensively in research (e.g., Cox 2008, Fern et al. 2015, Edil and Benson 2007, Altun et al. 2011, Duttine and Tatsuoka 2009, Hassen et al. 2016, Cai et al. 2016). Indices have been reported in the literature to quantify particle morphology and have been linked to granular materials' engineering behavior, such as shear strength and deformation characteristics.

However, the literature lacks a systematic experimental investigation incorporating the influence of particle morphology's quantitative measurements on sands' friction and dilatancy. Furthermore, the literature has not conclusively determined which of the input parameters influences sands' friction and dilatancy the most.

Developing models that define the relationship between shear strength parameters and morphology will not only enhance the development of constitutive models predicting granular materials' behavior but also impact many field applications (e.g., processing granular materials for industrial applications) and improve designs that use granular materials (e.g., backfill for mechanically stabilized earth walls). The proposed new models encompass deterministic parameters (i.e., normal stress and relative density) as well as more complex and problematic parameters (i.e., sphericity, roundness, and surface texture). Moreover, this thesis investigates which explanatory variables affect friction and dilatancy the most by conducting stepwise regression analysis as well as comparing standardized regression estimates. Lastly, the model was evaluated to prove that predicted values correlate to experimental measurements for both friction and dilatancy angles.

1.2 Objectives

The main objective of this thesis is to study the influence of particle morphology on sands' friction and dilatancy responses by proposing statistical models that outline the influential parameters (i.e., sphericity, roundness, and surface texture) on sands' friction and dilatancy while also considering normal stress and relative density effects. Laboratory direct shear experiments were conducted on dry sands with various densities, normal stresses, and particle morphologies. This thesis achieves the following:

- Determines the effect of normal stress and relative density on sands' friction and dilatancy.
- Determines the influence of particle morphology (i.e., sphericity, roundness, and surface texture) on sands' friction and dilatancy.
- Develops statistical models to predict critical state and peak friction angles as well as dilatancy angles by incorporating particle morphology's influence.

1.3 Thesis Outline

This thesis contains six chapters. Chapter 1 presents the motivation for and objectives of the thesis. For a better understanding of particle morphology, Chapter 2 presents a literature review along with a brief description of the direct shear experiment. Sphericity, roundness, and surface texture are defined; and the particles' 2D and 3D imaging methods are discussed. Chapter 2 also discusses previously reported literature on roundness and surface texture and their effects on friction and dilatancy angles. Chapter 3 describes the direct shear apparatus used for the laboratory experiments. Included are dimension details and the direct shear box's components, the Geojac Automated Load Actuator system, and the DigiShear program. Chapter 4 describes the experimental procedure for specimen preparation as well as background information about the statistical regression analysis assumptions and methods for modeling the shear strength parameters. Chapter 5 presents the results and discusses sand behavior based on direct shear experiments in which particle morphology was linked to experimental measurements of friction and dilatancy angles. Linear regression models were developed to predict sands' friction and dilatancy angles. Chapter 6 presents conclusions and recommendations for further research.

CHAPTER 2

LITERATURE REVIEW

2.1 Introduction

This Chapter briefly reviews the direct shear test and sand behavior during shear. The use of direct shear tests for determining shear strength, friction angle, and dilatancy is summarized. Particle morphology is defined, and different quantification techniques reported in the literature are summarized. Previous research investigating the effects of particle roundness and surface texture on shear strength parameters are discussed.

2.2 Direct Shear

Shear strength is an important property to accurately quantify granular materials for many applications in geotechnical engineering, manufacturing, and processing. Soil failure can result in the collapse of supported structures with a major impact on public safety. In addition, many industrial applications involve handling and processing granular materials. Direct shear testing is a common and simple procedure to determine granular materials' shear strength. Many researchers (e.g., Cox (2008), Fern et al. (2015), Edil and Benson (2007), Altun et al. (2011), Duttine and Tatsuoka (2009), Hassen et al. (2016), and Cai et al. (2016)) have used direct shear tests to study shear strength and sand behavior. The first researcher to use the direct shear test in 1776 was Coulomb, followed by other researchers who used it extensively. It is the oldest form of shear test (Lambe and Whitman 1969); and during the 20th century, many researchers refined the direct shear test to yield the current ASTM D3080 standard.

Considered a common test for sands, the direct shear test is inexpensive and simple. It can be used to measure the drained shear strength for both sands and clays. Although clay's

drained strengths can be measured, they may not always prove reliable because drainage conditions cannot be controlled other than by varying the loading rate (Coduto 2001). Other limitations of direct shear tests include technical difficulties when studying dilatancy (i.e., measuring partially saturated sand's volume change) (Fern et al. 2015) and forcing the shear failure along a pre-determined failure plane, which may not be the weakest in the specimen. Not allowing the sand to fail along the weakest shear surface may create nonuniform strains within the soil mass, resulting in inaccurate measurements during the experiment's strain-softening stage (Coduto 2001). For this thesis, the direct shear test is appropriate since it is repeatable and friction and dilatancy angles are obtainable for dry sand in order to develop better predictions of strength parameters.

2.3 Sand Behavior

In order to predict granular materials' behavior during the handling and processing stages in industrial applications as well as to estimate soils' bearing capacity, shear strength is required. Granular materials' ability to dilate influences the peak friction angle and ultimately the behaviors during shear failure. Edil and Benson (2007) found that friction angle is generally the most important property for mechanically stabilizing earth walls and reinforced slopes since granular material is the preferred fill; therefore, accurate predictions of friction and dilatancy angles are beneficial. Studying the behavior of shear strength and morphology will ultimately have a major impact on constitutive models that predict granular soils' behavior and will in turn influence field applications.

Friction plays a significant role since it contributes to the sand's shear strength. In nature, particularly for granular materials, there is potential for the development of slip planes (i.e., shear

bands), which are the prevailing failure mode for dense sands. According to Budhu (2011), since each contact of a sand particle with another is a potential micro slip plane, loading can cause multiple micro slip planes aligning in the direction of least resistance. Coulomb's frictional law suggests that soil's resistance to shearing is dependent on the applied normal stress and the coefficient of friction. The *friction angle* is defined as the angle between the normal force and the resultant force (Budhu 2011). The individual sand particles' frictional properties as well as the interlocking between the particles influence friction angle. Other factors influencing friction angle include mineralogy, morphology, gradation, and void ratio (Coduto 2001). However, this relationship ignores dilatancy contribution to the shear strength of sands. Reynolds (1885) introduced the concept of granular materials' dilatancy.

Since sand failure does not necessarily mean collapse, but the imminent movement of one rigid body relative to another on a slip plane, dilatancy significantly influences the sand's behavior during shear failures and should be studied. When sliding is initiated, loose sand tend to move into void spaces while dense particles ride over each other, resulting in expansion. The *dilatancy angle* refers to the sand's expansion and is calculated from the change in volumetric strain with respect to the change in shear strain (Budhu 2011). The dilation phenomenon is the ability of the particles to slide up or down in relation to each other during shearing, resulting in increased space between the particles when compared to their initial state. Since volume change is measured directly from normal displacement, dilatancy is easily calculated.

Dense and loose sand's typical behavior during direct shear testing is shown in Figure 2.1, where the sand reaches its critical state (i.e., it experiences continuous plastic shear strain with no additional volume change). For dense sand, as the shear strain increases, the shear stress reaches a peak followed by strain softening and eventually approaches the critical state. The

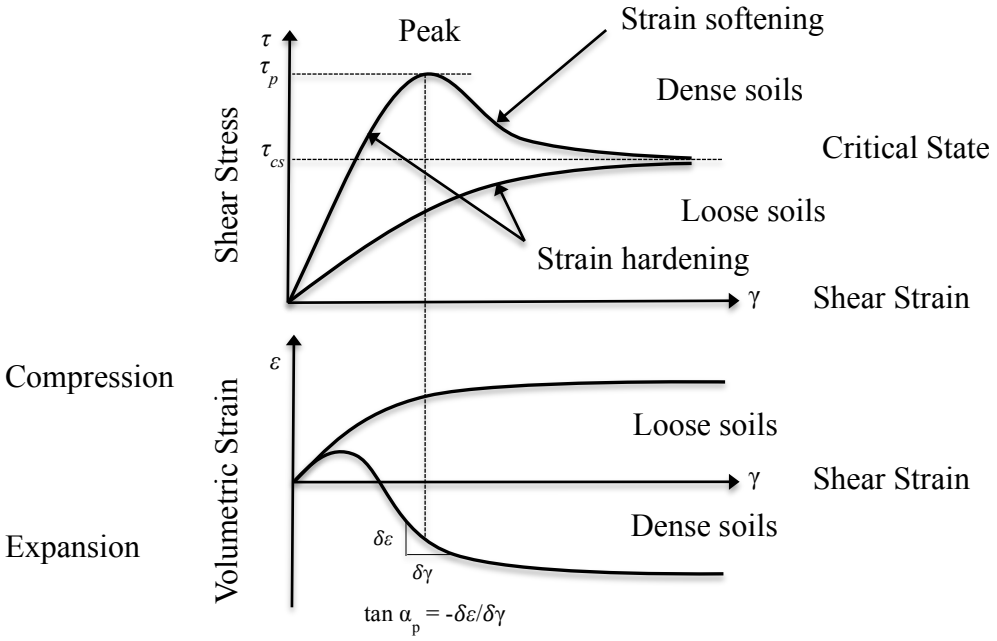

Figure 2.1. Shearing Behavior of Granular Soil, from (Budhu 2011)

specimens may initially experience volumetric contraction followed by expansion before reaching the critical state. Dense specimens experience more dilation because of the particles' arrangement and the distance the particles must translate in order to shear (Figure 2.2). When the specimen expands in volume, the particle translation adds to shearing resistance. On the other hand, for loose specimens, shear stress simply increases to a critical state as shear strain increases and is associated with volumetric contraction. According to Cox (2008), loose sands do not exhibit slip planes; however, slip planes are formed for dense sands since they occur at the peak shear strength. The following equations define the shear strength parameters from direct shear experiments:

$$\text{Peak friction angle:} \quad \phi'_p = tan^{-1}\frac{(\tau_f)_p}{\sigma_n} \tag{2.1}$$

$$\text{Critical state friction angle:} \quad \phi'_{cs} = tan^{-1}\frac{(\tau_f)_{cs}}{\sigma_n} \tag{2.2}$$

$$\text{Peak dilatancy angle:} \quad \psi_p = tan^{-1}\frac{\delta y}{\delta x} \tag{2.3}$$

where τ_f is the shear stress at peak or critical state denoted as p or cs, respectively; σ_n is the normal stress applied; and δ is shear or normal displacement denoted by x or y, respectively.

Normal stress is an important factor to investigate since it significantly influences friction and dilatancy. Typically, dense sands with low normal effective stress dilate more than sands with the same density and higher normal stress. As shown in Figure 2.3, as normal effective stress increases, the amount of dilatancy is suppressed. The curved failure envelope OBC, represents the dilatancy's influence with increasing normal effective stress, while the linear failure envelope OA represents the critical state (Figure 2.3). According to Cox (2008), increased

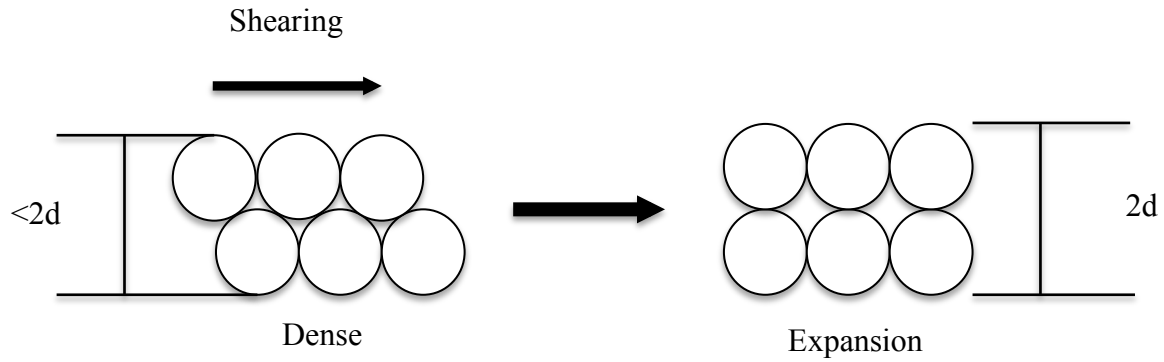

Figure 2.2. Dilation of Densely Packed Particles

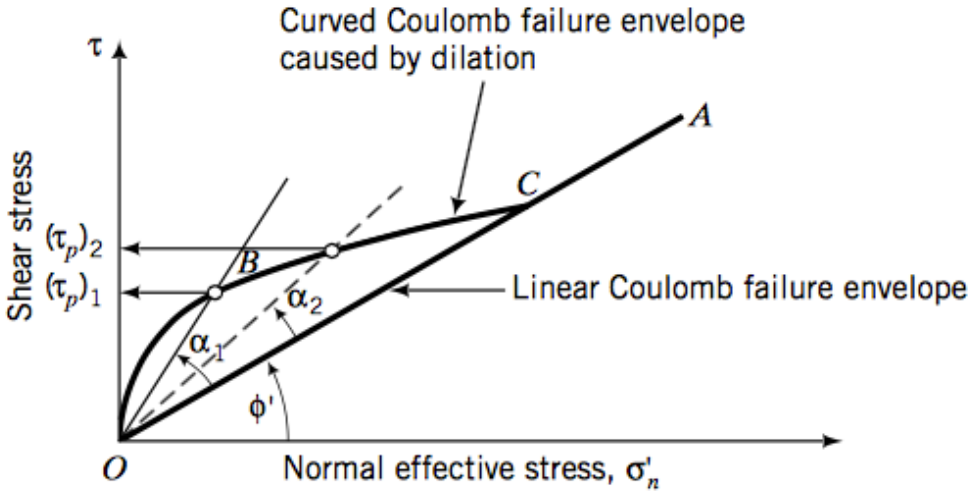

Figure 2.3. Effects of Dilation on Coulomb's Failure Envelope (Budhu 2011)

normal effective stress results in less potential for expansion since it suppresses the particles' typical behavior of sliding up.

Since dilatancy and friction are important contributors to granular soil's behavior, investigating the relationship between the dilation of the sand and friction angle is important. A loose sand with critical state as the shearing angle has zero dilation. However, the amount of sand expansion influences dense granular soils' peak friction angle. According to Coulomb's model, with an adjustment value A, friction and dilatancy are related as the following:

$$\phi'_p = \phi'_{cs} + A\,\psi_p \tag{2.4}$$

where ϕ'_p is peak friction angle, ϕ'_{cs} is critical state friction angle, A is the adjustment value depending on the test, and ψ_p is the peak dilatancy angle. Since both density and effective normal stress affect the rate of the sand's dilation, each ultimately influences the sand's strength (Bolton 1986; Cox 2008; Chakraborty and Salgado 2010; Siang et al. 2013). The sand's shear strength at failure under drained conditions based on Coulomb's friction law is expressed as the following:

$$\tau_f = (\sigma'_n)_f \tan(\phi'_{cs} \pm \psi_p) \tag{2.5}$$

where $(\sigma'_n)_f$ is normal effective stress at failure on the slip plane, ϕ'_{cs} is the effective critical state friction angle, and ψ_p is peak dilatancy angle. Positive dilatancy angle values represent expansion because of particle rearrangement and sliding (Budhu 2011).

The peak shear strength is caused by the combination of shear resistance resulting from sliding, dilatancy, crushing, and rearranging of particles. As shown in Figure 2.4, particle rearrangement and dilatancy are more prominent at low normal effective stresses. According to Altun et al. (2011), the rolling of particles is observed under very low shear forces and contact surfaces decrease because of this phenomenon. Therefore, because of the normal contact forces' high variability, very low shear forces lead to the particles' rolling. For a dense specimen, particles typically override and move from points of contacts during shear, resulting in dilation. However, Bolton (1986) found that at higher normal stresses, sand particles might be unable to override and ultimately reduce dilation because of particle crushing. If the particle's strength is less than the force that is being transferred, crushing may occur (Altun et al. 2011). At high normal effective stresses, particle crushing becomes the most influential contributor to shearing resistance while dilatancy is suppressed to a critical state (Figure 2.4).

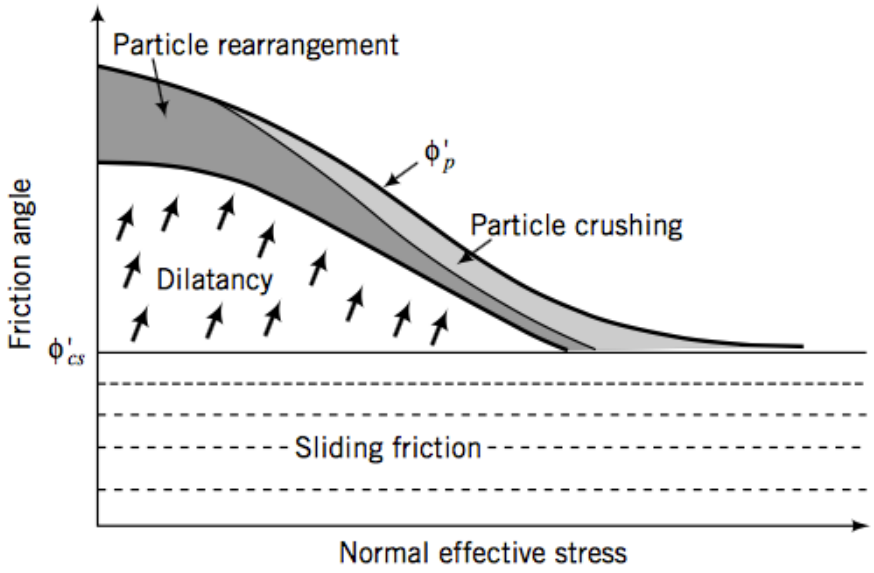

Figure 2.4. Contribution of Sliding Friction, Dilatancy, Crushing, and Rearrangement of Particles on the Peak Shear Strength (Budhu 2011)

Sands' shear strength is a function of the soil skeleton's deformation and the individual particles' relative translation. Moreover, Figure 2.4 shows that crushing results in reduced shear strength in granular soils when compared to particle translation and expansion. Nevertheless, it is difficult to quantify the shear strength contributed by crushing and rearranging particles from soil test results. Therefore, the assumption is that shear strength is the combination of shearing resistance because of both particles' frictional sliding and dilatancy. In other words, the shearing resistances resulting from crushing, rearranging particles, and dilatancy are combined (Budhu 2011).

2.4 Particle Morphology

Particle morphology is represented by sphericity, roundness, and surface roughness and is used to characterize granular particles. Morphology notably affects sand particles' geometric arrangement within the soil mass (Cox 2008) and influences sands' overall behavior (Alshibli et al. 2014). Consequently, few researchers have quantified morphology with improved techniques involving 2D and 3D images of sand particles.

2.4.1 Sphericity

Sphericity refers to a particle's general shape regardless of angularity characteristics such as corners and edge sharpness. According to Bowman et al. (2000), sphericity is typically most sensitive to the particle's elongation. Wadell (1932) defines *sphericity* as the ratio of the surface area of a sphere with equal volume as the particle of interest to the particle's actual surface area:

$$\frac{s}{S} = Degree\ of\ True\ Sphericity \tag{2.6}$$

where s is the surface area of the sphere with the same volume as the particle of interest and S is that particle's actual surface area. A maximum value of 1 represents a spherical particle's numerical value. Since particle morphology has scientific, industrial, and commercial importance (Wadell 1932), granular materials' sphericity should be investigated.

2.4.2 Roundness

Roundness, which is affected by a particle's corners and edge sharpness, greatly influences the sand's friction angle and strength. Wadell (1932) defines a particle's *roundness* as the ratio of the average radii of all particle corners to a circle's maximum radius:

$$\frac{\sum \frac{r}{R}}{N} = Degree\ of\ Roundness\ of\ a\ Particle\ in\ One\ Plane \tag{2.7}$$

where r is the curvature's radius in the corner, R is a circle's maximum radius, and N is the number of corners in the one plane. Therefore, an increase in edge sharpness would reduce a particle's roundness. Maximum roundness would result in a value of 1 in a given plane for Equation 2.7. Dodds (2004) reported that low particle roundness typically contributed to higher friction. Moreover, angular particles may increase friction because of a higher potential for sharp edges to interlock and resist sliding (Dodds 2004; Alshibli and Alsaleh 2004).

2.4.3 Surface Texture

Surface texture refers to the roughness of the particle's surface. Considering particle roughness is important in predicting frictional resistance and dilatancy of sands. According to Altun et al. (2011), sphericity and roundness as well as surface roughness affect particle

interlocking. Moreover, surface texture influences interparticle sliding resistance at particle-to-particle contacts. Since surface roughness may influence the contact points of two particle surfaces during particle rearrangement/translation, it may in turn affect the amount of dilation. Furthermore, Lambe and Whitman (1969) recognized that the friction mechanism could be explained such that on a submicroscopic scale, most surfaces are rough; therefore, two solids are in contact only where high asperities touch one another. Therefore, surface texture must be considered when investigating particle morphology's influence on granular materials' friction. It should be noted that surface roughness describes the detail of a particle's surface, but does not affect the overall shape (Alshibli et al. 2014).

2.5 Quantifying Morphology from 2D or 3D Images

In order to measure sphericity and roundness, previous analyses have typically been done visually using 2D images of particles. Since accurate volume and edge curvature measurements are difficult to achieve, charts have been developed. Consequently, the most common method to characterize particles is based on standardized charts with varying scales of particle roughness, roundness, and sphericity (Hyslip and Vallejo 1997). Researchers such as Dodds (2004) characterized roundness and sphericity using a chart developed by Krumbein and Sloss (1963) to compare selected particles using stereomicroscope analysis. A pinch of sand was analyzed using a Leica MZ6 stereomicroscope. As shown in Figure 2.5, when moving from left to right in the chart, the particle increases in roundness. Moving from the bottom to the top of the chart represents an increase in the particle's sphericity. It is important to note that a particle may possess a high degree of roundness, but not a high degree of sphericity (Wadell 1932).

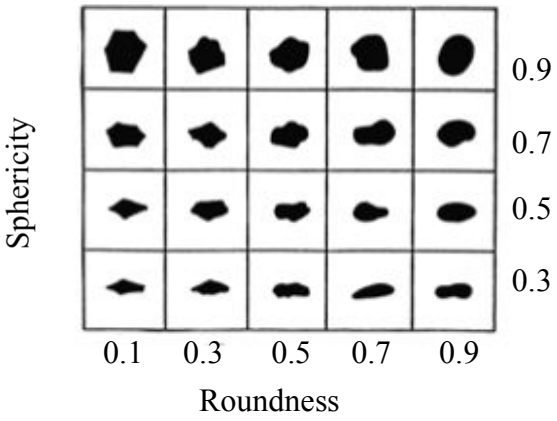

Figure 2.5. Characterization Chart: Particle Sphericity and Roundness
(Krumbein and Sloss 1963) (Font modifications by author)

According to Cox (2008), charts were later replaced by mathematical definitions such as the following:

$$Sphericity = \frac{R_I}{R_C} \tag{2.8}$$

$$Roundness = \frac{4A}{\pi L_{Major}^2} \tag{2.9}$$

where R_I is the inscribed circle's radius, R_C is the circumscribed circle's radius centered at the center of mass, A is the particle's cross sectional area, and L_{Major} is the length of the major axis.

Other morphology calculation methods using 3D imaging have emerged with advances in computer technology and research. Since sphericity relates to the particle's gross shape, measuring the particle's volume is required. Alshibli et al. (2014) used high-resolution 3D images to define particle sphericity ($\boldsymbol{I_s}$) and roundness ($\boldsymbol{I_R}$) indices. The *sphericity index* is defined as the following:

$$I_s = \frac{V_p}{V_s} \tag{2.10}$$

where V_p is the particle's actual volume and V_s is the volume of the sphere with a diameter equal to the shortest diameter of the particle that passes through the particle's center of mass. Spherical particles have a value equal to 1. According to Alshibli et al. (2014), particles with I_s values less than 1 indicate that the particle may be kidney-shaped or discoidal (Figure 2.6); but in most cases sphericity values are greater than unity. A particle's *roundness index* is defined as the following:

$$I_R = \frac{A_p}{4\pi\left(\frac{d_L+d_I+d_S}{6}\right)^2} \tag{2.11}$$

where A_p is the particle's actual 3D surface area, and d_L, d_I, and d_S represent the particle's longest, intermediate, and shortest diameters, respectively, passing through the center of mass. The denominator represents a sphere's surface area with the diameter equaling the average of d_L, d_I, and d_s. The roundness index with a value of 1 represents a particle with no asperities and with the same surface area as a sphere with an equal average diameter.

Alshibli et al. (2014) compared the 2D method to their 3D method and found that roundness and sphericity measurements do not produce the same results; 2D values yielded higher roundness values and lower sphericity values compared to 3D quantification. They concluded that since 2D measurements are dependent on the particle slice's orientation, the true short and long axes might not be shown. However, many studies still rely on 2D particle images while 3D images are rarely used; and when they are, it is usually for larger aggregate samples (Alshibli et al. 2014).

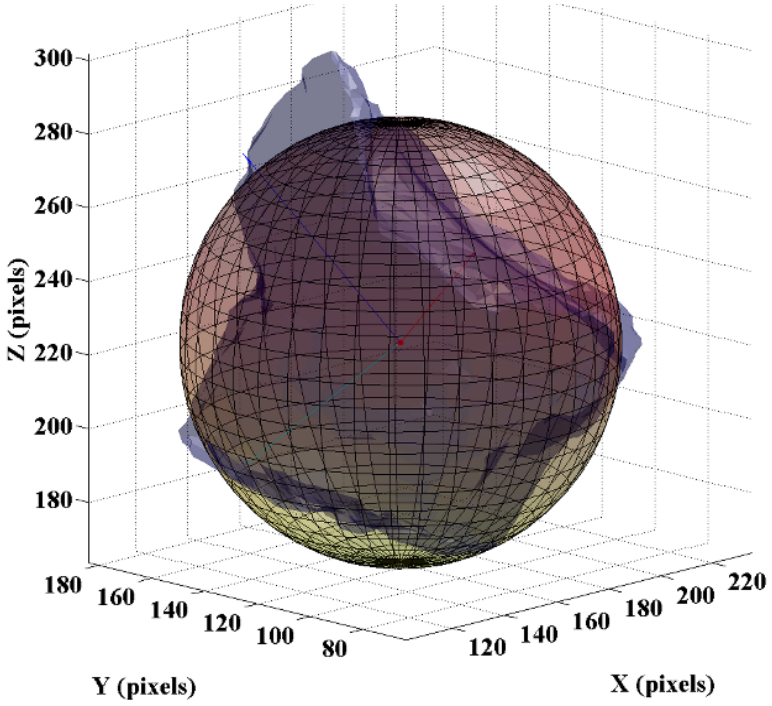

Figure 2.6. 3D Image of Particle Sphericity (Alshibli et al. 2014)

Masad et al. (2001) used the surface texture index (TI) to represent the particles' surface texture. Other approaches to measuring surface texture include fractal geometry (Hyslip and Vallejo 1997), fuzzy uncertainty texture spectrum (Lee et al. 1998), and optical interferometry (Alshibli and Alsaleh 2004). Surface texture measurements using an optical surface profiler provide a wide range of surface heights. When using optical interferometry, Alshibli et al. (2014) calculated the average roughness and root mean square roughness. The average roughness (R_a) is the arithmetic mean of the surface height's absolute values from the mean plane:

$$R_a = \frac{1}{MN}\sum_{i=1}^{M}\sum_{j=1}^{N}|Z_{ij}| \tag{2.12}$$

where M and N are the number of pixels in the X and Y directions, and Z_{ij} is the surface height at a specific pixel relative to the reference mean plane. Root mean square roughness (R_q) is calculated as the following:

$$R_q = \sqrt{\frac{1}{MN}\sum_{i=1}^{M}\sum_{j=1}^{N} {Z_{ij}}^2} \tag{2.13}$$

The main disadvantage of using both R_a and R_q is that the influence of a single nontypical peak or valley is averaged out and produces a small effect on the roughness results. However, using R_q is more advantageous since the heights are squared so peaks and valleys have more significance (Alshibli et al. 2014). A sample surface profile is displayed in Figure 2.7.

Overall, quantifying particle morphology with 3D imaging would provide a better particle representation when compared to 2D imaging since the particle's orientation would greatly influence 2D methods. If 2D imaging is preferred, scanning electron microscopes can display the particle's surfaces since magnification capabilities are advanced (Cox 2008). However, 3D particle morphology profiling by instruments such as X-ray computed tomography (CT) can give more powerful images with non-destructive techniques. 3D CT images also enable the observation of internal features to investigate real sand particles with a level of detail through section slices (Fonseca et al. 2012; Alshibli et al. 2014). Recently, synchrotron micro-computed tomography (SMT), an enhanced 3D imaging approach when compared to conventional CT images, has quantified particle morphology. Alshibli et al. (2014) introduced new sphericity and roundness indices through high-resolution 3D SMT images. Moreover, programs such as Avizo Fire can aid in post-processing 3D images to quantify particle morphology.

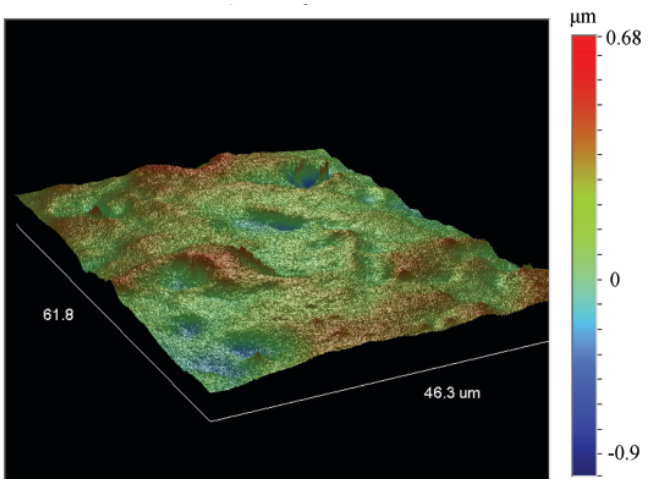

Figure 2.7. Surface Profile of GS#40 Columbia Sand (Alshibli et al. 2014)

2.6 Previous Research

The objective of this thesis is to investigate the relationship between particle morphology and dilatancy as well as particle morphology's relationship to friction. Dodds (2004) and Edil and Benson (2007) analyzed the influence of roundness on friction angle, and Alshibli and Alsaleh (2004) investigated surface texture's influence on friction and dilatancy angles. Other researchers such as Hasan and Alshibli (2010) have created models based on the influence of normal stress and relative density.

Dodds (2004) quantified roundness for sand and crushed rock using the charts produced by Krumbien and Sloss (1963) and measured the critical state friction angle for each material using procedures from Santamarina and Cho (2001). Dodds (2004) concluded that through rotational disturbance, roundness affects friction angle. Moreover, angular particles interlock; for angular particles to begin rearranging/translating, greater activation energy is required. Therefore, Dodds (2004) determined that the critical state friction angles of sand and crushed rock increase as roundness decreases (Figure 2.8).

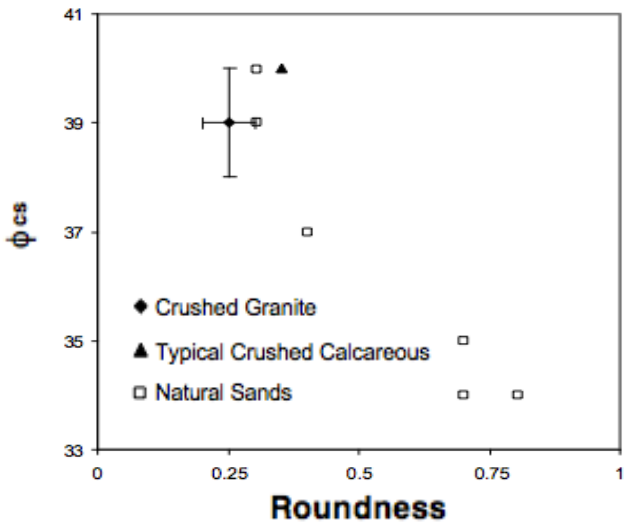

Figure 2.8. Roundness and Friction Angle Relationship (Dodds 2004)

Edil and Benson (2007) investigated granular materials for backfill in mechanically stabilized earth (MSE) walls. Direct shear tests were conducted on 30 sand samples throughout Wisconsin to research the relationship between particle roundness and friction. Particle roundness was quantified using a visual qualitative procedure conducted with an optical microscope and Krumbein (1941) morphology charts. As shown in Figure 2.9, Edil and Benson (2007) found that the friction angle decreases as roundness increases and that when comparing fine and medium sands, larger particles result in greater friction angles.

Other researchers have investigated surface roughness and its influence on friction and dilatancy. Using 3D imaging, Alshibli and Alsaleh (2004) analyzed three silica sands with different surface roughness and morphologies. They concluded that peak friction and dilatancy angles increase as surface roughness increases in all cases. Figures 2.10 and 2.11 display the effect of sand's surface roughness on peak friction and dilatancy angles, respectively, for various relative densities and confining pressures. Additionally, Alshibli and Alsaleh (2004) found that

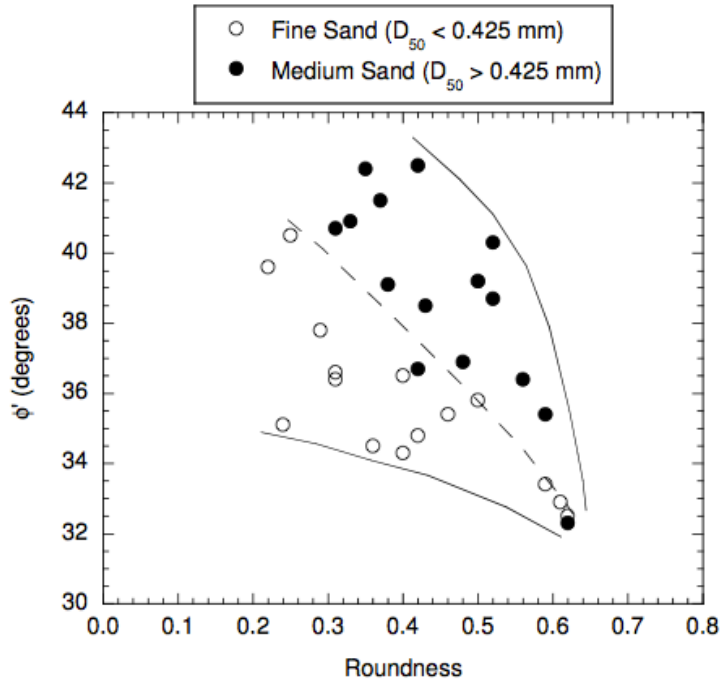

Figure 2.9. Roundness and Friction Angles of Fine and Medium Sand (Edil and Benson 2007)

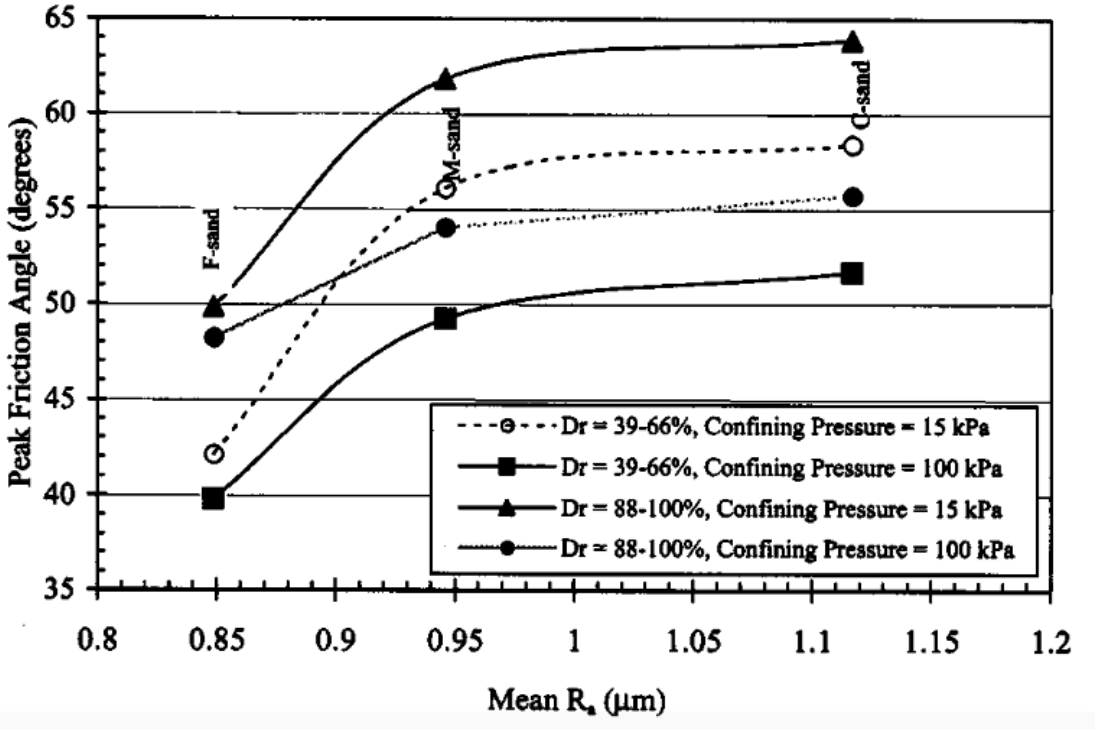

Figure 2.10. Effect of Surface Roughness on Peak Friction Angles (Alshibli and Alsaleh 2004)

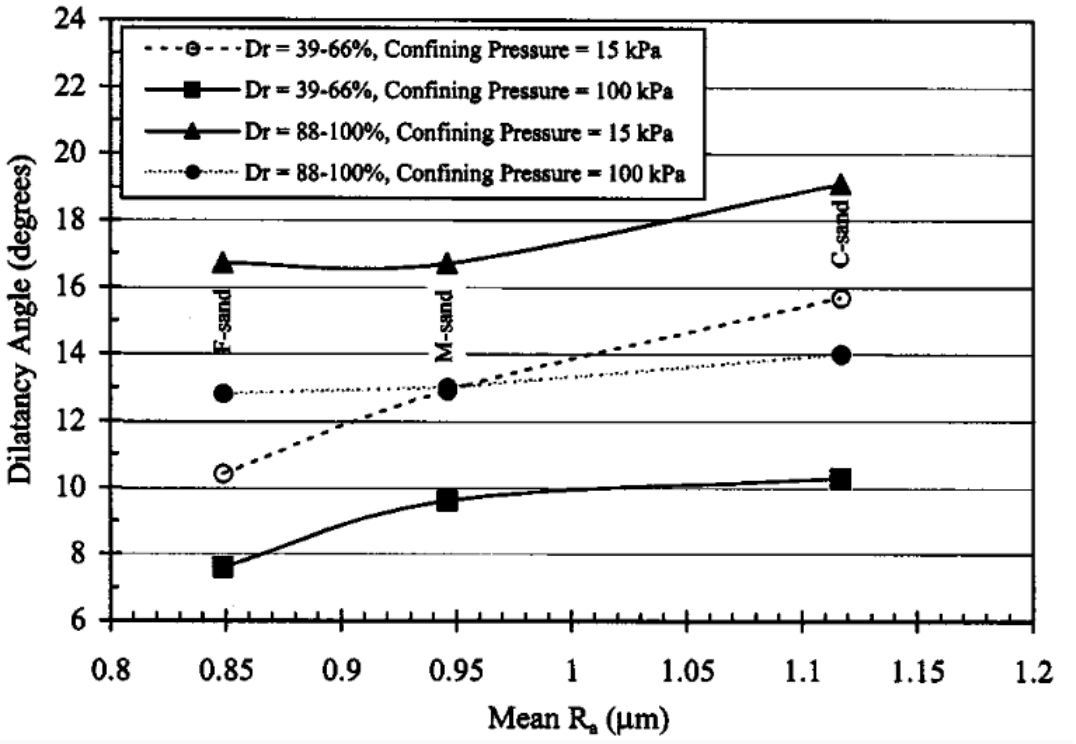

Figure 2.11. Effect of Surface Roughness on Dilatancy Angles (Alshibli and Alsaleh 2004)

dense specimens and low confining pressures resulted in higher peak friction angles as well as higher dilatancy angles.

Hasan and Alshibli (2010) investigated the influence of relative density and normal stress on peak friction angles using triaxial tests on lunar regolith. They developed a model for peak friction angles that is defined by the following:

$$\phi_p = \phi_{cs} + 16\frac{D_r^{0.9}}{p'^{0.1}_{cs}} \tag{2.14}$$

where p'_{cs} is the mean effective stress at critical state and D_r is relative density. As relative density increases, the peak friction angle increases according to Equation 2.14. On the other hand, increasing the mean effective stress would decrease the peak friction angle. Predictions based on relative density and mean effective stress are illustrated; however, the model did not incorporate particle morphology's influence. Since particle morphology is expected to affect friction and dilatancy, incorporating these parameters into the model is critical for more accurate predictions.

CHAPTER 3

EXPERIMENTAL WORK

3.1 Introduction

This Chapter describes the testing apparatus used to conduct the direct shear experiments on sands. More specifically, the box's dimensions and components for the direct shear test are presented along with a description of the Geojac Automated Load Actuator assembly. In addition, the Digishear software is described.

3.2 Direct Shear Description

Direct shear experiments are often used to measure sands' shear strength. According to Mitachi et al. (1997), the box for the direct shear test, which has been used worldwide, is classified into three types:

a) Type A: The top platen and upper portion of the shear box are independently allowed to move vertically and rotate (Skempton and Bishop 1950).
b) Type B: The top platen is fixed to the upper part of the shear box such that both move vertically or rotate together (Jewell and Wroth 1987).
c) Type C: The upper portion of the shear box is prevented from moving vertically or rotating; the top platen moves independently but can also be prevented from rotating (Mikasa 1960; Takada 1993).

The box for the direct shear test for this thesis was Type C, which prevented vertical (i.e., normal) movement of the shear box's upper portion while allowing the top platen to move independently. The direct shear tests consist of either a cylindrical or prismatic box dividing the soil specimen into two halves according to ASTM-D3080. The division's purpose was to fail the

soil at the specimen's center. Setup for direct shear tests typically includes cylindrical specimens, which range from 63.5-76.2 mm in diameter, subjected to a normal effective stress (Coduto 2001). A typical schematic of the test and sand specimen is depicted in Figure 3.1. Moreover, porous stones were essential for tests to allow the specimen to drain during shearing. The specimen is typically sheared at a constant displacement rate while maintaining a constant effective normal stress (σ'_N). The test was repeated on similar sand specimens to achieve at least three experiments at different effective normal stresses.

A shear box with a square cross section measuring 76.2 x 76.2 mm with a 25.4 mm fill height was used to prepare the specimens in this study. The rigid-wall system for each side of the custom-made box consisted of acrylic 18 mm thick. The specimen holder was 36.5 mm from the bottom porous stone to the top of the box. Two alignment and two gap screws secured the two halves of the box (Figure 3.2). Moreover, porous stones were placed at the bottom and the top of the specimen during the test, while two adapter pieces enabled the reaction arm to attach the horizontal load cell to the shear box.

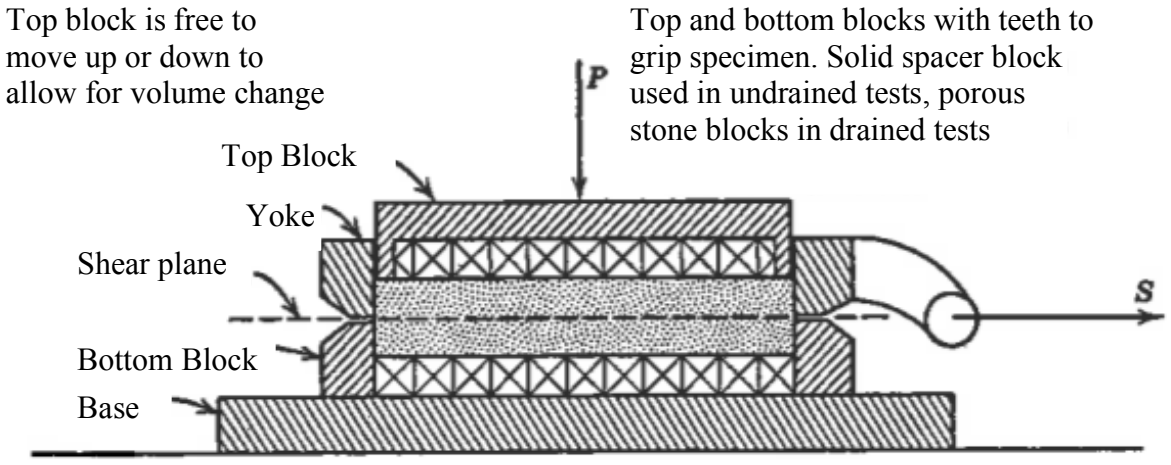

Figure 3.1. Direct Shear Box Assembly (Lambe and Whitman 1969)
(Font modifications by author)

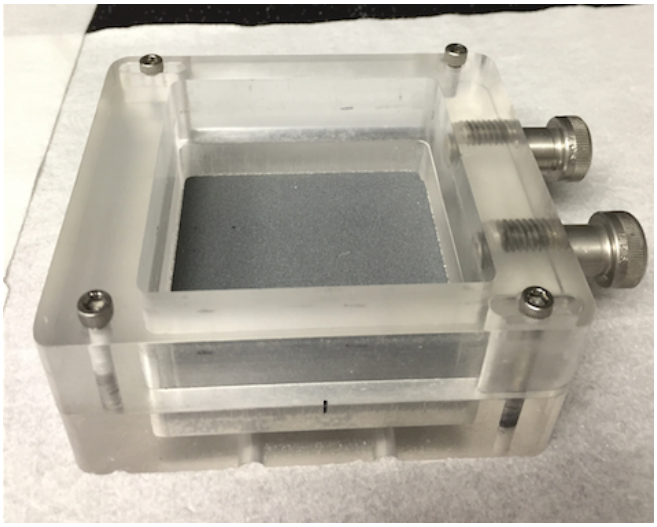

Figure 3.2. Photo of the Direct Shear Box

3.3 Geojac Automated Load Actuator System

The Geojac Automated Load Actuator System consists of a supporting frame holding two actuators to apply the shear and normal load as well as a shear box container to house the direct shear box (Figure 3.3). Moreover, sensors (i.e., vertical load cell, horizontal load cell, and linear variable differential transformer (LVDT)) acquired measurements for the experiments. The shear box container was attached to the horizontal Geojac piston adapter to impose lateral movement.

The LVDT was placed on the vertical load actuator's deformation rod to measure normal displacement as the specimen was sheared, while the vertical load cell was attached to the bottom of the load actuator to measure the normal force applied to the specimen (Figure 3.3). To measure the shear force, the horizontal load cell was attached to an adapter running through the alignment block. Lastly, cables connected each sensor to a network module to transmit the measurements to the DigiShear computer program.

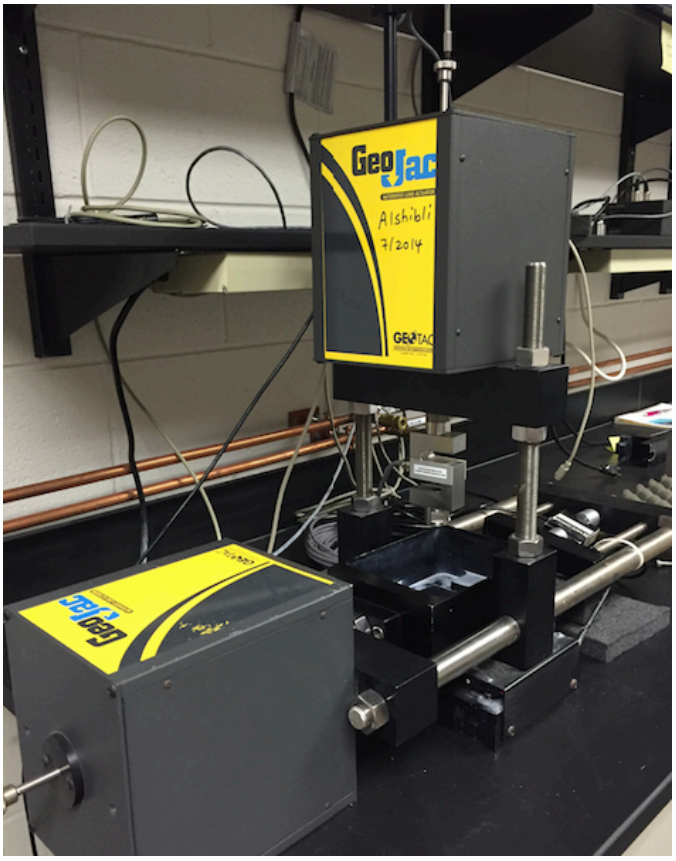

Figure 3.3. Geojac Automated Load Actuator System

3.4 DigiShear Program

The DigiShear program monitored and controlled the experiment by applying the desired shear displacement rate and normal load (Figure 3.4). Specimen information (e.g., height, cross sectional area, and type of sand tested) was entered into the system. Each sensor was logged in the program with its specific calibration factor to monitor the normal stress applied, normal displacement, and the specimen's shear stress. Lastly, the loading schedule and test data were entered to provide each experiment's normal load and displacement rate.

The program also has the capability to display the shear stress versus shear displacement measurements in real time as well as measurements for normal displacement versus shear displacement. These measurements are useful for determining when the experiment needs to be terminated when it reaches a critical state with no significant volume change.

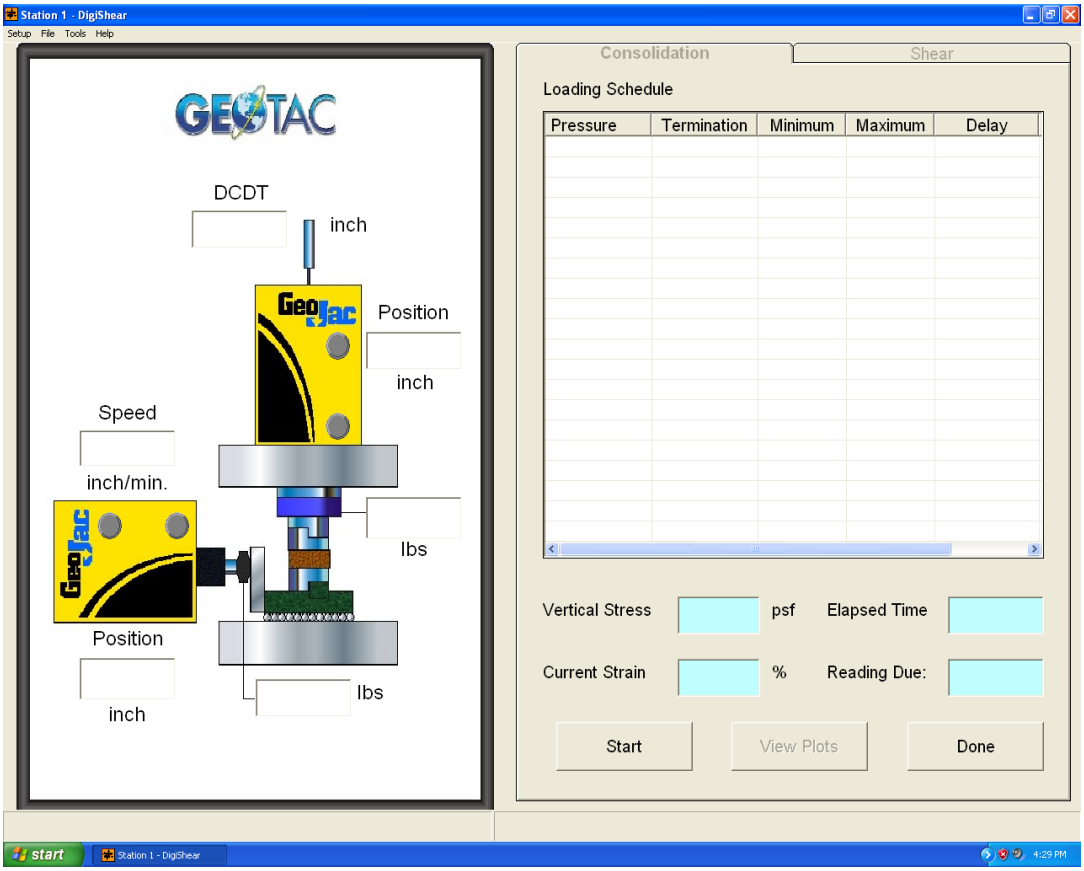

Figure 3.4. The DigiShear Computer Program's User Interface

CHAPTER 4

EXPERIMENTAL PROCEDURE AND STATISTICAL METHODOLOGY

4.1 Introduction

A detailed description of the experimental procedure for specimen preparation and the direct shear test is presented in this Chapter. The direct shear box's two halves were first secured, and then the sand specimen was prepared in the box to the correct density for testing. The application of normal stress is explained along with the specimen's shearing procedures. Lastly, the statistical methods are presented alongside the assumptions to develop the models.

4.2 Specimen Preparation

The direct shear box was assembled with a porous stone at the bottom and the alignment and gap screws properly placed. Each specimen was prepared within the shear box for the various dry uniform silica sands (i.e., #1 Dry Glass, GS#40, and F-35 Ottawa Sand) as well as the standard spherical glass beads. Scanning electron microscope (SEM) images of the sands are shown in Figures 4.1 and 4.2. All silica sands and glass beads had particle sizes between US sieves No. 40 (0.425 mm) and No. 50 (0.300 mm); and the specimens were prepared in loose, medium-dense, and dense states to investigate density's effect on the granular materials' friction and dilation. The range of dry densities to accomplish the various density states as well as the relative density and amount of sand used to prepare the specimens are summarized in Table 4.1.

The maximum and minimum void ratios determined by Alshibli et al. (2014) were used to calculate the sands' and glass beads' relative density, which is expressed as the following:

$$D_r = \frac{e_{max} - e}{e_{max} - e_{min}} \tag{4.1}$$

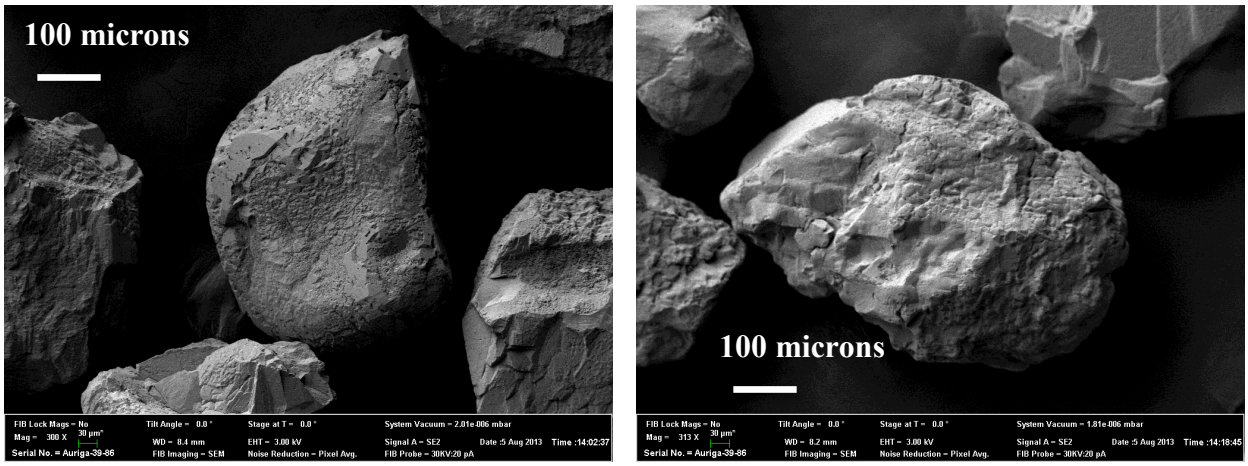

a) #1 Dry Glass Sand

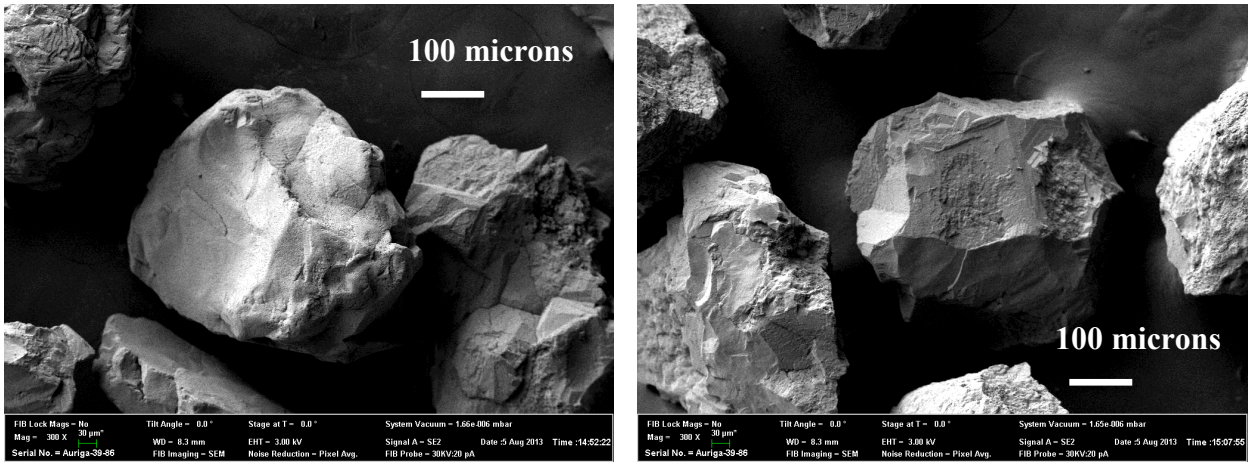

b) GS#40 Columbia Sand

Figure 4.1. SEM Images of #1 Dry Glass and GS#40 Columbia Sand

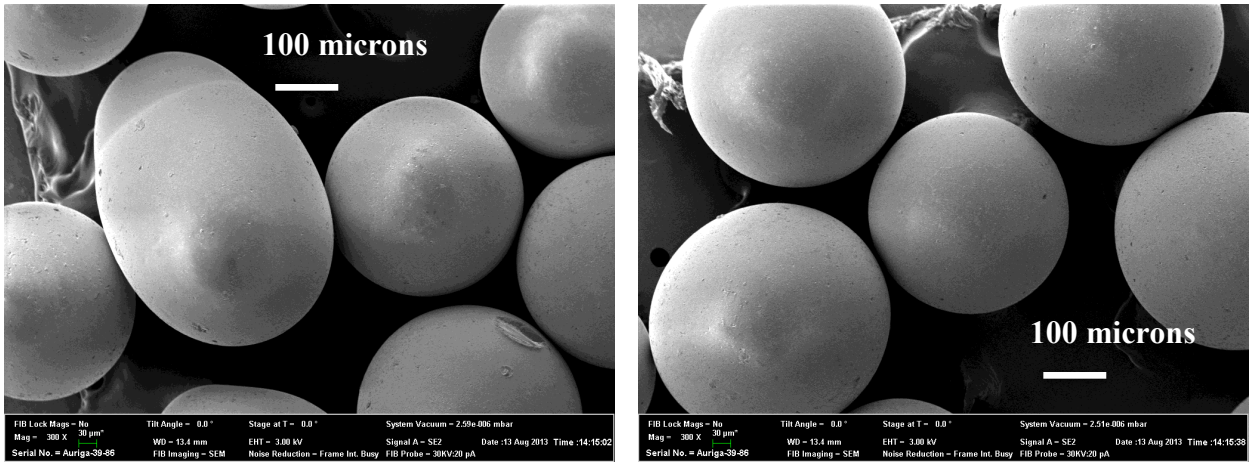

a) Glass Beads

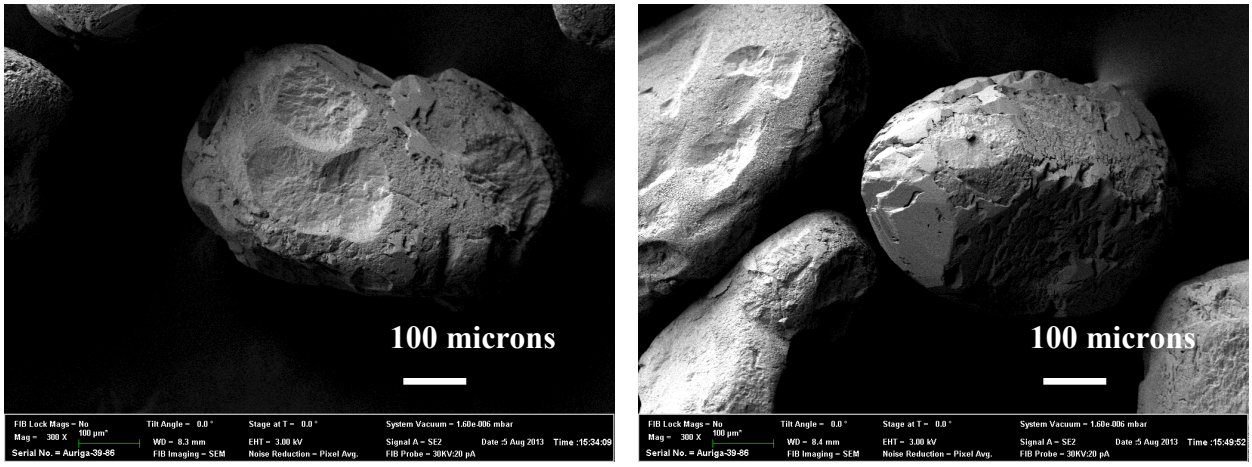

b) F-35 Ottawa Sand

Figure 4.2. SEM Images of Glass Beads and of F-35 Ottawa Sand

Table 4.1. Various Sands with Differing Dry Density States

Material	Density State	Dry Mass (g)	Dry Density (g/cm^3)	D_r (%)
#1 Dry Glass Sand	Loose	203.53	1.38	11.9
	Medium Dense	219.75	1.49	73.0
	Dense	242.48	1.60	125.6
GS#40 Columbia Sand	Loose	203.53	1.38	10.5
	Medium Dense	221.23	1.50	71.2
	Dense	235.06	1.60	114.8
F-35 Ottawa Sand	Loose	225.65	1.53	16.5
	Medium Dense	241.87	1.64	76.6
	Dense	257.64	1.76	133.7
Glass Beads	Loose	218.28	1.48	68.2
	Medium Dense	228.60	1.55	136.5
	Dense	245.13	1.62	198.8

where e_{max} is the maximum void ratio, e_{min} is the minimum void ratio, and e is the specimen's void ratio. The dry sand's mass needed in order to achieve the target loose and medium-dense conditions was calculated for the specimens, and that amount correlated to the shear box's volume. The dry sand was then carefully poured into the direct shear box.

Loose conditions were achieved by depositing the sand through a funnel with an inner-stem diameter of 9.55 mm. The sand was slowly deposited until the shear box was filled using a 5 mm drop height, which reduced the energy of the sand particles as they were placed in the direct shear box. Once the first layer was placed, the process was repeated to deposit the remaining layers. After reaching the target height, the top porous stone was secured.

A medium-dense state was achieved using a similar procedure and a larger funnel with an inner-stem diameter of 14.25 mm. The sand was slowly deposited using a 30 mm drop height, allowing more energy for the sand deposit. After the mass of sand was deposited, the specimen was typically less dense than the target density. The porous stone, cap, and small mass were placed on top of the specimen; and all four sides of the direct shear box were gently tapped with

a rubber mallet to achieve a denser state. The small mass of 1000 g was placed on top to help densify the specimen.

The same method used for the medium-dense state was attempted for a dense state with more taps to the sides, but was insufficient to yield the target density. Therefore, air pluviation (i.e., raining) of sand was adopted with a large drop height to achieve a dense state using Al-Shibli et al.'s (1996) apparatus. As shown in Figure 4.3, the dry air pluviation apparatus consisted of four identical No. 4 sieves (4.75 mm) with openings staggered at 45 degrees to provide more energy to the sand particles. Dry sand flowed out of a funnel with an inner-stem diameter of 14.25 mm and was diffused through the sieves, which were 0.254 m below the funnel. The drop height to the top of the specimen was 0.967 m. The direct shear box was placed in a bucket so that the sand could rain into a larger radius than the specimen holder's. The mass of dry sand and density achieved for each specimen using air pluviation is shown in Table 4.1.

Figure 4.3. Air Pluviation Apparatus

4.3 Test Procedure

The specimen within the direct shear box was placed into the Geojac Automated Load Actuator assembly with a snug fit at the bottom of the box. The loading cap was placed on top of the porous stone with a loading ball assembly, and the reaction arm connecting the horizontal load cell to the top half of the box was then positioned and tightened. A normal force applied by the actuator was determined by the target normal stresses of 15, 50, 100, and 400 kPa and were calculated based on the specimen area. Different load cells were selected for each normal stress to ensure accurate measurements. The 50 lb (222 N) load cell, which was ± 0.03% accurate, was used for the 15 kPa experiments, while the 250 lb (1112 N) load cell, which was ± 0.025% accurate, was used for the 50 and 100 kPa normal stresses. The 500 lb (2224 N) load cell, which was ± 0.053% accurate, was used for the 400 kPa normal stress experiments. Horizontal load cells measuring the shear force consisted of a load cell of 250 lb (1112 N) for the 15 kPa normal stress experiment while the 500 lb (2224 N) load cell, which was ± 0.025% accurate, was used for the 50, 100, and 400 kPa tests. The LVDT used for all the experiments had a range of 76.2 mm (± 0.05 mm accuracy).

The sensor properties were verified with appropriate calibration factors and then zeroed within the DigiShear program. The loading schedules were entered to apply a constant normal stress throughout the experiment. Specimen data, test data, and a displacement rate of 0.40 mm/min were used for all experiments; after the normal stress was applied, the alignment screws were removed to allow the bottom half of the box to slide once the experiment began. Then, a ¼ turn of the gap screws was executed to lift the top half of the box approximately 0.15 mm to create a gap between the two acrylic halves, thus reducing any friction the specimen holder caused when sliding. The direct shear test was started, and the data acquisition system recorded

and saved the results. After the specimen sheared and experienced failure with no significant volume change, the experiment was terminated. Then the sand was collected for fracture investigations whereby the sand was passed through sieve No. 50 (0.300 mm), and the percentage of particles fractured during testing was calculated.

4.4 Statistical Regression Methodology

Regression analysis is one of the most widely used statistical methods describing the relationship between explanatory variables and a response variable. Multiple assumptions for the analysis as well as the stepwise regression's variable selection method are discussed in this section. Once the models were developed, an evaluation was performed, including investigation of Cook's D, analysis of variance, collinearity by variance of inflation, nonlinearity and outliers based on residuals, normality of residuals, and goodness of fit. Lastly, predicted values were compared to experimental calculations. Since 3D imaging was not performed for each experiment, random sampling from previous research was used to link particle morphology to friction and dilatancy angles.

The experimental response variables as well as morphology data were compiled for each experiment using the Statistical Analysis System (SAS) Enterprise Guide 7.1, a software system used for statistical analyses. Random sampling with one standard deviation about the mean on the statistical summary from Alshibli et al. (2014) was conducted to determine values for sphericity, roundness, and surface texture for each test. Since these measurements were taken for individual particles, determining each specimen's morphology by random sampling was advantageous compared to using a constant value per sand because random sampling was more rigorous by providing more variance of values for the sands as opposed to assuming constant

morphology indices (e.g., mean value). Moreover, random sampling allowed each experimental observation value of morphology to be drawn independently. The linear regression was investigated after the experimental calculations and morphology indices were compiled.

The linear regression method evaluated the relationship of the response variables (i.e., friction and dilatancy) to the explanatory variables (i.e., normal stress, relative density, sphericity, roundness, and surface texture). One requirement for this method includes unit-of-association, which states that these explanatory variables are indeed related to friction and dilatancy. Since evidence in the literature indicates that deterministic (i.e., normal stress and relative density) and problemistic variables (i.e., morphology) influence friction and dilatancy, the unit-of-association requirement is satisfied (i.e., Dodds 2004; Cox 2008; Edil and Benson 2007; Alshibli and Alsaleh 2004).

The data under investigation was used to fit a prediction line including the dependent variable (y) and independent variables (x), where the slope is constant as x changes (Longnecker and Ott 2010). The linear regression function is expressed as the following:

$$y = \beta_0 + \beta_1 x_1 + \beta_2 x_2 \ldots + \varepsilon \tag{4.2}$$

where y is the dependent variable, x are the independent variables, β_0 is the intercept, β is the coefficient of predicted change in y when there is one-unit change in x, and ε is the random error term. According to Longnecker and Ott (2010), the formal assumptions for regression analysis include that the relationship is in fact linear, that all errors have the same variance and are independent of each other, and that the errors are normally distributed. These errors are called residuals and are investigated to determine if the linear regression's assumptions are violated.

The residuals were investigated after the regression analysis (stepwise regression) was performed and the model was observed.

The stepwise regression procedure was conducted to select the best linear regression models for friction and dilatancy angles. This process determined each explanatory variable's significance and enabled the model building to begin by adding one variable at a time until the criterion was satisfied. The model's initial most-influential variable was chosen based on the F-test for regression, whereby SAS compared calculated F-values to the ones at the desired significance level. This step of introducing one additional variable was repeated to produce the largest F-value for the regression, thus creating a more successful model. During this process, variables that had previously entered the model could be dropped after other terms were added to improve the model. Thus, adding or removing variables based on their overall significance developed the linear regression model. This process was conducted with a significance level of 0.15 to enter the model and a significance level of 0.05 to remain in the model.

After the regression was selected, the parameter estimates were observed before investigating the assumptions to ensure that the models were worth considering. Cook's D and the analysis of variance are two forms of observations that are critical for determining a model's success. Cook's D statistics aids in identifying highly influential observations. According to Longnecker and Ott (2010), it is recommended that D values greater than 1 be investigated. Once a highly influential observation (e.g., one GS#40 Columbia experiment) is identified, how the model changes with the omission of that observation is assessed. Therefore, Cook's D statistics was conducted and one highly influential observation was omitted (i.e., GS#40 Columbia with normal stress of 15 kPa under dense conditions). Then the analysis of variance was performed to

provide information on the variability within the model. Evaluating the large F-value associated with a small p-value, SAS indicated that these models were worth investigating.

Since there was evidence that these models were worth considering, collinearity was investigated. A collinearity problem indicates that two or more of the predictors are highly correlated and that only one of those predictors is needed to explain the variation in friction and dilatancy. The process of determining collinearity issues includes analyzing the explanatory variables' variance of inflation (VIF) values (i.e., the amount of variance of a coefficient is increased because of collinearity). Small VIF values ensure that experimental procedures are uniformly conducted across all experimental components. A VIF value greater than 10 indicates a serious issue with collinearity (Longnecker and Ott 2010).

Nonlinearity and outliers should then be evaluated by visually observing the residuals to find evidence of how accurately the model predicts actual values. This observation includes looking at the residuals' size based on the residual standard deviation (s_ε) when plotting studentized residual versus predicted value. Any value greater than $\pm 3s_\varepsilon$ should be examined to explore if it is an outlier and a poor fit to the model. Studentized residuals falling within $\pm 3s_\varepsilon$ indicates no outliers for the model. In general, another indicator of a model's satisfactory fit is the display of randomly scattered residuals (Stevens 1984).

Normality of residuals was the last model evaluation performed to satisfy the assumption for a regression model. The residuals' quartile-quartile plots were observed, and the residuals' normality was judged by a close fit to the 1:1 line. Moreover, the Shapiro-Wilk test, a statistics measurement for normality, was conducted to ensure that the residuals were indeed normally distributed.

The adjusted coefficient of determination, adj. R^2, was then evaluated to determine the proportion of variation in friction and dilatancy. Adj. R^2 is advantageous over R^2 since increasing the number of terms in the model would not always increase the value, thus penalizing adj. R^2 for including variables that do not reasonably improve the model (Longnecker and Ott 2010). An adj. R^2 value of 0.90 would indicate that the explanatory variables' linear combination would explain approximately 90% of the variation in the response variable. According to Anastas's (1999) study on the interpretation of correlations' strength, an R^2 value of 0.64 or greater represents a strong relationship. Lastly, predicted values from the model were evaluated, including assessment of predicted versus experimental values and a 95% prediction interval. The prediction interval was displayed to show the range for 95% of future predictions when using the developed models.

CHAPTER 5

RESULTS AND DISCUSSION OF GRANULAR SOIL MODEL

5.1 Introduction

This Chapter presents the experimental results as well as the statistical analyses. The direct shear test results are discussed in detail for the various sands and glass beads, which includes the normalized shear stress and the normal displacement versus shear displacement and the measured friction and dilatancy angle. Particle fracture analysis is presented as well as the typical trends for particle morphology. Statistical modeling and evaluation of the results are summarized for critical state friction, peak friction, and dilatancy angles. The most influential variable (i.e., normal stress, relative density, sphericity, roundness, or surface texture) that constituted the models for the shear strength parameters is presented. Finally, predicted values from the model are compared to the experimental measurements.

5.2 Direct Shear Experiments

Direct shear experiments were performed on three types of silica sands and glass beads to determine the friction and dilatancy angles. The resulting shear stress normalized by the normal stress applied during shearing (τ/σ_N) versus shear displacement as well as the normal displacement versus shear displacement relationships are depicted for glass beads and silica sands. In this thesis, specimen dilation (i.e., expansion) is considered positive, which is the opposite of the convention used in Figure 2.1. Initial experiments under the same conditions were conducted with repetitive results and are shown in the Appendix; therefore, for this study one set for each condition is reported. Based on the relationship of normalized shear stress versus shear displacement, the peak and critical state friction angles were determined using Equations

2.1 and 2.2. Moreover, the relationship of normal versus shear displacement was used to determine peak dilatancy angles based on Equation 2.3.

A statistical summary of morphology parameters is presented in Table 5.1 for the tested sands and glass beads. The particle morphology indices were determined by Alshibli et al. (2014) using Equations 2.10, 2.11, and 2.13 for sphericity, roundness, and surface texture, respectively. A value of unity for $\mathbf{I_S}$ and $\mathbf{I_R}$ represents the most spherical particle with round edges. A value much greater than unity represents a non-spherical particle, while roundness has a maximum value of 1. On the other hand, surface texture depends on the surface heights' deviation, where a larger value represents a rougher particle surface. The sands and glass beads were ranked in ascending order of roundness: GS#40 Columbia, #1 Dry Glass, F-35 Ottawa, and glass beads. The materials were also ranked in ascending order of sphericity: F-35 Ottawa, #1 Dry Glass, GS#40 Columbia, and glass beads. Glass beads did not prove to be perfectly round and spherical because of manufacturing defects. In ascending order of surface texture, the materials were ranked as glass beads, GS#40 Columbia, #1 Dry Glass, and F-35 Ottawa Sand.

Table 5.1. Statistical Summary of Sphericity, Roundness, and Surface Texture Indices (Alshibli et al. 2014)

Material	Parameter	$\mathbf{I_S}$	$\mathbf{I_R}$	$\mathbf{R_q}$
#1 Dry Glass Sand	Mean	1.704	0.937	1.990
	SD	0.859	0.106	1.135
GS#40 Columbia Grout Sand	Mean	1.674	0.924	1.923
	SD	0.799	0.099	1.986
Glass Beads	Mean	1.096	0.965	0.381
	SD	0.443	0.043	0.947
F-35 Ottawa Sand	Mean	1.872	0.959	2.084
	SD	0.732	0.083	1.693

Note: $\mathbf{I_S} = 1$ indicates a spherical particle.

5.2.1 #1 Dry Glass Sand

Figures 5.1(a) and 5.1(b) show the normalized shear stress versus shear displacement and the normal versus shear displacement, respectively, for dense #1 Dry Glass at different normal stresses. As shear displacement increased, τ/σ_N increased to a peak and then decreased and approached a critical state at about 5 mm of shear displacement. All dense specimens followed similar trends. The dense packing resulted in a peak shear stress caused by a higher degree of interlocking and interaction among the particles. Particle crushing was not a significant factor since fracture analysis indicated only a very small amount of fracture for the sands and glass beads. A critical state was reached when there was no additional volume change as shearing continued. As normal stress increased, τ/σ_N decreased because dilatation was suppressed as a result of increased normal stress suppressing the potential of particles to roll over each other. As shown in Figure 5.1(b), the specimen slightly contracted and then dilated and eventually reached a critical state. This response correlates with the critical state in the normalized shear stress versus the shear displacement relationship in which there is no additional change in volume with continued shearing.

At the beginning of the experiment (Figure 5.1(b)), a small contraction occurred as a result of the particle rearrangement from the normal stress's initial application. Afterwards, the rate of dilation was high and then decreased to approach the critical state. Therefore, expansion occurred from the particles' initial dense state to a looser state until a critical void ratio was reached. As shearing occurred, particles rolled over each other causing dilation because dense specimens' sliding is typically initiated on an inclined plane rather than a horizontal plane (Budhu 2011).

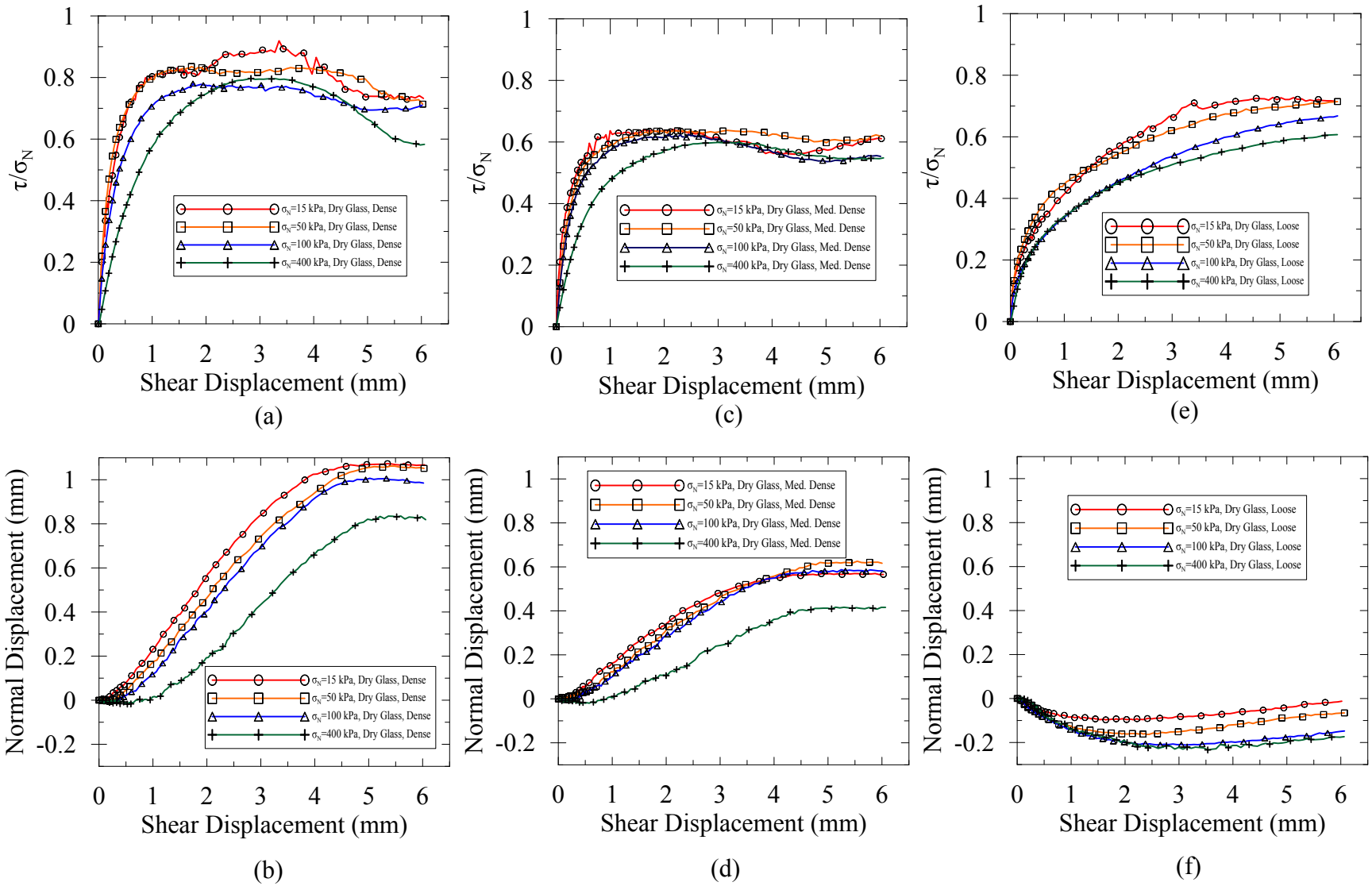

Figure 5.1. Normalized Shear Stress and Normal Displacement versus Shear Displacement for #1 Dry Glass Sand

Figures 5.1(c) through 5.1(f) display the normalized shear stress versus the shear displacement as well as the normal displacement versus the shear displacement of medium-dense and loose specimens. Similar behaviors are displayed in Figure 5.1(c) when compared to Figure 5.1(a) with τ/σ_N reaching a peak and then decreasing to a critical state with further shearing for medium-dense and dense conditions. The sand and glass beads reached a band range of critical state. When the relative density was decreased from a dense to a medium-dense condition, each corresponding experiment decreased in τ/σ_N. The normalized peak shear stress values for the dense specimens ranged from approximately 0.75 to 0.90 while the medium-dense specimens' values were typically 0.6. An increase in sand density increased the number of particle contacts, increasing shear strength because of interlocking.

The normal versus shear displacement for medium-dense specimens (Figure 5.1(d)) had trends similar to those shown in Figure 5.1(b) with an initial contraction and then dilation to a critical state. When the relative density was varied from dense to medium dense, the specimen did not dilate as much for the medium-dense condition. For a dense specimen, the normal displacement at the critical state was approximately 1.05 mm while for a medium-dense specimen it was approximately 0.58 mm because the more densely packed particles, compared to looser ones, had more potential to roll over each other and then expand.

Figure 5.1(e) displays the loose specimens' normalized shear stress versus shear displacement, following a relatively different trend. The loose specimens' τ/σ_N gradually increased until reaching a critical state value where there was no increase in τ/σ_N with further shearing. Therefore, τ/σ_N did not exhibit a peak state and simply increased to a critical state for loose specimens.

Only a small amount of dilation was displayed for the loose specimens. As shown in Figure 5.1(f), the loose specimens contracted and then slightly dilated as shear displacement increased until the end of the experiment. Specimens with normal stresses of 50, 100, and 400 kPa contracted and then slightly expanded, but did not achieve the initial height because particles within loose specimens typically slide/roll on the horizontal plane and then move into void spaces, resulting in compression. Once compressed to a denser state, the specimens slightly expanded. For normal stress of 15 kPa with loose conditions, the specimen initially contracted and then dilated slightly above its initial height. More dilation occurred because at low normal stresses, the specimen was less suppressed as it was sheared. Overall, the loose specimens contracted more than the medium dense and dense specimens.

In summary, the peak and critical state friction angles from the normalized shear stress versus shear displacement relationship are displayed in Table 5.2 as well as the dilatancy angles from the normal versus shear displacement relationship. The friction and dilatancy angles were calculated using Equations 2.1 through 2.3. Moreover, initial dry densities, void ratios, and relative densities are displayed for each experiment. The dense specimens' relative density values were greater than 100% since the specimens' void ratio was smaller than the sand's typical $\boldsymbol{e_{min}}$ values. Therefore, the air pluviation technique employed in this study produced specimens with higher densities than the maximum index density based on the ASTM D4253 procedure.

Higher density and a low normal stress resulted in a higher τ/σ_N followed by a more pronounced approach to a critical state. However, looser specimens exhibited larger τ/σ_N than medium-dense specimens, which was slightly larger than expected. The typical trend for friction angle is that as normal stress increases, friction angle decreases. For example, with normal

Table 5.2. Summary of #1 Dry Glass Sand's Measured Friction and Dilatancy Angles

Summary #1 Dry Glass							
Test	σ_N **(kPa)**	γ_d **(g/cm^3)**	e	D_r **(%)**	ϕ_p **(deg.)**	ϕ_{cs} **(deg.)**	ψ **(deg.)**
Loose	15	1.377	0.924	10.0	N/A	36.0	2.3
	50	1.382	0.917	12.5	N/A	36.3	2.3
	100	1.378	0.922	10.3	N/A	34.2	1.8
	400	1.382	0.916	13.2	N/A	31.2	1.8
Medium Dense	15	1.491	0.777	73.4	32.5	31.5	11.5
	50	1.486	0.783	70.7	32.5	31.3	10.0
	100	1.489	0.779	72.2	31.8	29.1	9.1
	400	1.493	0.774	74.3	30.9	28.7	8.4
Dense	15	1.596	0.660	123.7	41.6	36.5	18.1
	50	1.605	0.651	127.5	39.9	36.0	16.6
	100	1.604	0.651	127.6	38.0	35.0	16.0
	400	1.601	0.654	126.2	38.5	30.2	15.4

stresses of 15, 50, 100 and 400 kPa for a dense specimen, the peak friction angles were found to be 41.6°, 39.9°, 38.0°, and 38.5°, respectively, because for dense sands, the peak friction angle at peak shear stresses was dependent on granular soil dilation. At low normal stresses, dilatancy and particle rearrangement are the main contributors in influencing shearing resistance when compared to higher normal stresses. Therefore, at low normal effective stress more dilation occurs, increasing peak friction. However, increased normal stress suppresses the specimen as shear displacement is increased; therefore, the specimen is not as free to expand. When varying from a dense to a loose specimen, the dilatancy angles decrease. For example, with 15 kPa normal stress, the dilatancy angles were 18.1, 11.5, and 2.3° for dense, medium-dense, and loose specimens, respectively. The loose specimens' dilatancy angle significantly decreased because the particle contracted more and then only slightly expanded to a critical state.

5.2.2 GS#40 Columbia Sand

Figures 5.2(a), 5.2(c), and 5.2(e) display the normalized shear stress versus shear displacement for GS#40 Columbia Sand dense, medium-dense, and loose specimens, respectively. A similar trend for τ/σ_N was observed when compared to #1 Dry Glass Sand except the medium-dense specimens had a less defined peak. A higher density and low normal stress resulted in a higher τ/σ_N followed by a more pronounced approach to a critical state. Moreover, increasing density resulted in an increase in τ/σ_N and an emergence of a peak state while τ/σ_N of loose specimens gradually increased until reaching a critical state where τ/σ_N did not increase with further shearing. Figures 5.2(b), 5.2(d), and 5.2(f) display the normal versus shear displacement relationship for the dense, medium-dense, and loose specimens, respectively. The same trend of initially contracting and then dilating to a critical state was observed in each experiment. However, GS#40 Columbia Sand contracted less compared to #1 Dry Glass Sand. This result could be attributed to GS#40 Columbia Sand's particle morphology being less rounded and having a rougher surface than #1 Dry Glass Sand. Moreover, during dilation to a critical state, the normal displacement was slightly less than #1 Dry Glass. Table 5.3 presents a summary of GS#40 Columbia Sand's results including friction angles, dilatancy angles, initial densities, void ratios, and relative densities.

5.2.3 Glass Beads

Figures 5.3(a), 5.3(c), and 5.3(e) display the normalized shear stress versus shear displacement for dense, medium-dense, and loose specimens, respectively, for glass beads. As shear displacement increased, τ/σ_N showed similar trends to those of GS#40 Columbia Sand. The medium-dense specimens only slightly peaked and then leveled to a critical state. The glass

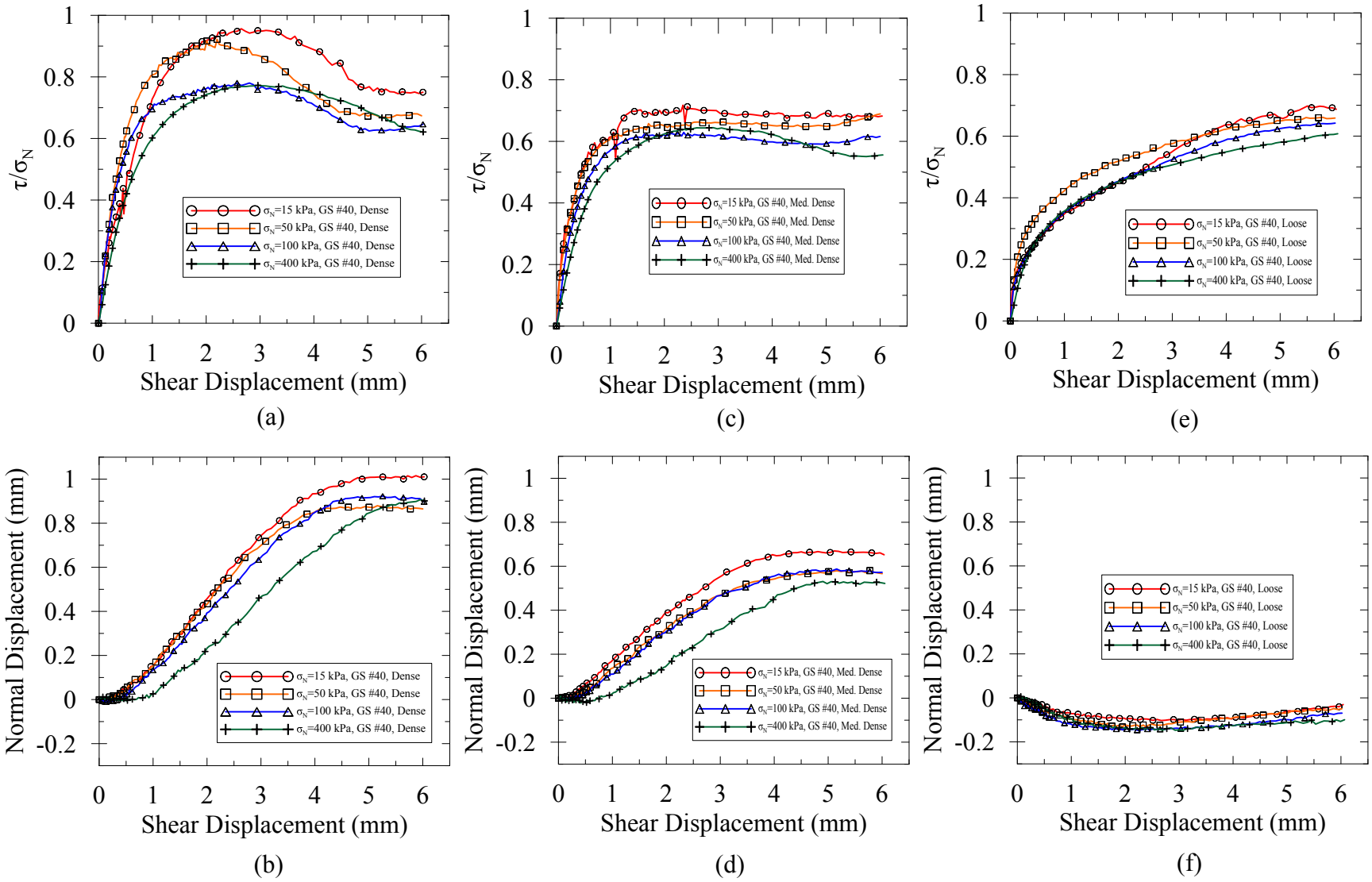

Figure 5.2. Normalized Shear Stress and Normal Displacement versus Shear Displacement for GS #40 Columbia Sand

Table 5.3. Summary of GS#40 Columbia Grout Sand's Measured Friction and Dilatancy Angles

Summary GS#40 Columbia Grout Sand							
Test	σ_N **(kPa)**	γ_d **(g/cm^3)**	e	D_r **(%)**	ϕ_p **(deg.)**	ϕ_{cs} **(deg.)**	ψ **(deg.)**
Loose	15	1.379	0.920	10.1	N/A	35.2	1.7
	50	1.382	0.916	11.7	N/A	34.0	1.6
	100	1.383	0.915	12.1	N/A	33.6	1.5
	400	1.379	0.920	10.1	N/A	31.7	1.0
Medium Dense	15	1.503	0.762	72.7	34.9	34.4	11.4
	50	1.501	0.764	71.8	33.5	33.1	9.5
	100	1.504	0.762	72.8	32.0	30.6	9.4
	400	1.501	0.764	71.7	32.8	28.9	8.8
Dense	15	1.596	0.659	113.2	42.2	36.8	17.3
	50	1.597	0.659	113.2	42.2	33.8	16.6
	100	1.598	0.657	114.0	37.8	32.2	16.6
	400	1.597	0.658	113.3	37.7	31.3	16.0

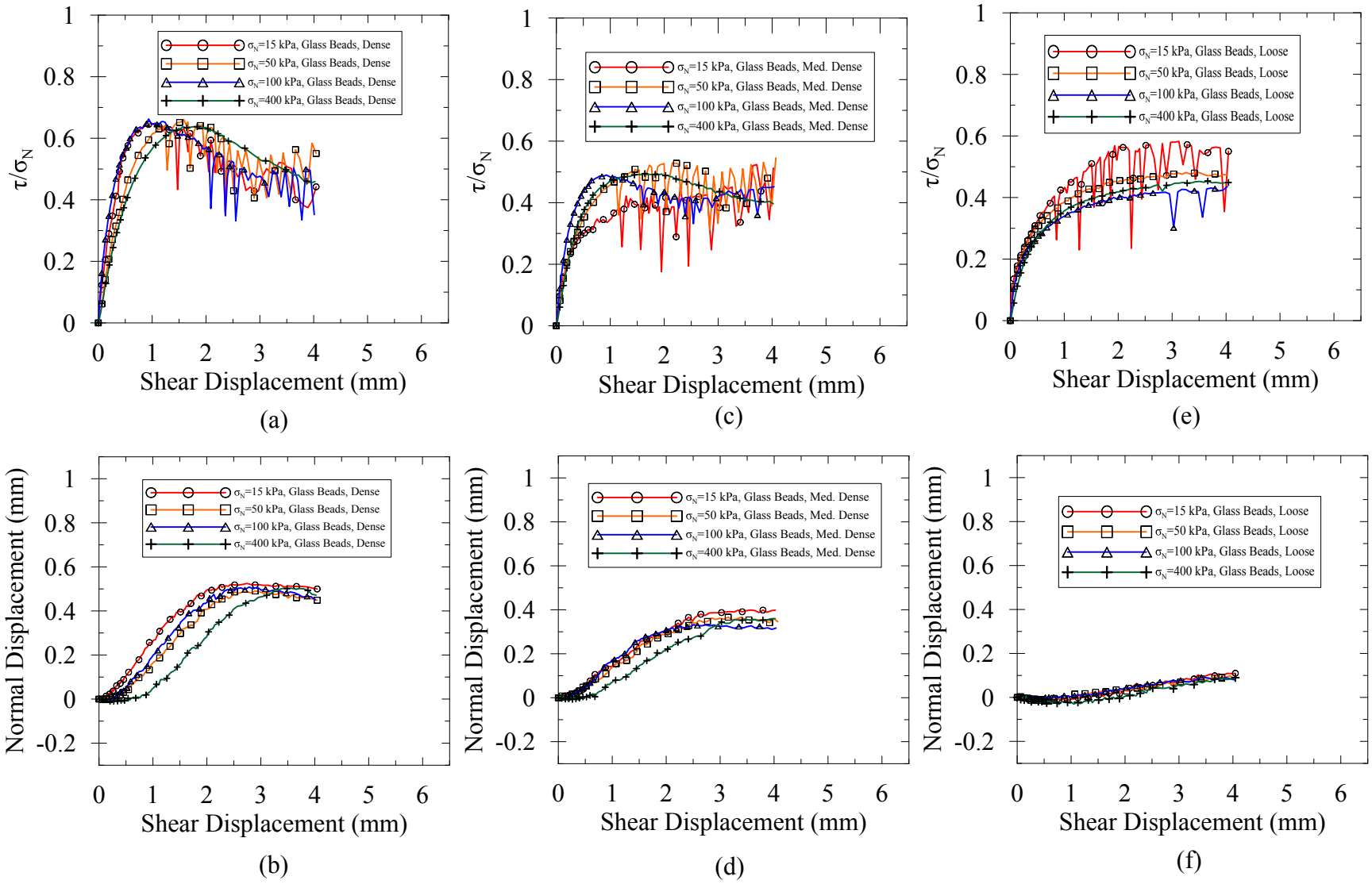

Figure 5.3. Normalized Shear Stress and Normal Displacement versus Shear Displacement for Glass Beads

beads' τ/σ_N measurements were not as smooth as the two previously discussed types of sands. This oscillation is attributed to the slip-stick behavior between the particles during shearing, when the particles momentarily stick, in turn causing constant resistance, and then slip causing a sudden drop. Glass beads have relatively uniform sphericity and roundness as well as a smoother surface when compared to the silica sands, thus causing the slip-stick behavior. Alshibli and Roussel (2006) also reported glass beads' slip-stick behavior.

Figures 5.3(b), 5.3(d), and 5.3(f) show the normal versus shear displacement for dense, medium-dense, and loose specimen, respectively. No significant contraction was observed at the beginning of the experiment for the dense and medium-dense specimens, unlike the expansion of #1 Dry Glass and GS#40 Columbia Grout Sand. Thus, as shear displacement increased, the specimens dilated until it reached a critical state at a smaller normal and shear displacement (3.5 mm). This phenomenon could be a result of the rough oscillatory behavior of glass beads as they are sheared. Figure 5.3(f) displays the results of experiments with loose specimens in which the behavior also differed from that of the two previous sands. As shear displacement increased, only very slight contraction occurred followed by dilation before reaching a critical state. The summary values for friction angles, dilatancy angles, initial densities, void ratios, and relative densities are shown in Table 5.4.

5.2.4 F-35 Ottawa Sand

Figures 5.4(a), 5.4(c), and 5.4(e) display the normalized shear stress versus shear displacement for dense, medium-dense, and loose specimens, respectively for F-35 Ottawa Sand. Figure 5.4(a) shows dense specimens with similar trends as those of the other three types of

Table 5.4. Summary of Glass Beads' Measured Friction and Dilatancy Angles

Summary Glass Beads							
Test	σ_N **(kPa)**	γ_d **(g/cm^3)**	e	D_r **(%)**	ϕ_p **(deg.)**	ϕ_{cs} **(deg.)**	ψ **(deg.)**
Loose	15	1.482	0.720	69.6	N/A	26.9	3.6
	50	1.476	0.727	63.5	N/A	25.9	2.8
	100	1.480	0.723	67.7	N/A	23.5	2.1
	400	1.479	0.724	66.9	N/A	23.4	2.2
Medium Dense	15	1.547	0.648	133.2	25.0	25.0	12.9
	50	1.552	0.642	138.5	26.6	23.8	10.8
	100	1.546	0.649	132.6	26.1	22.1	10.6
	400	1.547	0.648	133.6	26.2	21.6	8.6
Dense	15	1.620	0.573	198.8	32.9	26.0	19.3
	50	1.622	0.572	200.0	32.9	25.6	18.6
	100	1.614	0.579	193.9	32.8	24.7	17.7
	400	1.613	0.581	192.2	32.2	24.5	15.1

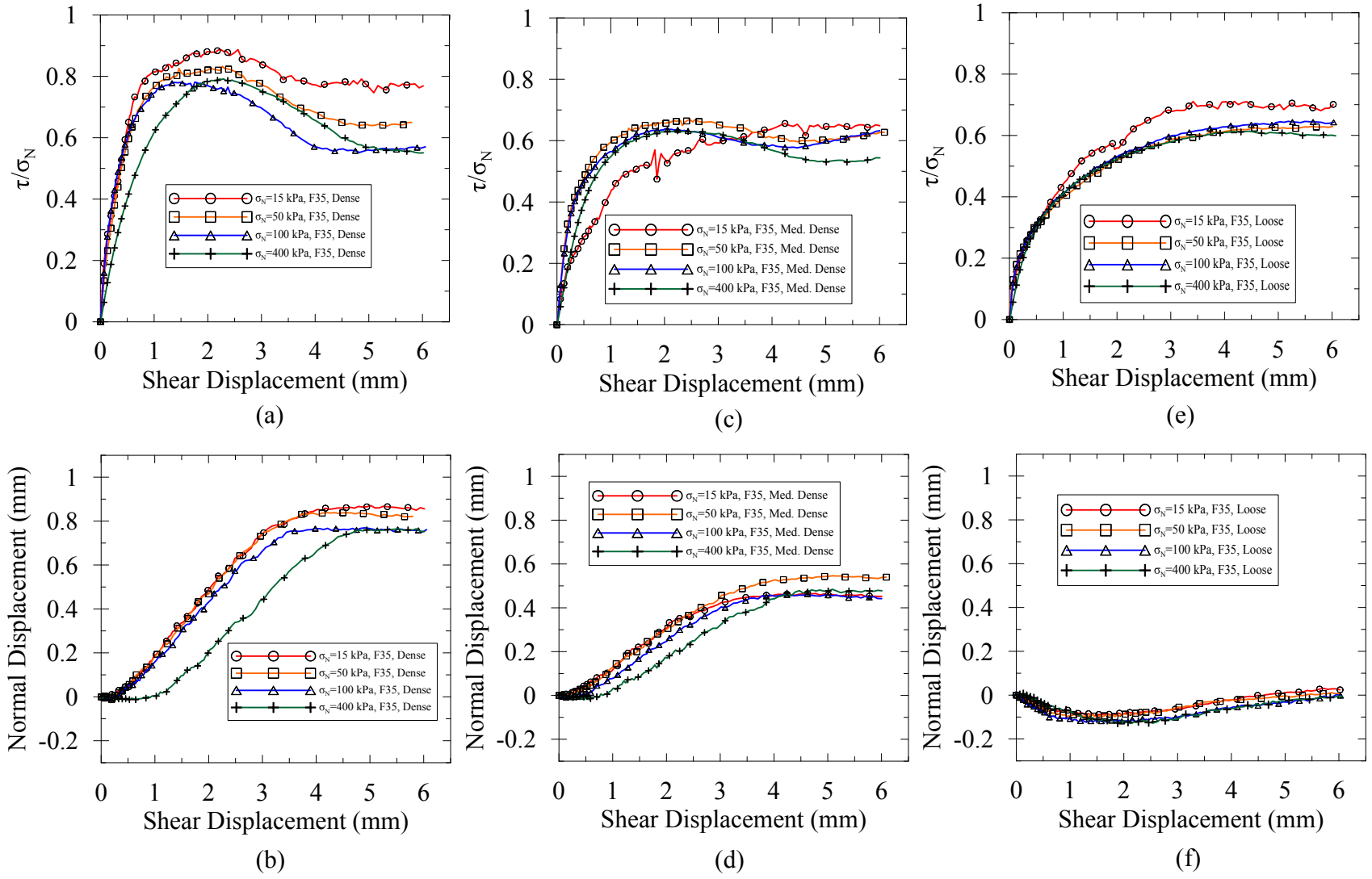

Figure 5.4. Normalized Shear Stress and Normal Displacement versus Shear Displacement for F-35 Ottawa Sand

sands'; where as shear displacement increased, τ/σ_N increased to a peak and then approached a critical state. Moreover, Figure 5.4(c) shows that the medium-dense specimens increased in τ/σ_N to a slight peak and then decreased to a critical state as shear displacement increased, while Figure 5.4(e) displays the results for loose specimens, in which τ/σ_N simply increased to a critical state. The same behavior was observed when normal stress with a constant density varied.

Figures 5.4(b), 5.4(d), and 5.4(f) display the normal versus shear displacement for dense, medium-dense, and loose specimens, respectively. Figures 5.4(b) and 5.4(d) do not show significant contraction, but rather expansion until reaching a critical state for dense and medium-dense specimens. On the other hand, Figure 5.4(f) shows that loose specimens contracted initially and then expanded to a critical state. Specimens with normal stress conditions of 50, 100, and 400 kPa dilated such that the final height was similar to the initial height. For the experiments with 15 kPa normal stress, the specimen contracted and then expanded past the initial height since less normal stress was suppressing the specimen's tendency to expand. The friction and dilatancy angles from the normalized shear stress versus shear displacement and normal versus shear displacement relationships are listed in Table 5.5.

Overall, increasing normal stresses decreased the shear strength parameters such as friction and dilatancy angles. This trend was evident throughout most of the experiments. The explanation for this trend is that the high normal stress suppressed the particles' ability to expand during shearing, resulting in smaller dilatancy and peak friction angles. Relative density's influence was also observed; while the specimen's density shifted from dense to loose, the friction and dilatancy angles decreased.

The slightly different behavior observed in the three types of silica sands and glass beads is most likely attributable to particle morphology. Increasing the particle's sphericity typically

Table 5.5. Summary of F-35 Ottawa Sand's Measured Friction and Dilatancy Angles

Summary F-35 Ottawa Sand							
Test	σ_N **(kPa)**	γ_d **(g/cm^3)**	e	D_r **(%)**	ϕ_p **(deg.)**	ϕ_{cs} **(deg.)**	ψ **(deg.)**
Loose	15	1.530	0.731	16.1	N/A	34.7	2.8
	50	1.530	0.732	16.2	N/A	32.6	2.9
	100	1.531	0.731	16.6	N/A	32.6	2.3
	400	1.529	0.732	15.7	N/A	30.9	2.3
Medium Dense	15	1.642	0.613	77.6	32.9	32.9	13.4
	50	1.641	0.614	77.2	33.4	31.0	12.2
	100	1.639	0.616	76.0	32.5	30.0	11.1
	400	1.643	0.613	77.8	32.21	28.1	8.8
Dense	15	1.757	0.507	132.5	40.00	36.1	19.1
	50	1.759	0.506	133.2	39.8	32.8	19.6
	100	1.753	0.511	130.6	38.0	29.4	18.9
	400	1.756	0.508	132.0	38.2	29.2	17.5

decreased the sands' and glass beads' τ/σ_N. For example, comparing the dense specimens' τ/σ_N for glass beads (i.e., spherical, smooth, and rounded particles) and for F-35 Ottawa Sand (i.e., less spherical, rougher surface, and less rounded particles), approximate values of 0.55 and 0.70, respectively, were found for τ/σ_N critical state. Therefore, less spherical particles contributed more to particle resistance such as interlocking, resulting in increased τ/σ_N. A less rounded particle with a rougher surface contributed to particle resistance and increased τ/σ_N as well. Particle morphology also attributed to the sands' slightly different dilation behaviors. Glass beads and F-35 Ottawa Sand specimens expanded to a normal displacement value of approximately 0.5 and 0.8 mm, respectively, for dense specimens. Thus, less spherical, rougher surfaces, and less rounded particles contributed to increased specimen expansion because of particle rearrangement/translation, unlike the stick-slip behavior of the spherical, smooth, and rounded particles of glass beads.

5.3 Particle Fracture Analysis

After each direct shear experiment, the sheared sand specimens were sieved to determine the amount passing through the US sieve No. 50 (0.300 mm). The passing amount represents the fracture the sand exhibited during the direct shear test. Comparing the fractured particles' weight divided by the total weight yielded the percentage of fractured particles. As normal stress increased, the sand typically exhibited more particle fracture. Once the particle's strength was less than the force being transferred, its limit was exceeded and hence particle fracture occurred. Moreover, increasing specimen density resulted in more fracture, as was expected. Since the particles were more densely packed initially, they had to overcome particle-on-particle resistance (e.g., rearranging and interlocking), which might have contributed to some of the particle fracture. The average percentage of particle fracture for each material's 12 tests is presented in Table 5.6. The sphericity, roundness, and surface texture rank is shown with a value of 1 being the least and 4 being the most. Internal composition and structure played a role, as well as particle morphology (e.g., fracturing of a particle's sharp edges during translation). Overall, the percentage of fractured particles was less than 1%, a very small percentage of the total amount of sand, demonstrating that particle fracturing was not a major contributor to frictional resistance.

Table 5.6. Average Fracture Percentages

Material	Fracture (%)	Sphericity Rank	Roundness Rank	Surface Texture Rank
#1 Dry Glass Sand	0.926	2	2	3
Glass Beads	0.542	4	4	1
GS#40 Columbia Sand	0.486	3	1	2
F-35 Ottawa Sand	0.104	1	3	4

5.4 Particle Morphology Trends

Before statistical modeling, typical trends were observed when the values of sphericity, roundness, and surface texture were carefully analyzed. For both peak and critical state friction angles, as sphericity increased in a value greater than unity, the friction angles increased. Therefore, a less spherical particle increases frictional resistance. As roundness increased, the critical state and peak friction angle slightly decreased in value. This finding indicates that a more rounded edge decreases friction. There was only a slight influence, which could have resulted from the small range of roundness for the tested sands (mean range = 0.204). As surface texture increased, both peak and critical state friction angles also increased.

For dilatancy angles, sphericity and surface texture had more influence than roundness. As the sphericity value increased past unity, dilatancy angles typically increased, indicating that a less spherical particle may result in more expansion. For roundness, the dilatancy angles barely decreased as the roundness value increased. As surface texture increased, the dilatancy angle slightly increased, possibly because smoother particles, such as glass beads, tend to slip, resulting in less expansion.

5.5 Statistical Modeling Evaluation and Results

Regression analysis, one of the most widely used statistical techniques, was adopted to model the relationship between explanatory variables and a response variable. The explanatory variables (i.e., normal stress, relative density, sphericity, roundness, and surface texture) were used to determine their effect on the sands' friction and dilatancy (i.e., response variables). A random sampling technique with one standard deviation was performed on the morphology indices listed in Table 5.1 to represent each experiment's morphology characteristics correlating

to friction and dilatancy angles summarized in Tables 5.2 through 5.5. Since multiple influential variables likely affect the critical state friction, peak friction, and dilatancy angles, a linear regression model determining which explanatory variables are significant should be developed. Evaluating multiple explanatory (or independent) variables using stepwise regression would determine which of these independent variables is most influential.

Using Cook's D, one extreme influential point had a value greater than 1, which according to Longnecker and Ott (2010) should be examined. Consequently, the experiment for GS#40 Columbia Sand with a normal stress of 15 kPa under dense condition was eliminated since this influential point caused minor inaccuracies in the models. Therefore, the final models discussed exclude this observation.

In this thesis, the variable $\boldsymbol{\beta_0}$ represents the intercept for each developed model. An increase in $\boldsymbol{I_S}$ indicates a less spherical value since unity represents a spherical particle. Because sphericity indices are greater than one, the proposed models hold true for sphericity values of one or more. For roundness, all indices that increase in $\boldsymbol{I_R}$ indicate a more round particle. Lastly, since surface texture depends on a particle's surface heights, an increase in $\boldsymbol{R_q}$ represents a rougher particle.

5.5.1 Critical State Friction Angle

Critical state friction angle was investigated using 47 observations from the direct shear experiments for this statistical analysis. Stepwise regression was applied using the SAS Enterprise Guide. The independent variables were entered based on a default and desired significance level of 0.15 (Montgomery and Runger 2011); they were then removed from the model if determined to be insignificant (0.05 level). Researchers have reported that normal stress

and relative density significantly influence peak friction and dilatancy angles, but not the critical state friction angle; therefore, normal stress and relative density were not included in the regression model for the critical state friction angle. However, the parameter of silica sand's true friction (ϕ_μ) was explored by assuming an intercept value of 22°, similar to the sand's true friction (23°) reported by Rowe (1962). Consequently, the model evaluation was conducted with this intercept by analyzing ($\phi_{CS} - \phi_\mu$) values as the response variable. Table 5.7 summarizes the stepwise regression for critical state friction angle. The order of the variable entry depended on its F-value and significance to the model. The largest F-value was placed into the model first, and then its significance based on its p-value determined if the variable should be removed. All independent variables were entered except roundness, which did not meet the significance level of 0.15. Therefore, the model indicated that roundness does not significantly influence critical state friction angles.

The analysis of variance's results (i.e., the degree of freedom (DF), sum of squares, mean square, F-value, and p-value) for the critical state friction angle linear regression model are listed in Table 5.8. The F-test determined if the combination of variables explained variance in the response variable (i.e., critical state friction angle) and if it indicated a significant model. A large F-value and a small p-value provide evidence of a good model. The analysis of variance summary indicates that the model was significant with F(2,45) = 346.82 and p-value less than 0.0001. Overall, the model's adj. R^2 is 0.936, verifying that the model was important enough to

Table 5.7. Stepwise Regression Summary for Critical State Friction Angle Using SAS

Step	Variable Entered	Variable Removed	Model R-Square	F-Value	P-Value
1	$\boldsymbol{I_S}$		0.891	377.34	<0.0001
2	$\boldsymbol{R_q}$		0.939	35.26	<0.0001

Table 5.8. Final Analysis of Variance for Critical State Friction Angle Using SAS

Source	DF	Sum of Squares	Mean Square	F-value	P-value
Model	2	3855.51	1927.75	346.82	<0.0001
Error	45	250.13	5.56		
Corrected Total	47	4105.64			

investigate since the variables' linear combination accounts for approximately 93.6% of variance in the critical state friction angle.

Once the analysis of variance proved that this was a substantial model to investigate, each variable's parameter estimates were observed and evaluated. Table 5.9 summarizes each variable's parameter estimates with the degree of freedom, standard error, p-value, standardized estimate, and variance of inflation. For each variable, all VIF values were less than 2. A VIF of 10 or more indicates a problem with collinearity. Since all VIF values were less than 10, collinearity was not an issue for this linear regression model.

Outliers and violation of assumptions were then investigated to ensure an accurate model. A scatter plot of the studentized residual (RStudent), which are the residuals divided by an estimate of their standard deviation, was used when evaluating these issues. The studentized residuals versus predicted value with $\pm 2s_\varepsilon$ boundary lines are shown in Figure 5.5. All but two studentized residuals lay within $\pm 2s_\varepsilon$ and all lay within $\pm 3s_\varepsilon$, indicating outliers were not an issue. Moreover, no noticeable pattern was seen in the residuals; therefore, the linearity assumption was not violated.

The regression model's normality of residuals was another assumption that had to be evaluated. Based on a visual evaluation, the residuals lay close to the 1:1 line, indicating that the

Table 5.9. Parameter Estimates for the Critical State Friction Angle Model

Variable	DF	Parameter Estimate	Standard Error	Pr>|t|	Standardized Estimate	VIF
I_S	1	3.405	0.470	<0.0001	0.550	4.253
R_q	1	2.596	0.437	<0.0001	0.451	4.253

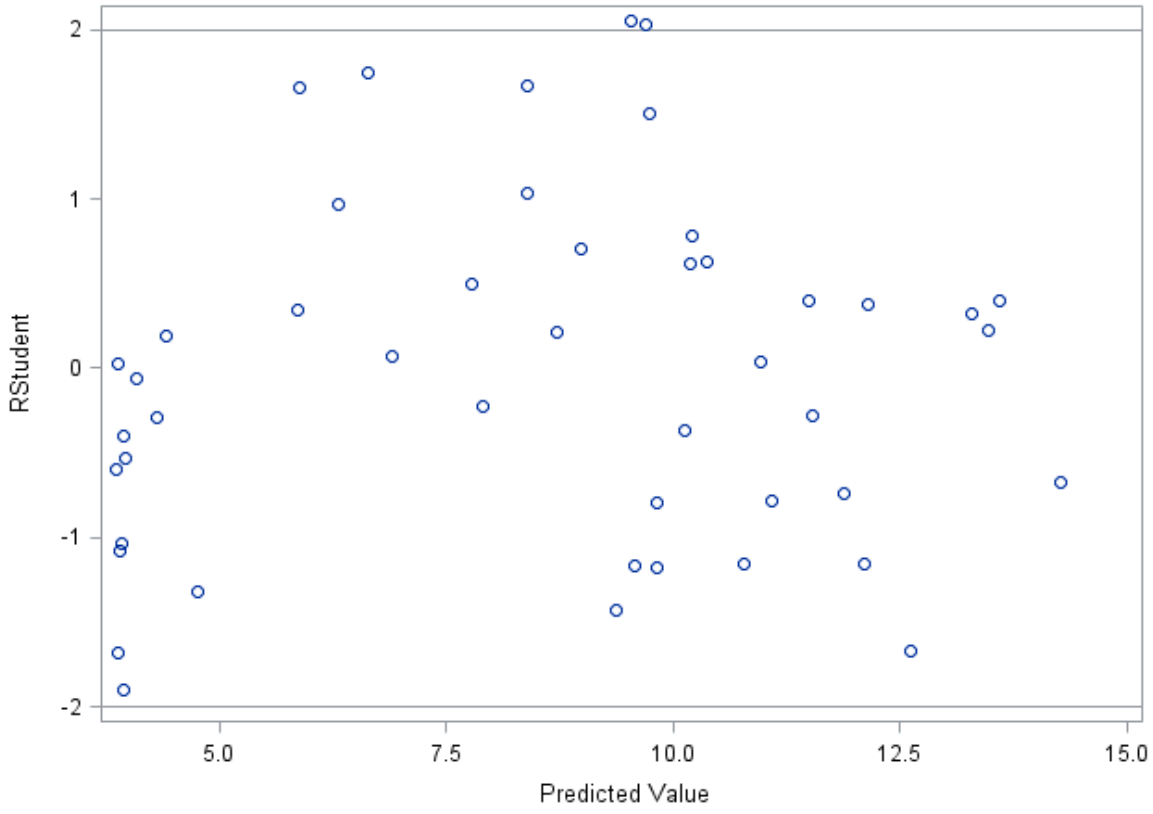

Figure 5.5. Studentized Residual versus Predicted Value for Critical State Friction Angle

residuals were indeed normal (Figure 5.6). Moreover, a p-value of 0.291 was found using the Shapiro-Wilk test for normality. According to Longnecker and Ott (2010), a p-value between 0.10 and 0.50 for assessing normality provides a good fit. Therefore, the residuals were found to follow a normal distribution, and no assumptions were violated.

Since no assumptions for a linear regression were violated, the model could be confidently outlined. Sphericity and surface texture (i.e., the explanatory variables) were input parameters for the critical state friction angle linear regression model:

$$\boldsymbol{\phi_{CS}} = 22° + 3.405\,\boldsymbol{I_S} + 2.596\,\boldsymbol{R_q} \tag{5.1}$$

Equation 5.1 corresponds to the parameter estimates shown in Table 5.9. The most influential variable was based on the standardized regression estimate (β), which for this model correlated with the significance of the stepwise regression summary selection (Table 5.7). The standardized regression estimates measured the dependent variable's standard deviation increase as a single independent variable experiences one standard deviation change. Since larger values indicated the most effect, the most influential variable was determined to be the sphericity index (β=0.550), which is positively related to the critical state friction angle. An increase in sphericity index resulted in an increase in critical state friction angle. This finding suggests that as a particle becomes less spherical, the critical state friction angle increases. Moreover, spherical particles may have fewer particle contacts that would attribute to frictional resistance when compared to a less spherical particle.

Surface texture (β=0.451) is the second-most significant variable affecting critical state friction angle. Moreover, surface texture was positively related to the critical state friction angle.

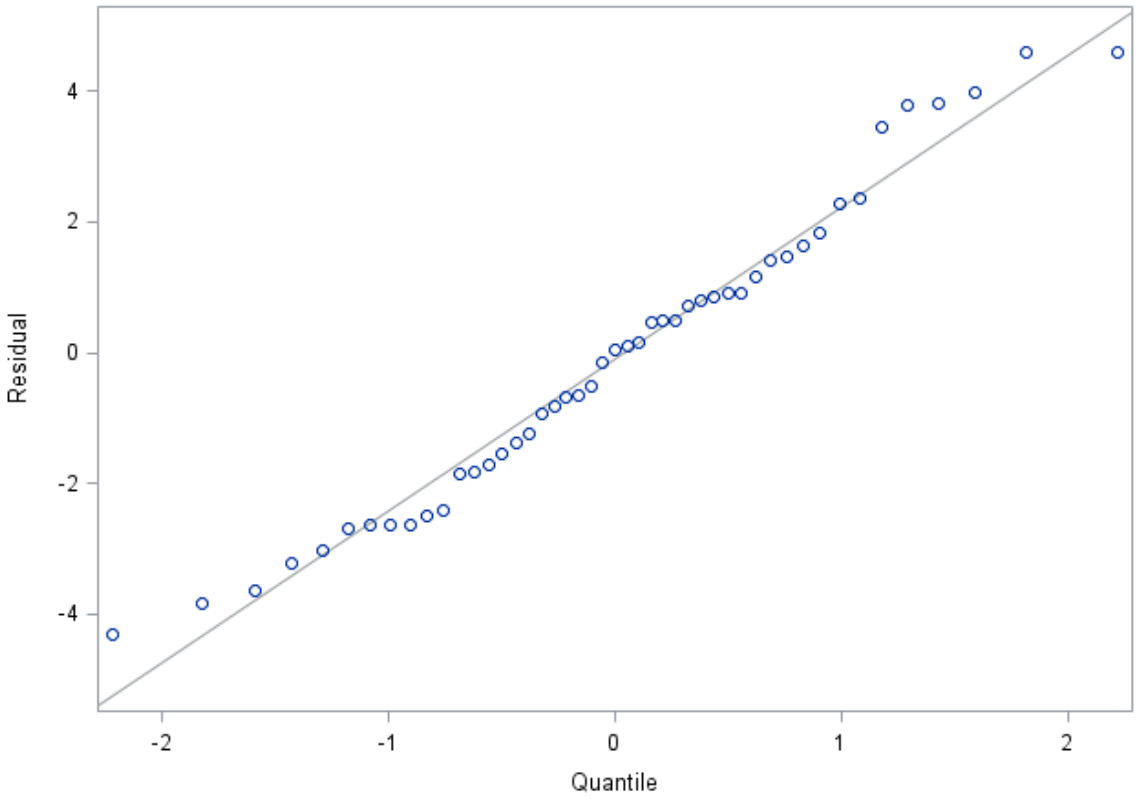

Figure 5.6. Quartile-Quartile Plot for Critical State Friction Angle

Surface texture caused more frictional resistance since it may have contributed to particle rearrangement and translation capabilities influenced by particle-on-particle contacts.

Although some studies (e.g., Dodds 2004 and Edil and Benson 2007) have reported that as roundness increases, critical state friction angle decreases, roundness was not found to be an influential factor in this study. Since roundness was determined to be insignificant (0.05 level), some reasons include that the other explanatory variables overpowered the significance of roundness. However, the range of roundness indices was narrow for the sands selected for this study. The range for roundness was 0.204 with the lowest and highest values being 0.837 and 1.041, respectively. For sphericity and surface texture, the range was 1.471 and 2.933, respectively. Therefore, experiments with a larger range of roundness indices should be conducted.

The predicted values from the linear regression model were compared to experimental values displayed in Figure 5.7 to investigate the model's reliability. The values lay close to the 1:1 line, indicating that the model produced reliable predictions. A grouping of the glass beads was identified with lower critical state friction angle values (Figure 5.7). Moreover, to display the linear regression model's goodness of fit, the coefficient of determination was 0.939 with an adj. R^2 of 0.936. With the linear combination of variables, the model explained 93.6% of the variability of critical state friction angle. A 95% prediction interval (i.e., estimating where 95% of future observations will lie) is shown in Figure 5.8.

5.5.2 Peak Friction Angle

Peak friction angle was investigated using 31 observations since all loose states did not exhibit a peak behavior. Stepwise regression was applied with the same independent variables

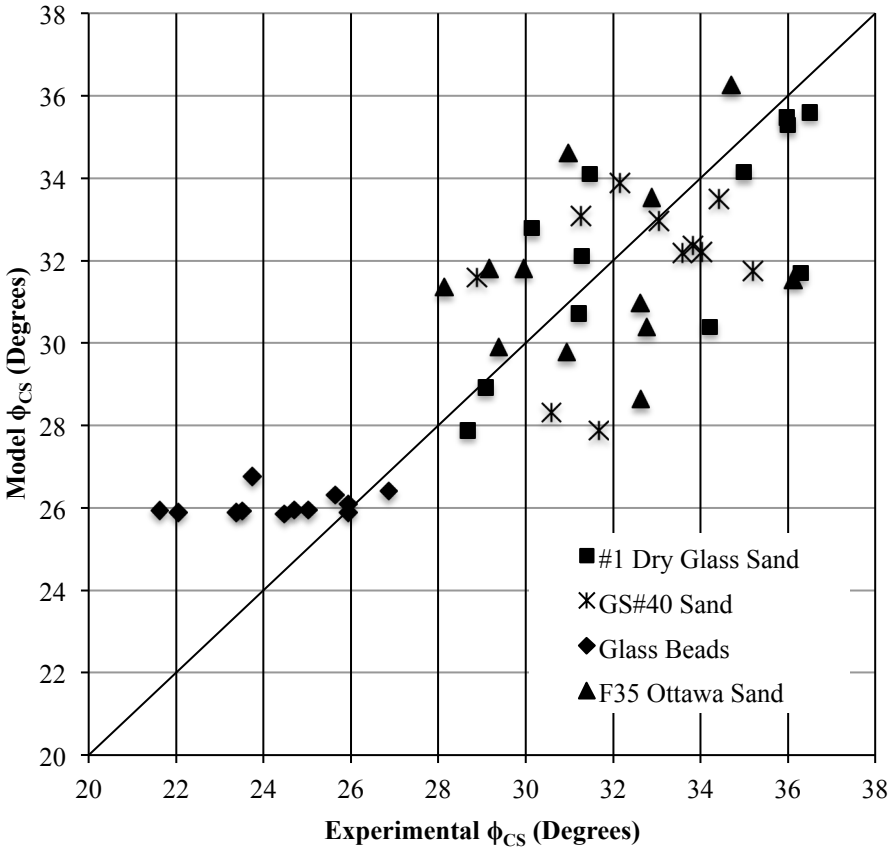

Figure 5.7. Model versus Experimental for Critical State Friction Angle

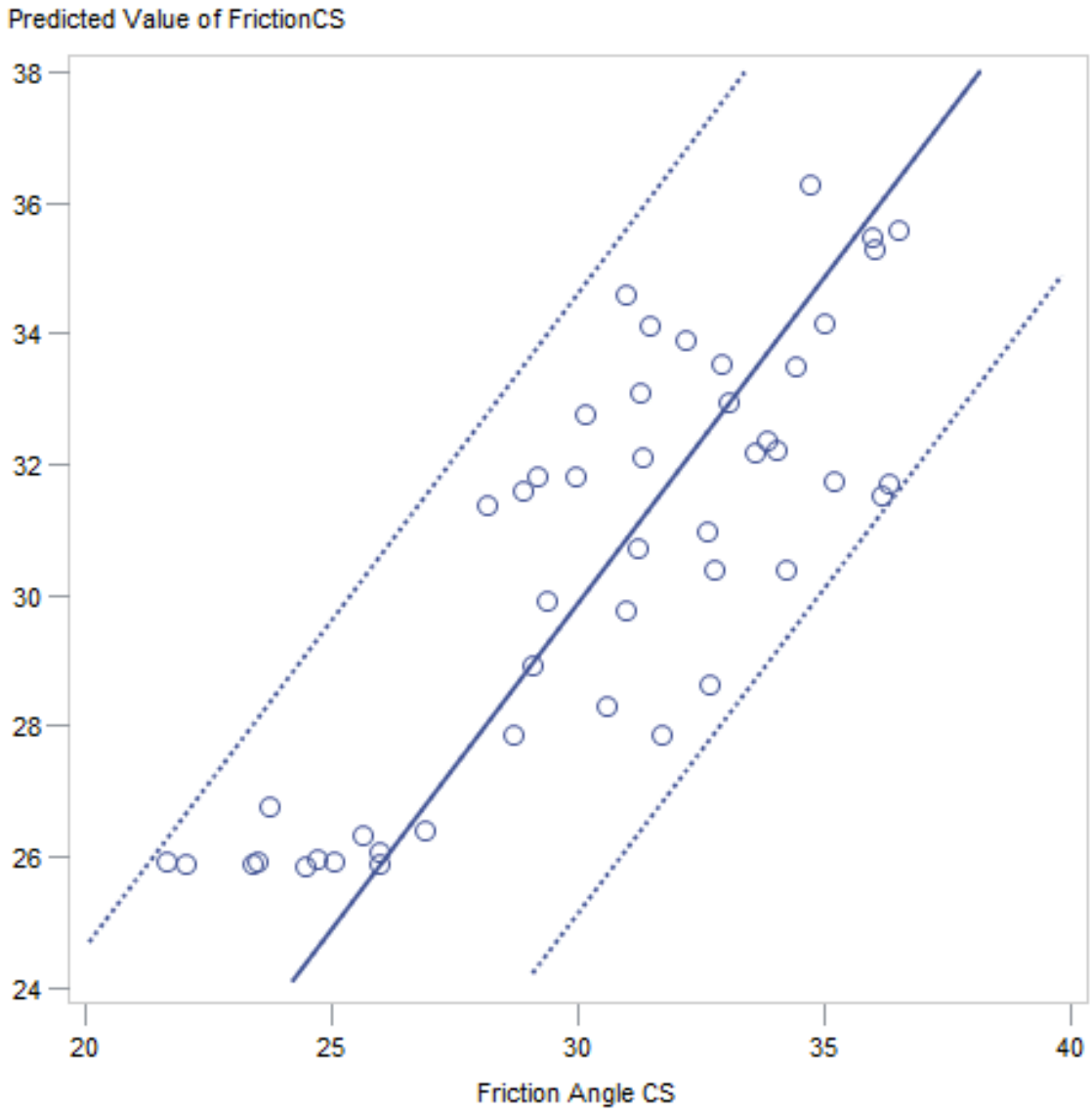

Figure 5.8. Model versus Experimental Measurements with a 95% Prediction Interval for Critical State Friction Angle

with the addition of relative density and normal stress. Table 5.10 shows the stepwise regression summary along with the F-value and p-value for each step. Since researchers have reported that normal stress is an influential variable to peak friction angle, a model with normal stress was preferred; therefore, normal stress was placed in the model before the stepwise regression was applied. With normal stress included, each variable was considered significant to the 0.05 level, and the model's R^2 increased with each additional variable entered.

Table 5.11 presents the results of the analysis of variance for the peak friction angle model. The degree of freedom, sum of squares, mean square, F-value, and p-value for the model are shown. The analysis indicated a significant model with F(5,25) = 18.31 and a p-value less than 0.0001. The adj. R^2 for the model was 0.743, indicating that the variables' linear combination in this model accounted for approximately 74.3% of variance in peak friction angle, in turn suggesting the model was substantial enough to investigate.

Because the model proved to be substantial enough to investigate, parameter estimates were observed and evaluated. Parameter estimates as well as the degree of freedom, standard error, p-value, standardized estimate, and VIF for peak friction angle are shown in Table 5.12. Each variable had a VIF value less than 2, indicating that there was no problem with collinearity within the model since VIF was less than 10.

Other assumptions such as outliers and residuals were investigated to ensure an accurate model. Figure 5.9 shows the studentized residual versus predicted value with $\pm 2s_\varepsilon$ boundary lines. Outliers were not an issue since all but two studentized residuals lay within $\pm 2s_\varepsilon$ and all within $\pm 3s_\varepsilon$. Moreover, the linearity assumption was not violated since no obvious patterns of the residuals were observed.

Table 5.10. Stepwise Regression Summary for Peak Friction Angle Using SAS

Step	Variable Entered	Variable Removed	Model R-Square	F-Value	P-Value
1	I_S		0.491	27.39	<0.0001
2	I_R		0.611	7.78	0.0096
3	D_R		0.666	4.30	0.0481
4	R_q		0.786	13.95	0.0010

Table 5.11. Final Analysis of Variance for Peak Friction Angle Using SAS

Source	DF	Sum of Squares	Mean Square	F-value	P-value
Model	5	490.07	98.01	18.31	<0.0001
Error	25	133.80	5.35		
Corrected Total	30	623.871			

Table 5.12. Parameter Estimates for the Peak Friction Angle Model

Variable	DF	Parameter Estimate	Standard Error	Pr>|t|	β	VIF
β_0	1	43.093	10.434	0.0004	0	0
σ_N	1	-0.002	0.003	0.4638	-0.077	1.264
D_R	1	0.053	0.013	0.0003	0.474	1.523
I_S	1	6.568	1.079	<0.0001	0.618	1.203
I_R	1	-29.163	10.084	0.0078	-0.298	1.238
R_q	1	2.256	0.604	0.0010	0.459	1.761

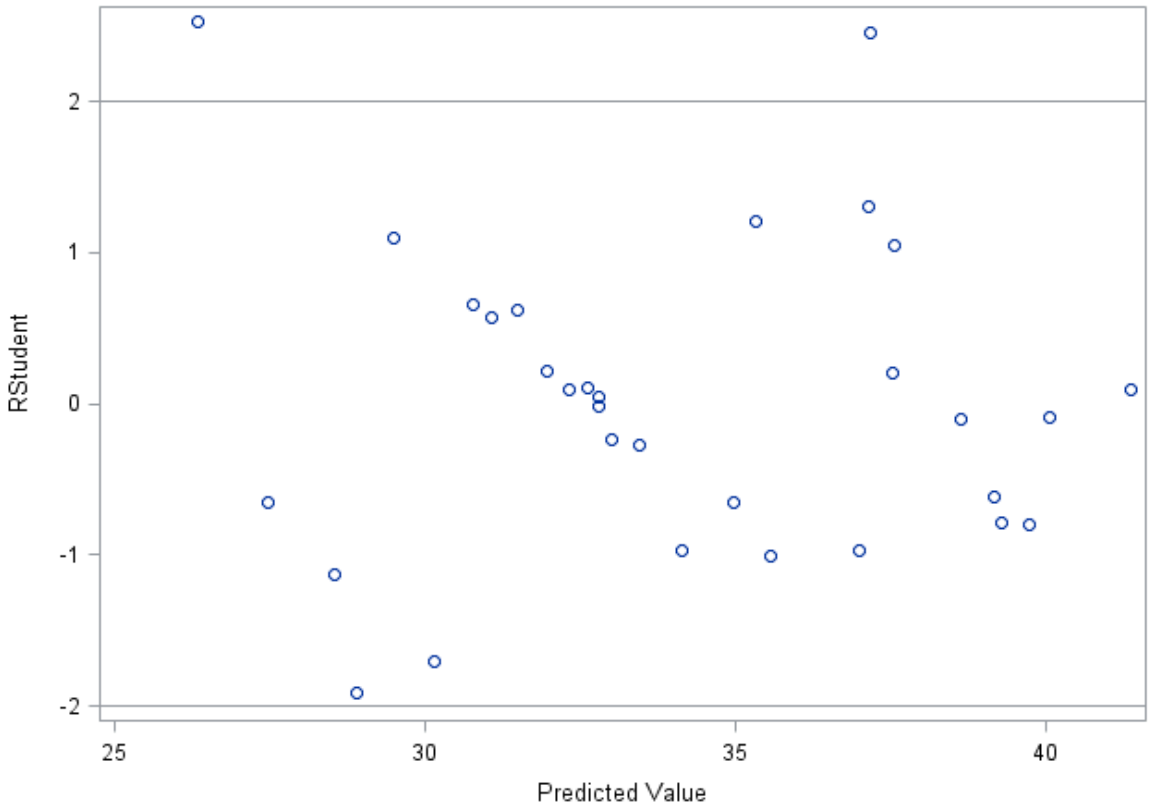

Figure 5.9. Studentized Residual versus Predicted Value for Peak Friction Angle

The residuals' assumption of normality for the linear regression was then evaluated. The residuals were indeed normal since they lay close to the 1:1 line as shown in Figure 5.10. Moreover, the Shapiro-Wilk test for normality found a p-value of 0.542, indicating that the residuals were normal. According to Longnecker and Ott (2010), a p-value greater than 0.50 for the normality assessment provides an excellent fit. Therefore, the residuals were an excellent fit for normality.

No assumptions for a linear regression were violated; therefore, the linear regression could be outlined with confidence. Corresponding to the parameter estimates shown in Table 5.12 and the inclusion of normal stress, all explanatory variables (i.e., relative density, sphericity, roundness, and surface texture) are input parameters for the peak friction angle linear regression model:

$$\boldsymbol{\phi_P} = 43.093 - 0.002\,\boldsymbol{\sigma_N} + 0.053\,\boldsymbol{D_R} + 6.568\,\boldsymbol{I_S} - 29.163\,\boldsymbol{I_R} + 2.256\,\boldsymbol{R_q} \qquad (5.2)$$

Based on the standardized regression estimate, the variables in descending order from most to least significant were sphericity, relative density, surface texture, roundness, and normal stress (Table 5.12). A large sphericity index (β=0.618) resulted in an increase in peak friction angle, indicating that a less spherical particle results in an increase in peak friction angle. Since the specimen's particle rearrangement and dilation were associated with peak friction angle, a less spherical particle resulted in increased volume because more stress was needed to force the particle to translate/rotate, in turn increasing peak friction angle.

The second-most influential variable was relative density (β=0.474), which had a positive relationship with peak friction angle, indicating a denser specimen would increase peak friction

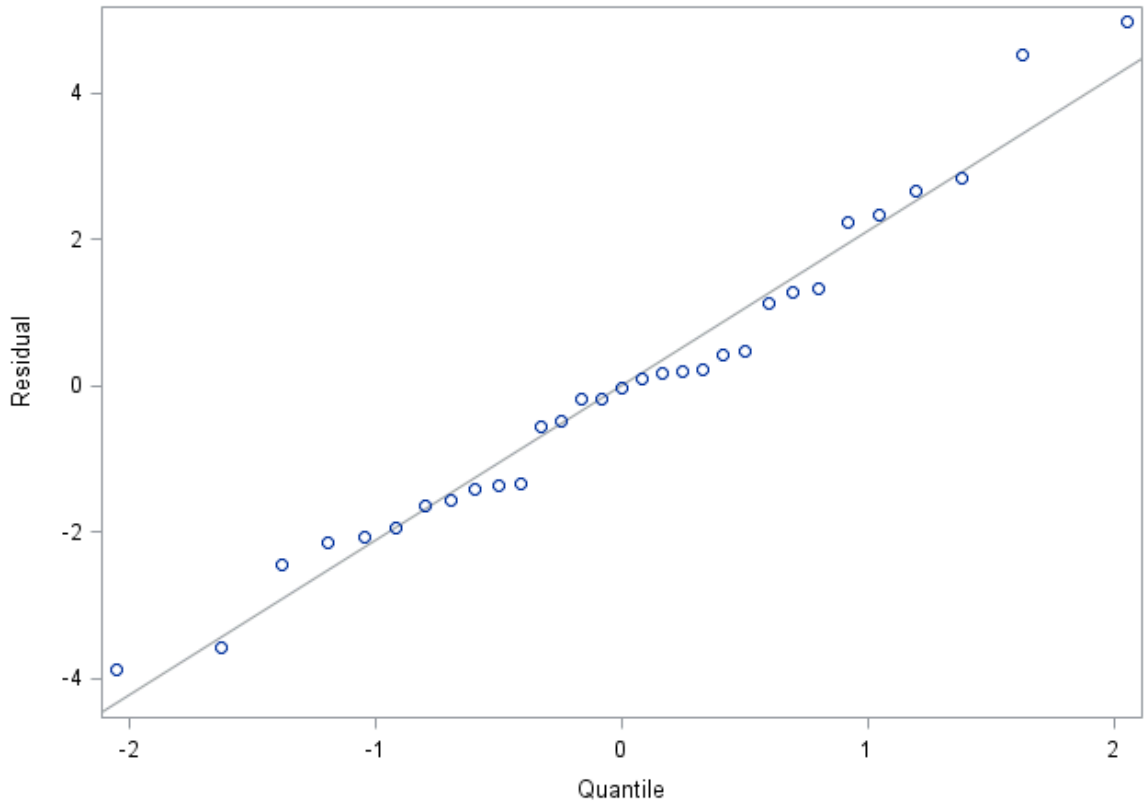

Figure 5.10. Quartile-Quartile Plot for Peak Friction Angle

angle. As relative density increased, the particles' packing was tighter and resulted in more particle contacts. More particle-to-particle contacts resulted in the morphology's more influential behavior (i.e., frictional resistance from surface texture or interlocking because of the particle's sphericity and roundness). Moreover, increased relative density typically increases dilation and rearrangement of particles, which based on previous research results in an increase in peak friction angle.

Surface texture (β=0.459) was the peak friction angle's third-most influential variable. An increase in surface roughness resulted in increased peak friction angle. The particles' behavior at particle-to-particle contacts may be influenced by surface texture, thus identifying surface texture's significance within the peak friction angle model.

The fourth-most significant variable based on the standardized regression estimates was roundness (β=-0.298). The relationship between roundness and the peak friction angle is inversely related (i.e., as roundness increased, the peak friction angle decreased). Since a less-rounded particle indicates sharper edges, decreased roundness may increase both the number of particle contacts as well and particle interlocking. Moreover, increasing particle interlocking increases resistance and therefore the sands' peak friction angle.

Lastly, normal stress (β=-0.077) was evaluated to determine its influence in the model. As normal stress increased, the peak friction angle decreased, meaning they were inversely related. It is well known that increasing normal stress suppresses dilation and particle rearrangement, thus explaining the decrease in peak friction angle.

The predicted values from the peak friction angle model were compared to experimental values to determine the model's reliability as shown in Figure 5.11 The model produced reliable predictions since the values lay close to the 1:1 line. Moreover, R^2 was 0.7855 while adj. R^2 was

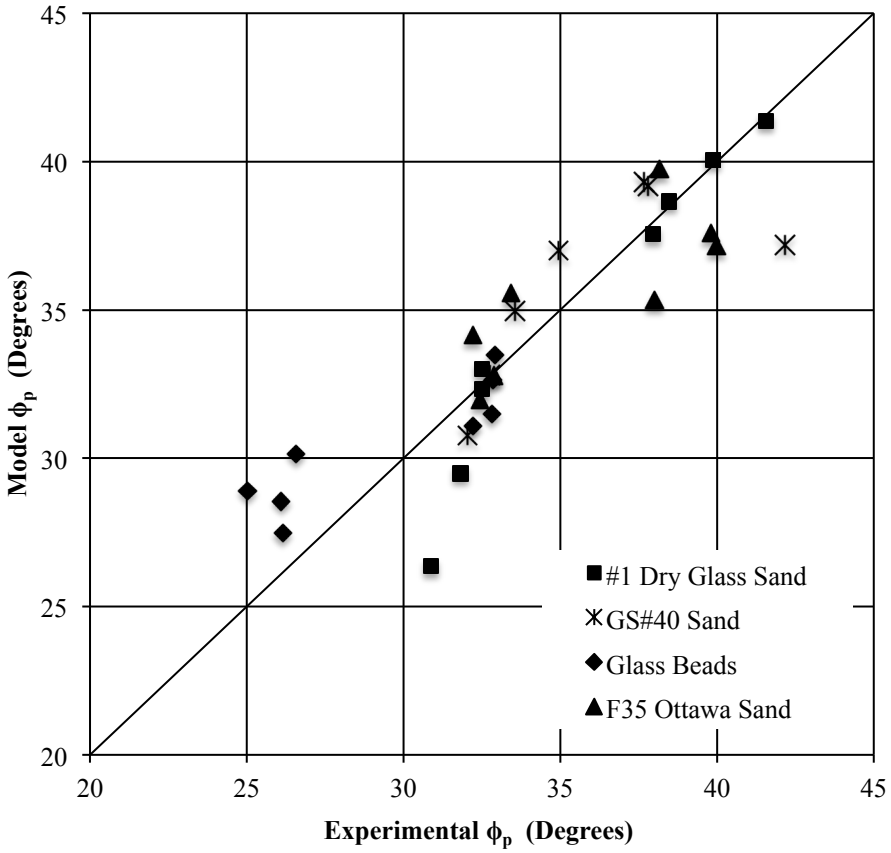

Figure 5.11. Model versus Experimental for Peak Friction Angle

found to be 0.7426. Therefore, the variables' linear combination explains 74.26% of the peak friction angle's variation. Figure 5.12 displays the 95% prediction interval, where 95% of future observations would fall.

5.5.3 Dilatancy Angle

The dilatancy angle was investigated using 47 observations. Stepwise regression was applied to investigate the explanatory variables' significance to the dependent variable dilatancy angle. The stepwise regression summary, F-value, and p-value for each variable are shown in Table 5.13. Similar to the peak friction angle, researchers have reported normal stress as an influential factor to dilatancy angle; therefore, normal stress was included in the model. All other variables except roundness were significant to the 0.05 level, and the model's R^2 increased with each additional variable.

The results of the analysis of variance (including the degree of freedom, sum of squares, mean square, F-value, and p-value) for the dilatancy angle regression model are summarized in Table 5.14. A large F-value and the small p-value of less than 0.0001 indicated a significant model with $F(4,42)=119.53$. The model's adj. R^2 was 0.912, indicating that approximately 91.2% of variance in the dilatancy angle is explained by the variables' linear combination. Therefore, the model was significant and the assumptions needed to be evaluated.

Each variable's parameter estimates were evaluated since the analysis of variance proved that this was a substantial model. The parameter estimate, degree of freedom, standard error, p-value, standardized estimate, and VIF are presented in Table 5.15. All VIF values were less than 10 for each variable, indicating that collinearity within the model was not a problem.

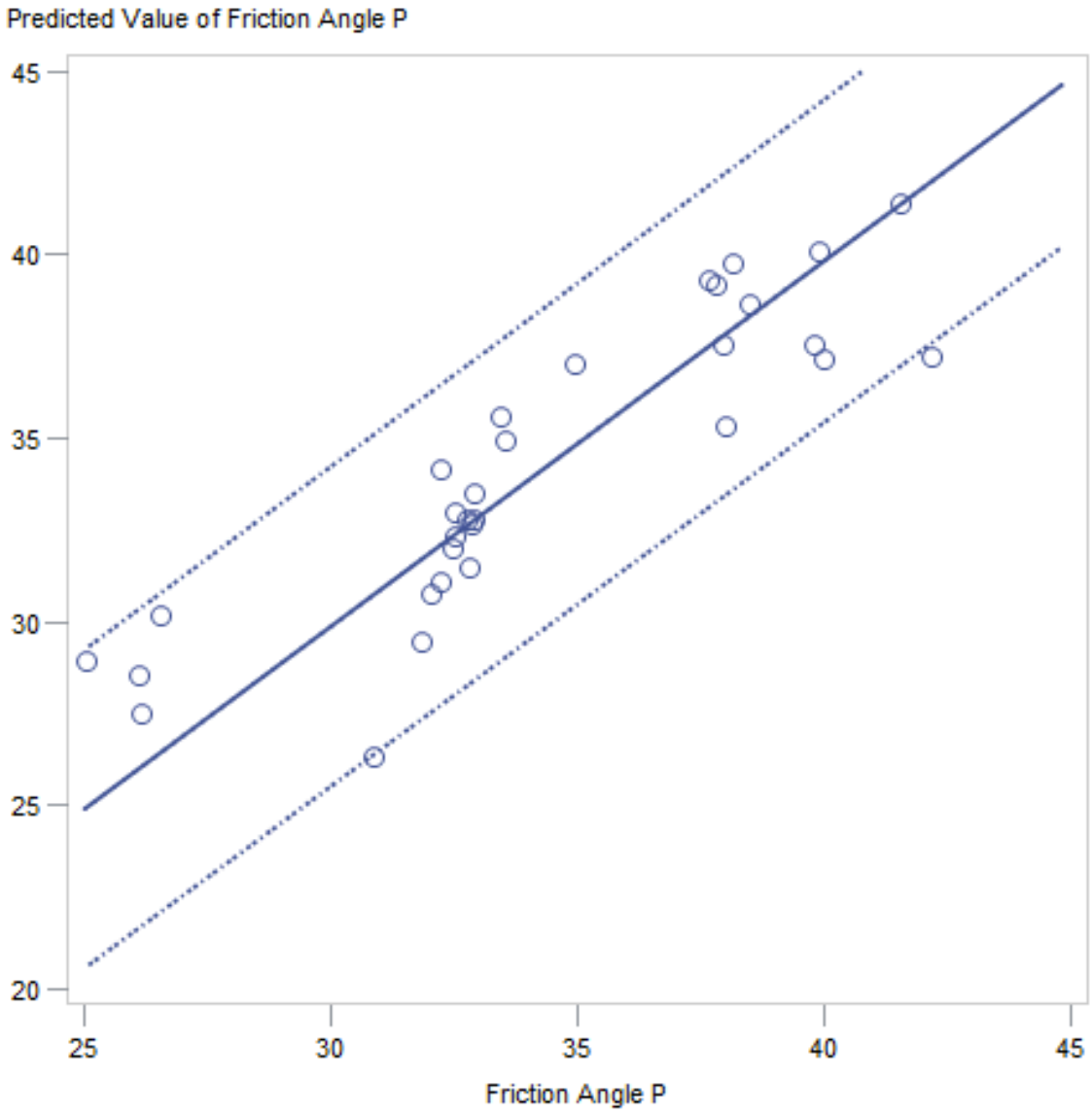

Figure 5.12. Model versus Experimental Measurements with a 95% Prediction Interval for Peak Friction Angle

Table 5.13. Stepwise Regression Summary for Dilatancy Angle Using SAS

Step	Variable Entered	Variable Removed	Model R-Square	F-Value	P-Value
1	$\boldsymbol{D_R}$		0.7710	146.20	<0.0001
2	$\boldsymbol{I_S}$		0.8819	40.36	<0.0001
3	$\boldsymbol{R_q}$		0.9193	19.43	<0.0001

Table 5.14. Final Analysis of Variance for Dilatancy Angle Using SAS

Source	DF	Sum of Squares	Mean Square	F-value	P-value
Model	4	1720.77	430.19	119.53	<0.0001
Error	42	151.16	3.60		
Corrected Total	46	1871.92			

Table 5.15. Parameter Estimates for the Dilatancy Angle Model

Variable	DF	Parameter Estimate	Standard Error	Pr>|t|	$\boldsymbol{\beta}$	VIF
$\boldsymbol{\beta_0}$	1	-7.499	1.283	<0.0001	0	0
$\boldsymbol{\sigma_N}$	1	-0.001	0.002	0.5346	-0.028	1.058
$\boldsymbol{D_R}$	1	0.113	0.005	<0.0001	0.990	1.118
$\boldsymbol{I_S}$	1	3.849	0.780	<0.0001	0.246	1.289
$\boldsymbol{R_q}$	1	1.647	0.374	<0.0001	0.233	1.447

Once collinearity was evaluated, the studentized residuals determined that the linear regression had no outliers and did not violate its assumptions. The studentized residual versus predicted value with the $\pm 2s_\varepsilon$ boundary is shown in Figure 5.13. All but three studentized residuals lay within $\pm 2s_\varepsilon$ while one value was close but not outside the range of $\pm 3s_\varepsilon$. Moreover, with no noticeable pattern for the residuals, no assumptions were violated.

Normality of residuals based on visual evaluation and the Shapiro-Wilk test ensured that the normality assumption was not violated. Figure 5.14 displays the Quartile-Quartile plot and indicates that the residuals were normal since they lay close to the 1:1 line. Moreover, the Shapiro-Wilk test for normality yielded a p-value of 0.957 and indicated an excellent fit. Therefore, no assumption was violated and the residuals followed a normal distribution.

The dilatancy angle model, corresponding to the parameter estimates shown in Table 5.15, could be confidently outlined since no assumptions for a linear regression were violated. Normal stress, relative density, sphericity, and surface texture (i.e., the explanatory variables) were significant to the model:

$$\boldsymbol{\psi_p} = -7.499 - 0.001\boldsymbol{\sigma_N} + 0.113\,\boldsymbol{D_R} + 3.849\,\boldsymbol{I_S} + 1.647\,\boldsymbol{R_q} \tag{5.3}$$

Roundness did not prove significant to the 0.15 level, possibly indicating that the other variables were far more significant or that the tested sands' range of roundness was somewhat limited. Based on the standardized regression estimates, relative density (β=0.990) was the dilatancy angle model's most influential factor. Relative density was positively related to dilatancy, meaning with increasing relative density, the expansion of the specimen increased. A more densely packed specimen increases dilatancy since during shear the particles must ride up and roll over other particles, resulting in the sands' expansion.

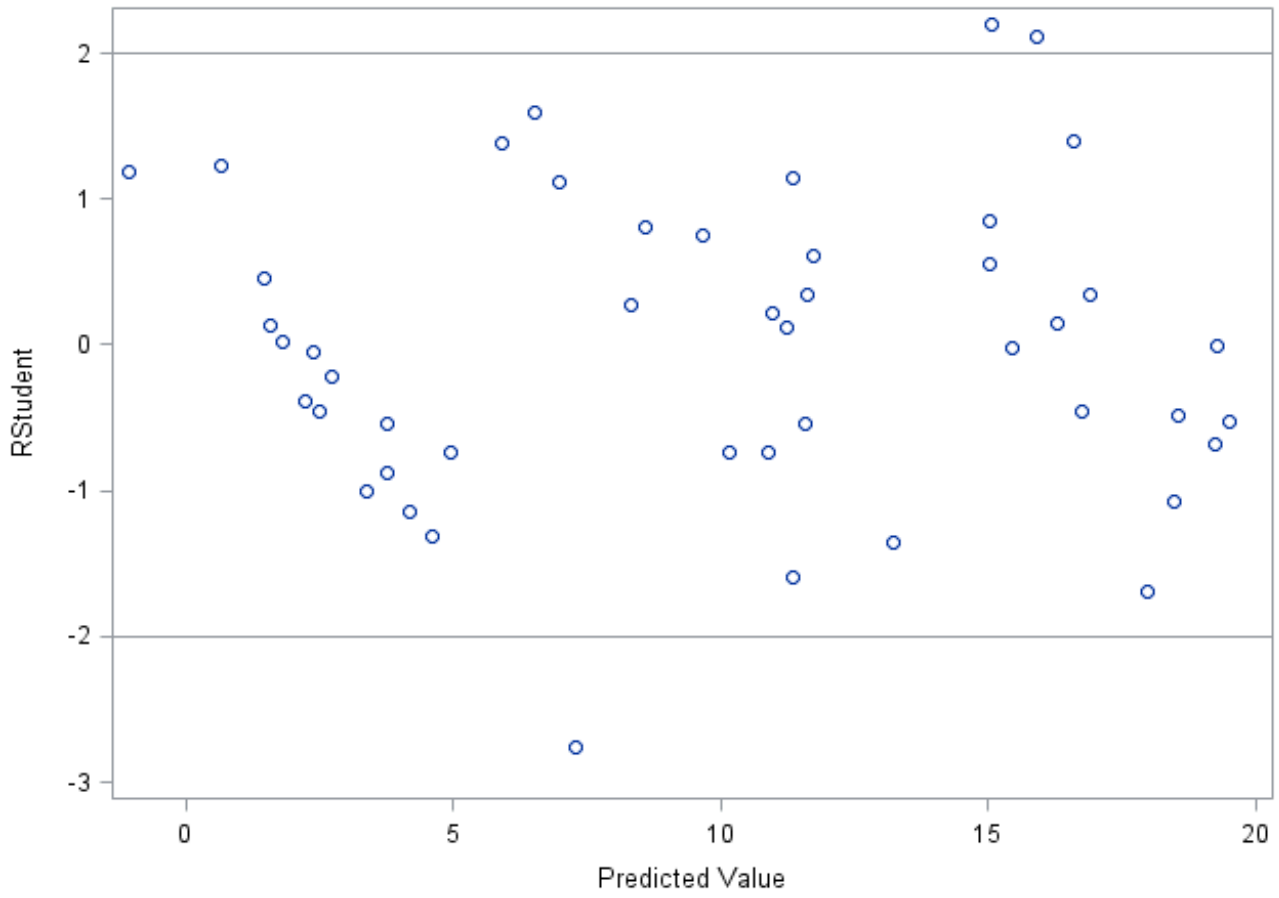

Figure 5.13. Studentized Residual versus Predicted Value for Dilatancy Angle

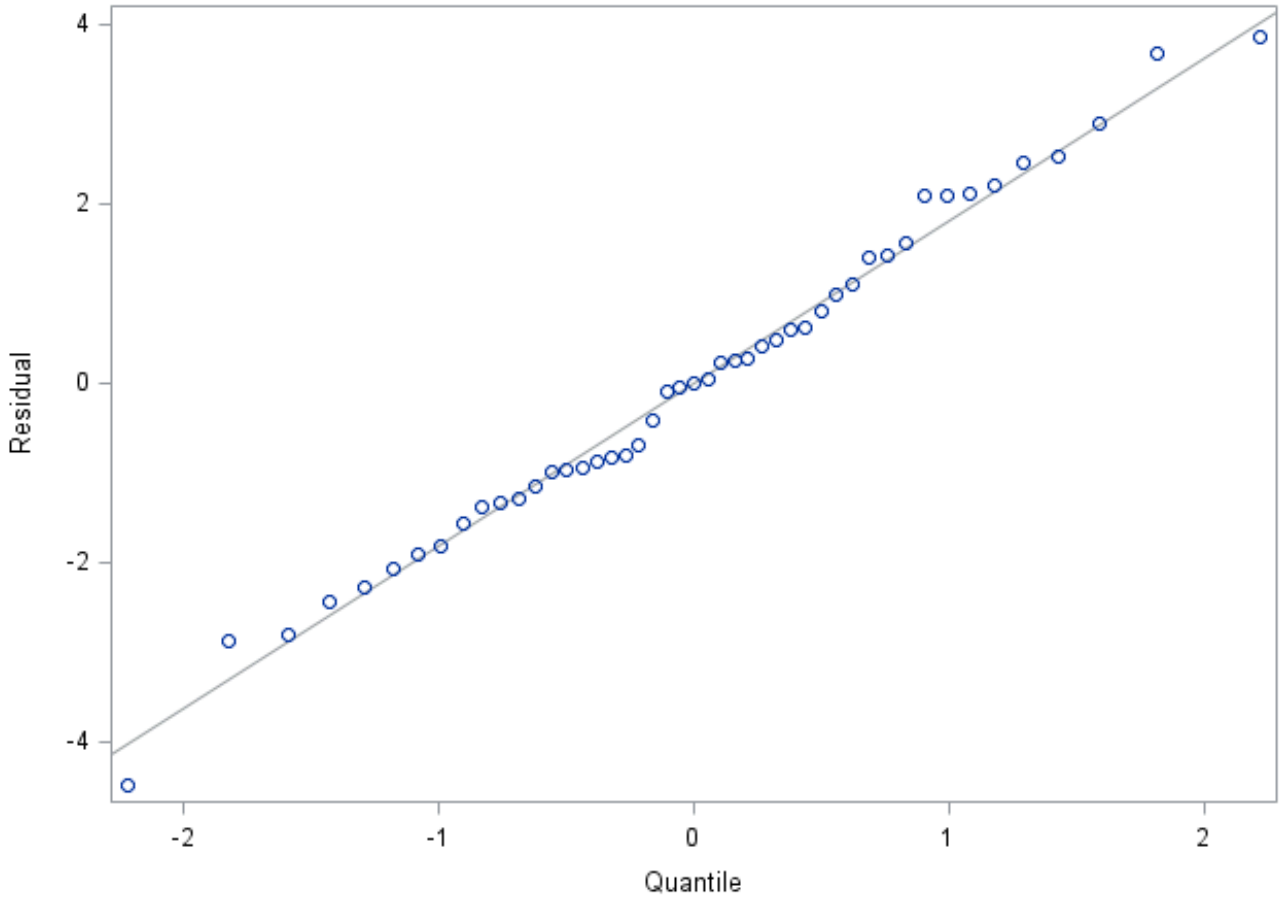

Figure 5.14. Quartile-Quartile Plot for Dilatancy Angle

Sphericity (β=0.246) was the second-most influential variable to dilatancy. With an increased sphericity index, dilatancy angle was increased. Thus, as a particle becomes less spherical, the sand's tendency to dilate increases. A less spherical particle may have contributed to more particle rearrangement, therefore increasing dilatancy.

The third-most significant variable is the particle's surface texture (β=0.233), which has a positive relationship with the dilatancy angle. As a particle's surface becomes rougher, more expansion is exhibited. However, at particle contact points, a smoother particle may tend to roll over another particle but then slip, such as in the glass beads' stick-slip phenomenon.

Lastly, normal stress (β=-0.028) was included to determine its influence in the model. Normal stress demonstrated an inverse relationship with dilatancy angle, indicating that as the specimen's normal stress increased, the dilatancy angle decreased, hence suppressing specimen expansion. A specimen at lower normal stress increased the dilatancy angle.

The model's predicted values were compared to experimental values shown in Figure 5.15 to determine the model's reliability. The values indicated that the model produced reliable predictions since the values lay close to the 1:1 line. The coefficient of determination was found to be 0.919 while adj. R^2 was 0.912. Therefore, through this linear combination of variables, the model explains 91.2% of the dilatancy angle's variability. The model displayed an excellent correlation to the experimental values. The 95% prediction interval is shown in Figure 5.16, estimating where 95% of future observations will fall.

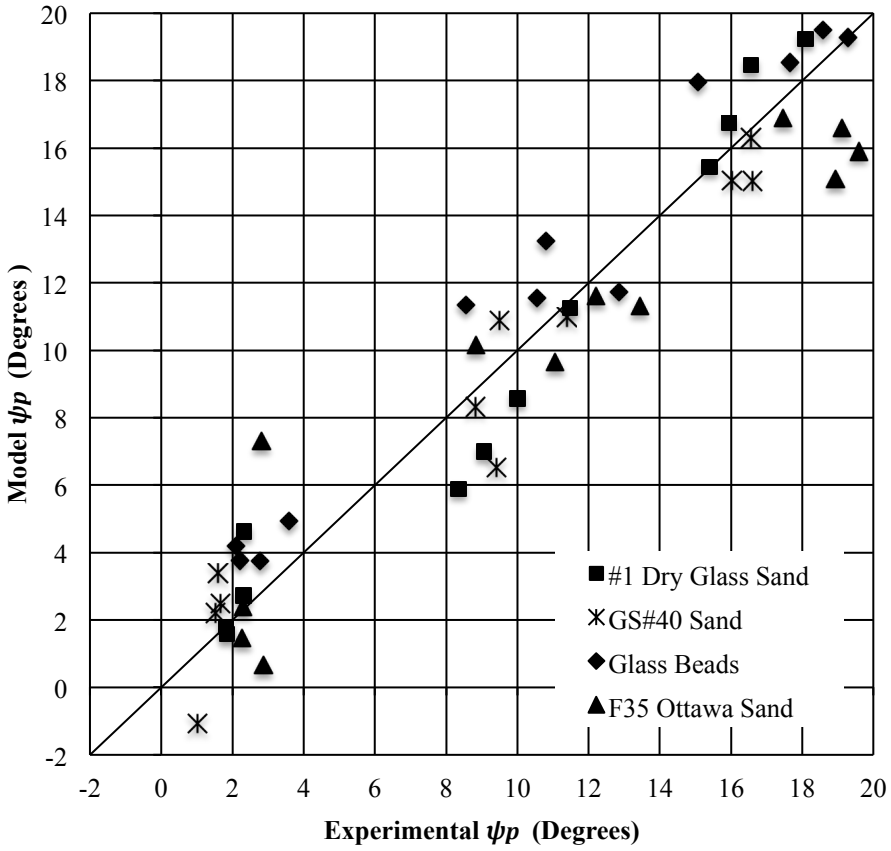

Figure 5.15. Model versus Experimental for Dilatancy Angle

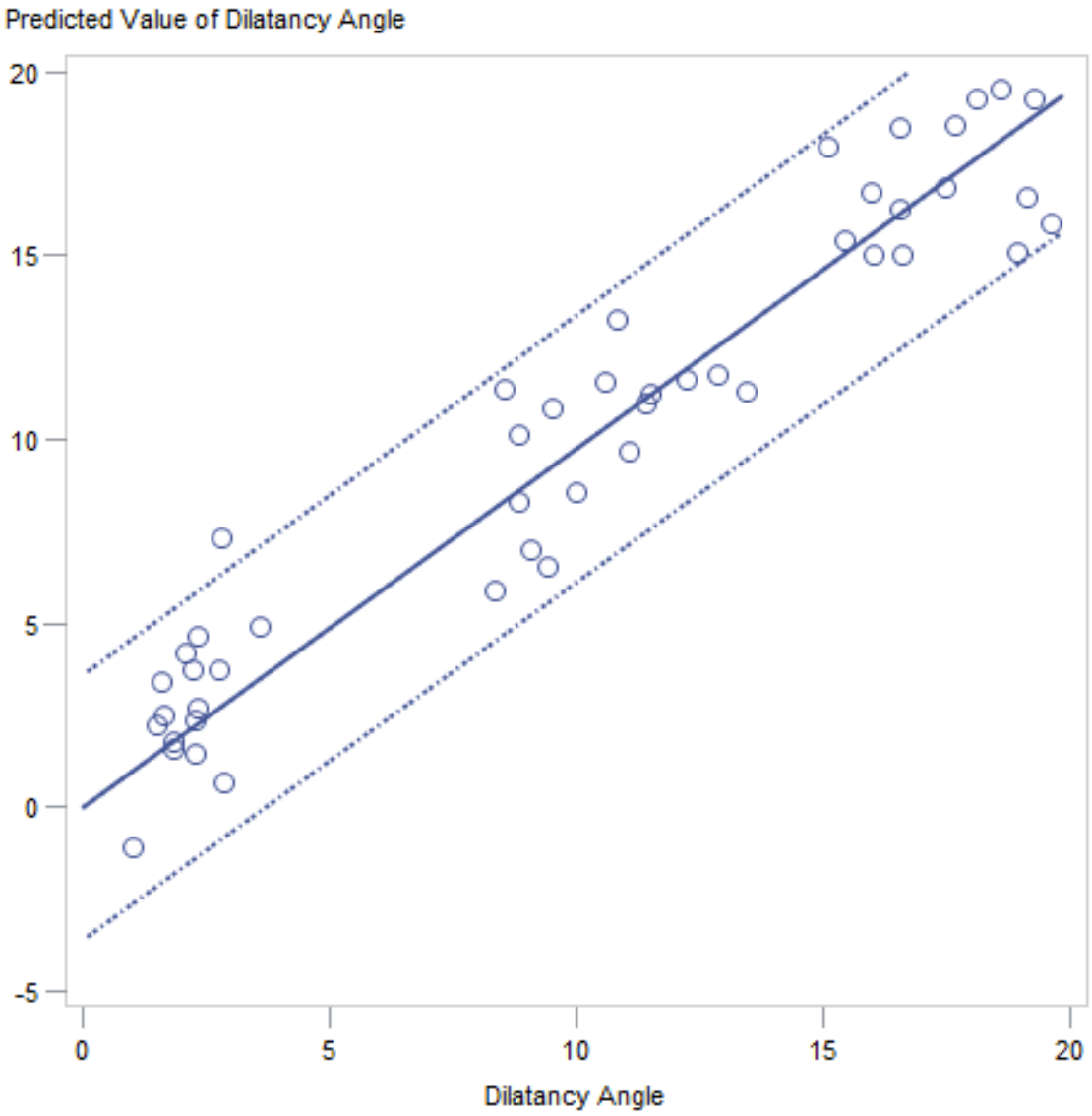

Figure 5.16. Model versus Experimental Measurements with a 95% Prediction Interval for Dilatancy Angle

CHAPTER 6

CONCLUSIONS AND RECOMMENDATIONS

6.1 Conclusions

This thesis investigated the effect of sphericity, roundness, and surface texture, as well as normal stress and relative density, on uniform sands' friction and dilatancy. Direct shear experiments on glass beads and three types of silica sands with different particle morphologies and the same gradation was conducted at four different normal stresses to investigate particle morphology's impact on granular materials' shear strength. Moreover, particle morphology indices from 3D images reported by Alshibli et al. (2014) provided a valuable source for random sampling, and particle morphology significantly influenced granular material's shear strength. Stepwise regression along with the evaluation of peak friction angle, critical state friction angle, and dilatancy angle models were conducted using the SAS Enterprise Guide. Based on the experimental work, morphology indices from literature, and statistical analyses, the following conclusions are drawn:

- The effect of normal stress and relative density on the shear response of the silica sands and glass beads was demonstrated using direct shear. An increase in normal stress decreased or suppressed the sands' peak friction and dilatancy angles. The models developed for peak friction and dilatancy angles confirmed this relationship by displaying a negative parameter estimate for normal stress. Therefore, low normal stresses increase both peak friction and dilatancy angles.
- Relative density considerably influenced the sands' peak friction angles and dilatancy angles. As relative density increased, peak friction and dilatancy angles increased; therefore, the positive parameter estimate for relative density was displayed. This finding agrees with

previous research since densely packed particles tend to dilate when they are sheared whereas loosely packed particles typically contract. Based on statistical analyses, relative density was determined to be the most influential explanatory variable for dilatancy angle and the second-most influential variable for peak friction angle when evaluating the standardized regression estimates.

- Particle morphology influenced the sands' shear strength parameters with at least two morphology parameters included in each model. More specifically, sphericity and surface texture are included in all three of the developed linear regression models.
- Sphericity influenced the critical state friction, peak friction, and dilatancy angles. Sphericity played a critical role in the peak and critical state friction angle linear regression models by being the most significant variable based on standardized regression estimates. Moreover, sphericity was the second-most significant variable for the dilatancy angle model. Each model demonstrated that as particles become less spherical, the peak, critical state friction, and dilatancy angles increased. Therefore, sphericity is considered the most significant particle morphology parameter of granular materials' shear strength.
- Roundness did not prove to be as influential to the models when compared to the particles' sphericity and surface texture. No significant effect (0.15 level) on critical state friction angle and dilatancy angle was observed by SAS; therefore, roundness was excluded from the models. On the other hand, roundness affected the sands' peak friction angle; however, it was not as significant as sphericity or surface texture based on the standardized regression estimates. As roundness increased, peak friction angle decreased, indicating that a particle with sharp edges increase peak friction angle. The range of roundness tested was

considerably less than the range of sphericity and surface texture; therefore, testing more sands with a wider range of roundness indices would be valuable.

- Surface texture's effect was significant to all models. The critical state friction angle linear regression model showed that surface texture was the second-most influential variable. Moreover, peak friction angle and dilatancy angle models demonstrated that surface texture was the third-most influential variable. Thus, as the particle's surface roughness increases, peak and critical state friction angles as well as dilatancy angles are expected to increase.
- The critical state friction angle resulted in an Adjusted R^2 of 0.936 while peak friction angle and dilatancy angle resulted in an Adjusted R^2 of 0.743 and 0.912, respectively. The linear regression for critical state friction angle explained more variability based on its linear combination of variables and the suggested intercept of 22°. The intercept value was investigated to account for silica sands' true friction and provided a good fit in the model.
- Random sampling with one standard deviation from Alshibli et al.'s (2014) indices sufficiently captured particle morphology's influence. The SAS Enterprise Guide software with its capabilities of stepwise regression and model evaluation was a useful tool in this study. Ultimately, model evaluation based on the analysis of variance, variance of inflation, and residuals proved that no collinearity issues existed and that all assumptions for the linear regression were met. Friction and dilatancy angles for the model correlated well with experimental measurements, and the prediction interval was developed.

This study investigated multiple explanatory variables that predicted granular materials' friction and dilatancy. The models incorporated multiple variables; therefore, the most influential parameters were identified. The linear regression models accurately predict friction and dilatancy angles from the experiments conducted. Understanding particle morphology and its relationship

to shear strength parameters has the potential to enhance the development of advanced constitutive models describing granular materials' behavior.

6.2 Recommendations

Experimental work and particle morphology indices from Alshibli et al. (2014) provided well-correlated models to predict experimental values for friction and dilatancy angles. This thesis builds on previous research regarding particle morphology's influence by investigating multiple explanatory variables' effects as an alternative to merely studying roundness or surface texture. Encompassing more than one parameter provides a more accurate model. Thus, the results lead to the following recommendations for future research:

- Evaluate a wider range of granular materials with a larger variance of particle morphology indices, especially the parameter roundness.
- Test with more sphericity values less than unity to model kidney-shaped particles.
- Investigate other morphology indices based on 2D and 3D imaging.
- Perform experiments using another type of test, such as the triaxial test.
- Increase the number of observations for more robust shear strength models.
- Investigate how particle morphology changes after shearing.

REFERENCES

Al-Shibli, K., Macari, E., and Sture, S. (1996). "Digital Imaging Techniques for the Assessment of Homogeneity of Granular Materials." *Journal of the Transportation Research Board*, DOI: 10.3141/1526-15, 121-128.

Alshibli, K. A., and Alsaleh, M. (2004). "Characterizing surface roughness and shape of sands using digital microscopy." *Journal of Computing in Civil Engineering,* 10.1061/(ASCE) 0887-3801(2004) 18:1(36), 36-45.

Alshibli, K., Druckrey, A., Al-Raoush, R., Weiskittel, T., and Lavrik, N. (2014). "Quantifying morphology of sands using 3D imaging." *Journal of Materials in Civil Engineering*, DOI: 10.1061/(ASCE) MT.1943-5533.0001246, 04014275.

Alshibli, K. A. and Roussel, L. (2006). "Experimental investigation of slip-stick behavior in granular materials." *International Journal for Numerical and Analytical Methods in Geomechanics*, 30(4), 1391-1407, DOI: http://dx.doi.org/10.1002/nag.517.

Altun, S., Sezer, A., and Goktepe, B. A. (2011). "Relationships between shape characteristics and shear strength of sands." *Japanese Geotechnical Society*, 51(5), 857-871.

Anastas, J. W. (1999). "Research Design for Social Work and the Human Services." *Methods of Data Analysis and Dissemination*, Columbia University Press, New York, 464.

ASTM D3080/D3080M-11. Standard Test Method for Direct Shear Test of Soils Under Consolidated Drained Conditions. American Society for Testing and Materials International, Vol. 4.08. 2011.

ASTM D4253. Standard Test Methods for Maximum Index Density and Unit Weight of Soils using a Vibratory Table. American Society for Testing and Materials International, Vol. 4.08. 2016.

Bolton, M. D. (1986). "Strength and dilatancy of sands." *Geotechnique*, 36(1), 65-78.

Bowman, E.T., Soga, K., and Drummond, T. W., (2000). "Particle Shape Characterization using Fourier Analysis." CUED/D-Soils/TR315.

Budhu, M. (2011). "Soil Mechanics and Foundations." *Soils Investigation and Shear Strength of Soils,* John Wiley & Sons, Inc., Hoboken, NJ, 45, 261-264, 270-272, 280-286.

Cai, Y. Q., Wang, J., Liu, F. Y. and Wang, P. (2016). "Particle size effects on coarse soil-geogrid interface response in cyclic and post-cyclic direct shear tests." *Geotextiles and Geomembranes*, 44(1), 854-861.

Chakraborty, T., and Salgado, R. (2010). "Dilatancy and Shear Strength of Sand at Low Confining Pressures." *Journal of Geotechnical and Geoenvironmental Engineering*, 10.1061/(ASCE) GT.1943-5606.0000237, 136(3), 527-532.

Coduto, D. P. (2001). "Foundation Design Principles and Practice." *Laboratory Shear Strength Tests: Direct Shear Test*, Prentice-Hall, Inc., Upper Saddle River, NJ, 82-83, 91-92.

Cox, M. R. (2008). "The Influence of Grain Shape on Dilatancy." Doctoral dissertation, The University of Arizona, Tucson, AZ.

Dodds, J. S. (2004). "Particle Shape and Stiffness." M.S. thesis, Georgia Institute of Technology, Atlanta, GA.

Duttine, A. and Tatsuoka, F. (2009). "Viscous Properties of Granular Materials Having Different Particle Shapes in Direct Shear." *Japanese Geotechnical Society*, 49(5), 777-796.

Edil, T. B., and Benson, C. H. (2007). "Determination of Shear Strength Values for Granular Backfill Material Used by the Wisconsin Department of Transportation." Report submitted to Wisconsin Department of Transportation (WIDOT), Madison, WI, Report No. WHRP 07-09. Available: http://wisdotresearch.wi.gov/wp-content/uploads/05-08shearstrengthvalues1.pdf.

Fern, J., Robert, D. J., and Soga, K. (2015). "Shear strength and dilatancy of partially saturated sand in direct shear tests." *Proceedings International Symposium on Geomechanics from Micro to Macro*, Cambridge, UK, 1391-1396.

Fonseca, J., O'Sullivan C., Coop, M. R., and Lee, P. D. (2012). "Non-invasive characterization of particle morphology of natural sands." *Soils and Found*ations, 52(4), 712-722.

Hasan, A., and Alshibli, K. A. (2010). "Discrete Element Modeling of Strength Properties of Johnson Space Center (JSC-1A) Lunar Regolith Simulant." *Journal of Aerospace Engineering*, 23(3), 157-165.

Hassen, G., Yavari, N., Tang, A. M., and Pereira, J. (2016). "Effect of temperature on the shear strength of soils and the soil-structure interface." *Canadian Geotechnical Journal*, 53(1), 1186-1194.

Hyslip, J. P., and Vallejo, L. E. (1997). "Fractal analysis of the roughness and size distribution of granular materials." *Engineering Geology*, 48(3-4), 231-244.

Jewell, R. R. and Wroth, C. P. (1987). "Direct shear tests on reinforced sand." *Geotechnique* 37(1), 53-68.

Krumbein, W. C., and Sloss, L. L. (1963). "Stratigraphy and Sedimentation*." Characterization of Sphericity and Roundness*, W. H. Freenman and Company, San Francisco, CA, 660.

Krumbein, W. C. (1941). "Measurement and geological significance of shape and roundness of sedimentary particles." *Journal of Sedimentary Petrology*, 11(2), 64-72.

Lambe, T. W., and Whitman, R. V. (1969). "Soil Mechanics." *Tests to Measure Stress-Strain Properties,* John and Wiley & Sons, Inc., New York, NY, 62-66, 119-121.

Lee, Y. G., Lee, J. H. and Hsueh, Y. C. (1998). "Texture classification using fuzzy uncertainty texture spectrum." *Neurocomputing*, 20(1-3), 115-122.

Longnecker, M and Ott, L. R. (2010). "An Introduction to Statistical Methods and Data Analysis." *Linear Regression and Correlation*, Brooks/Cole, Belmont, CA, 265, 572-610, 618.

Masad, E., Olcott, D., White, T., and Tashman, L. (2001). "Correlation of fine aggregate imaging shape indices with asphalt mixture performance." *Transportation Research Record 1757*, Transportation Research Board, Washington, DC, 148-156.

Mikasa, M. (1960). "New direct shear test apparatus." *Proceedings 15th Annual Convention Japanese Society of Civil Engineers, Tokyo,* 45-48.

Mitachi, T., Shibuya, S., and Tamate, S. (1997). "Interpretation of direct shear box testing of sands as quasi-simple shear." *Geotechnique*, 47(4), 769-790.

Montgomery, D. C. and Runger, G. C. (2011). "Applied Statistics and Probability for Engineers" *Aspects of Multiple Regression Modeling*, John Wiley & Sons, Inc., Hoboken, NJ, 499.

Reynolds, O. (1885). "On the dilatancy of media composed of rigid particles in contact." *Journal of Science*, 20(5), 469-485.

Rowe, P. W. (1962), "The stress-dilatancy relation for static equilibrium of an assembly of particles in contact." *Department of Engineering*, University of Manchester, 500-526.

Santamarina, J. C., and Cho, G. C. (2001). "Determination of critical state parameters in sandy soils – simple procedure." *ASTM Geotechnical Testing Journal*, 24(2), 185-192.

Skempton, A. W. and Bishop, A. W. (1950). "The measurement of the shear strength of soils." *Geotechnique*, 2, 188-192.

Siang, A., Wijeyesekera, D., and Zainorabidin, A. (2013). "The Effect of Particle Morphology of Sand on the Relationship Between Shear Strength and Dilatancy." *Electronic Journal of Geotechnical Engineering*, 18, 1537-1546.

Stevens, J. P. (1984). "Outliers and Influential Data Points in Regression Analysis." *Psychological Bulletin*, 95(2), 334-344.

Takada, N. (1993). "Mikasa's direct shear apparatus, testing procedures and results." *Journal of Geotechnical Testing*, 16(3), 314-322.

Wadell, H. (1932). “Volume shape and roundness of rock particles.” *The Journal of Geology*, 40(5), 443-451.

APPENDIX

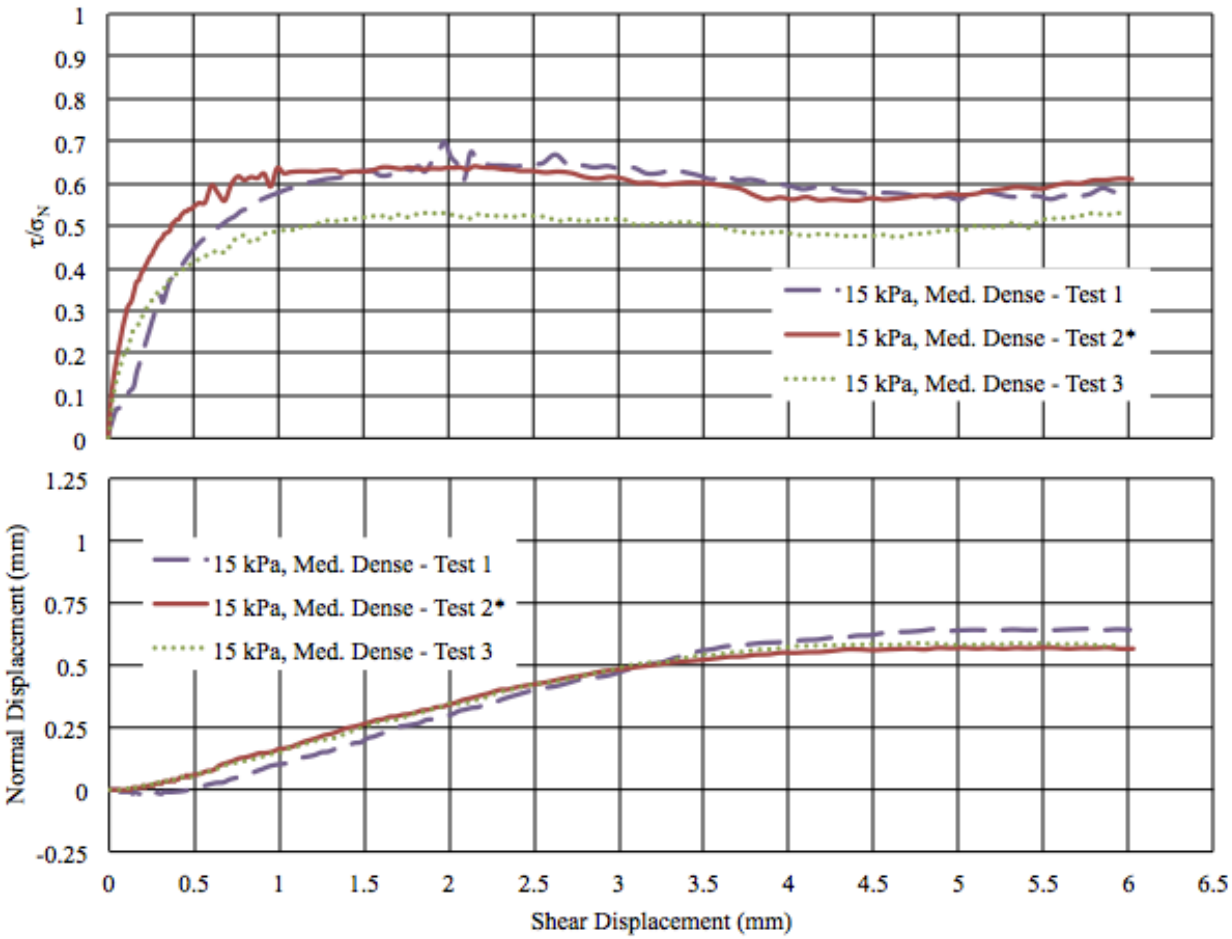

Note: * indicates the test used for statistical modeling.

Normalized Shear Stress and Normal Displacement versus Shear Displacement for #1 Dry Glass Sand, 15 kPa, Medium-Dense Specimens

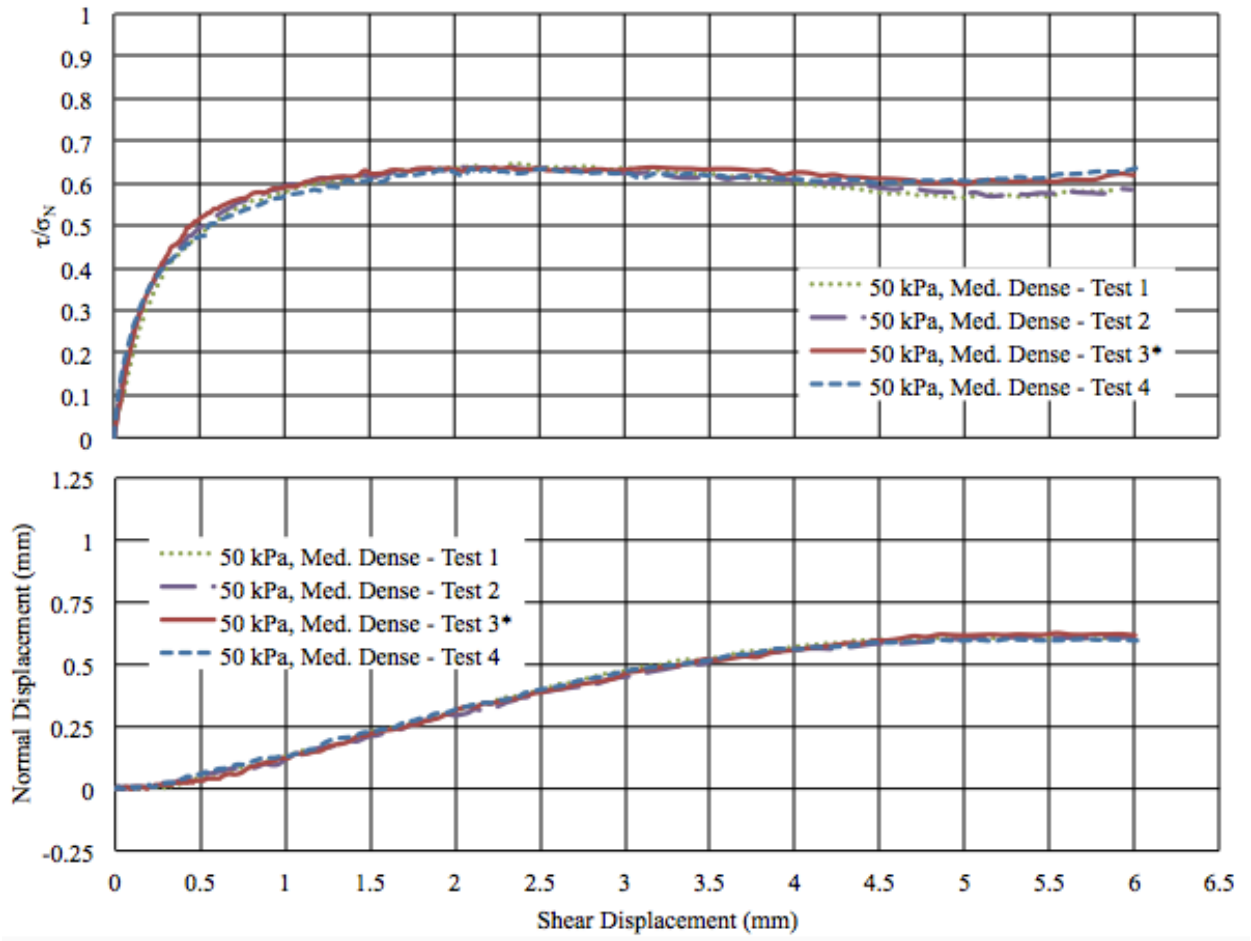

Note: * indicates the test used for statistical modeling.

Normalized Shear Stress and Normal Displacement versus Shear Displacement for #1 Dry Glass Sand, 50 kPa, Medium-Dense Specimens

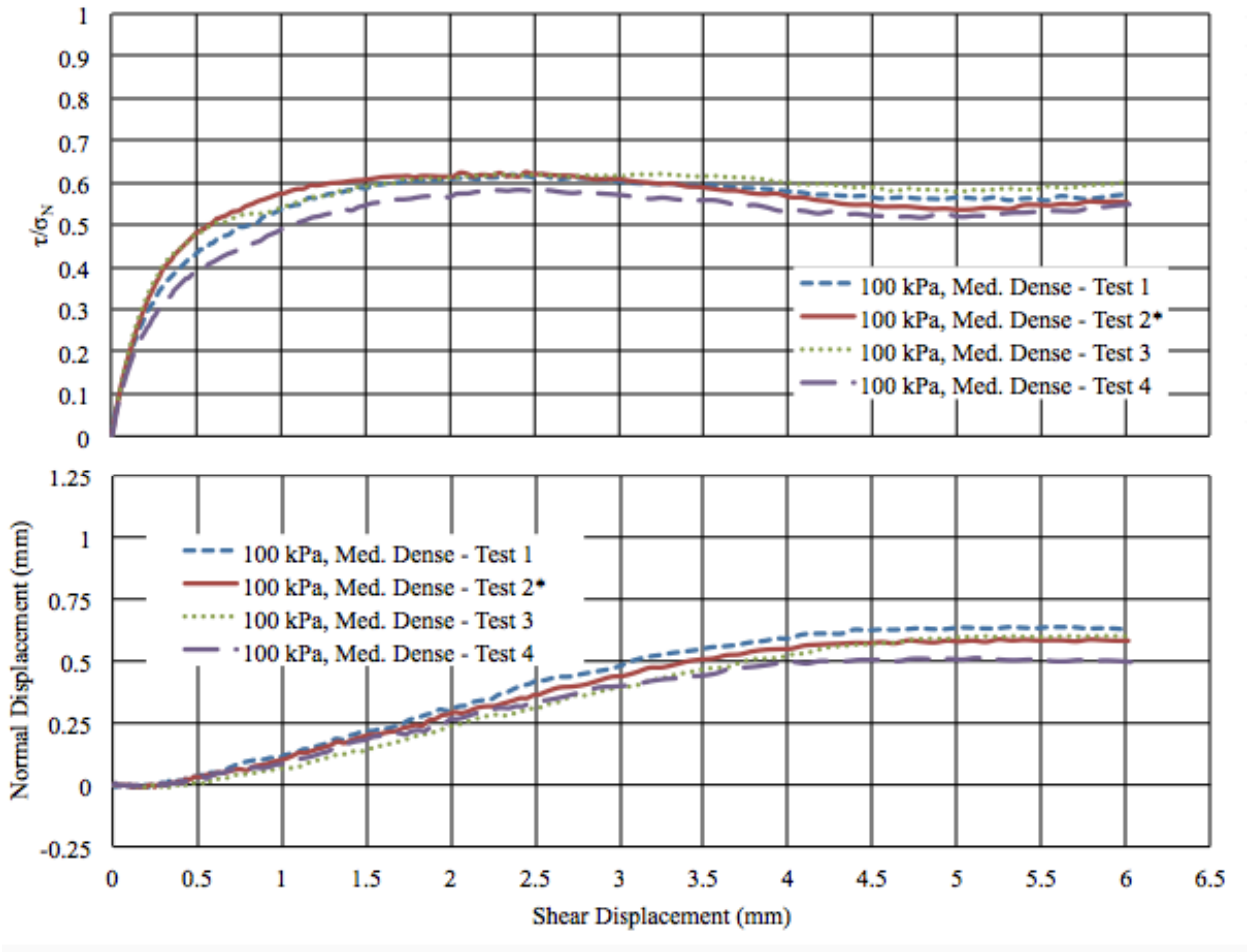

Note: * indicates the test used for statistical modeling.

Normalized Shear Stress and Normal Displacement versus Shear Displacement for #1 Dry Glass Sand, 100 kPa, Medium-Dense Specimens

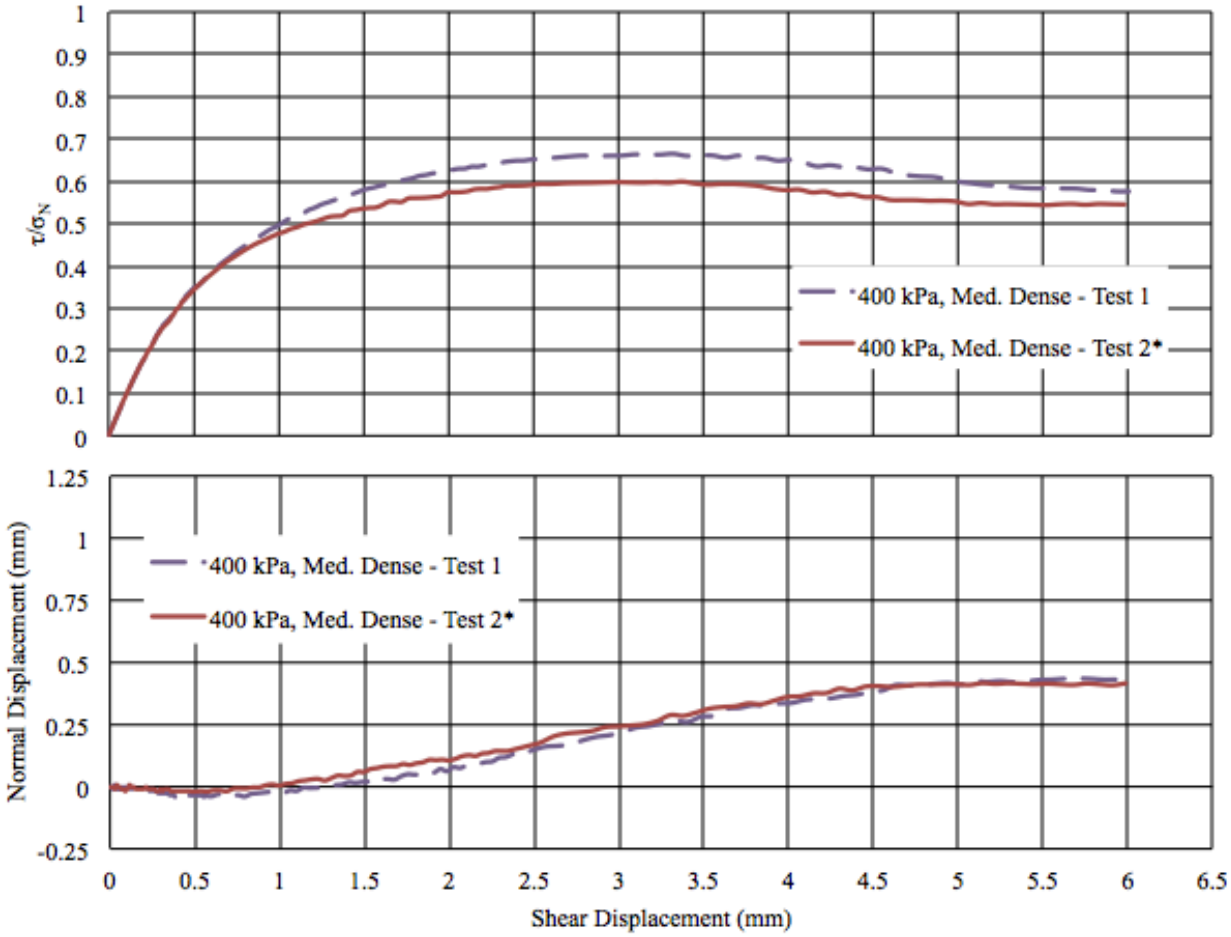

Note: * indicates the test used for statistical modeling.

Normalized Shear Stress and Normal Displacement versus Shear Displacement for #1 Dry Glass Sand, 400 kPa, Medium-Dense Specimens

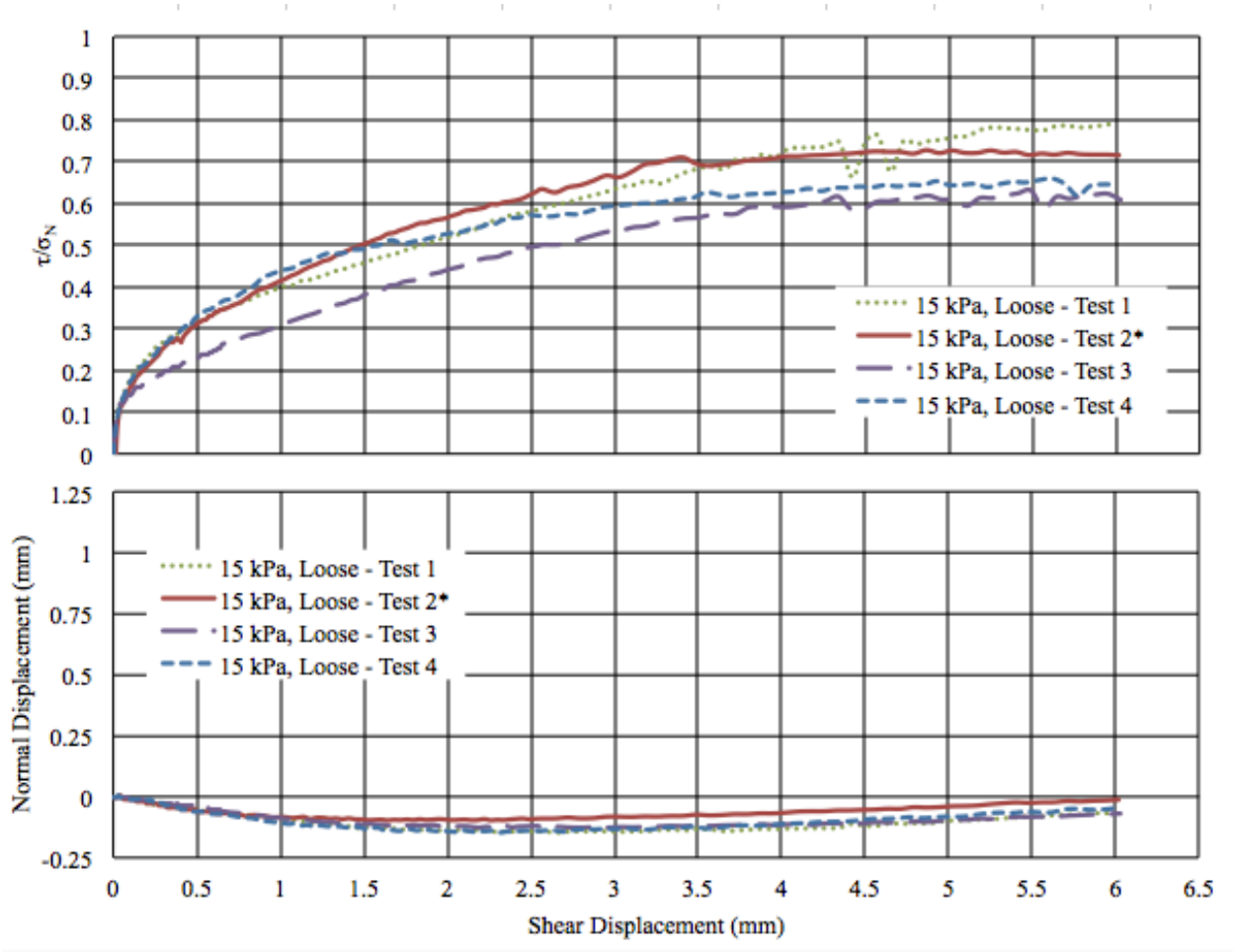

Note: * indicates the test used for statistical modeling.

Normalized Shear Stress and Normal Displacement versus Shear Displacement for #1 Dry Glass Sand, 15 kPa, Loose Specimens

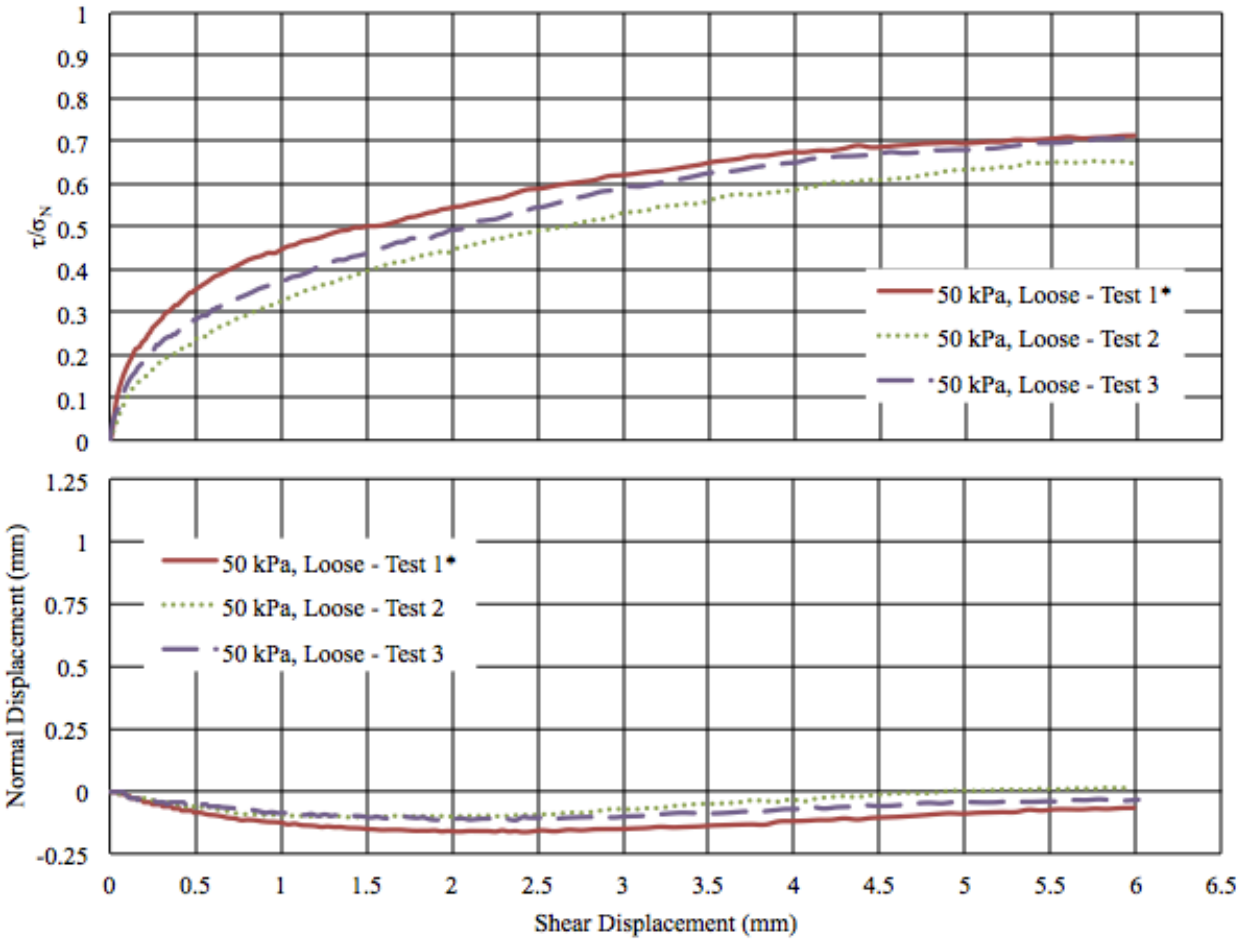

Note: * indicates the test used for statistical modeling.

Normalized Shear Stress and Normal Displacement versus Shear Displacement for #1 Dry Glass Sand, 50 kPa, Loose Specimens

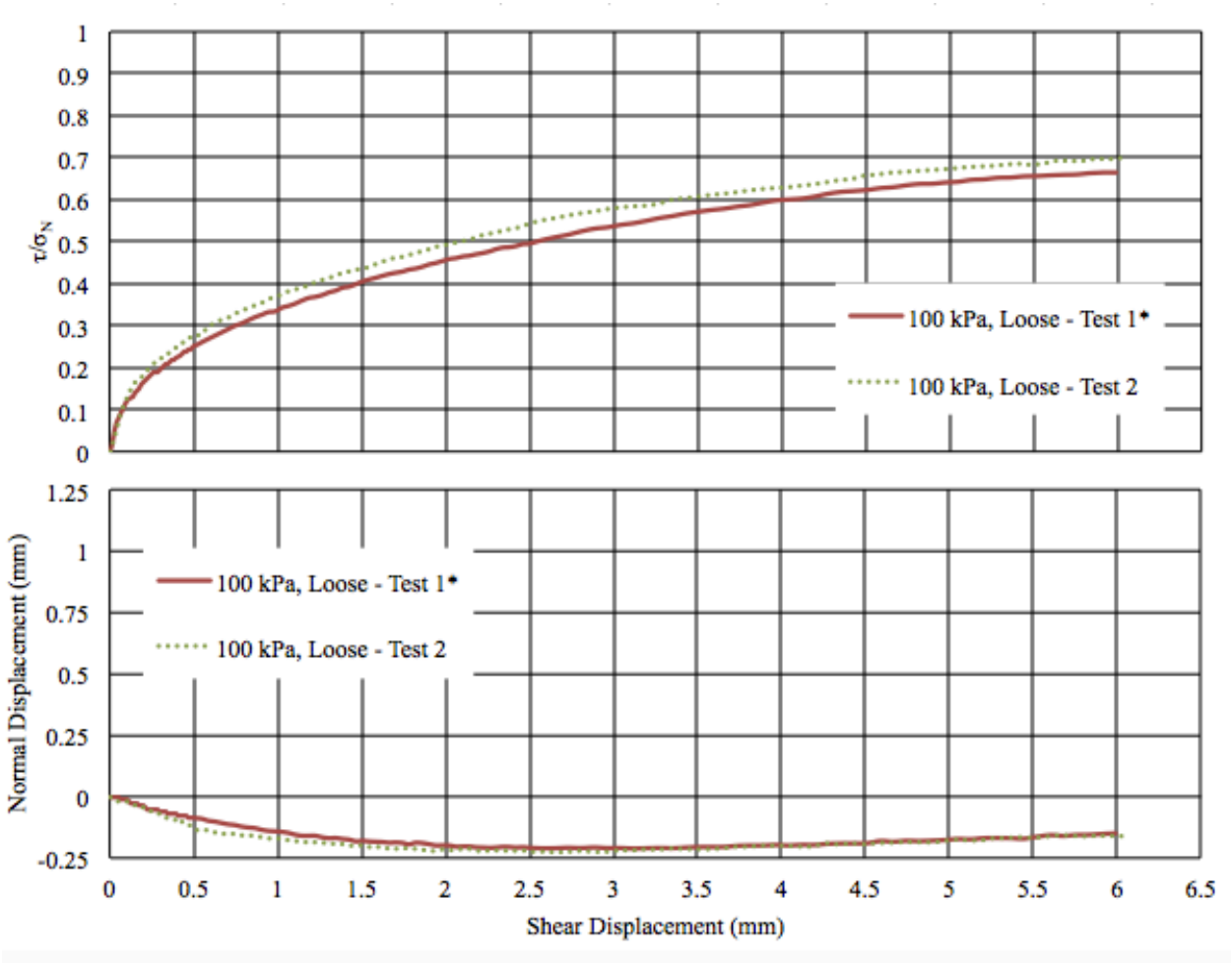

Note: * indicates the test used for statistical modeling.

Normalized Shear Stress and Normal Displacement versus Shear Displacement for #1 Dry Glass Sand, 100 kPa, Loose Specimens

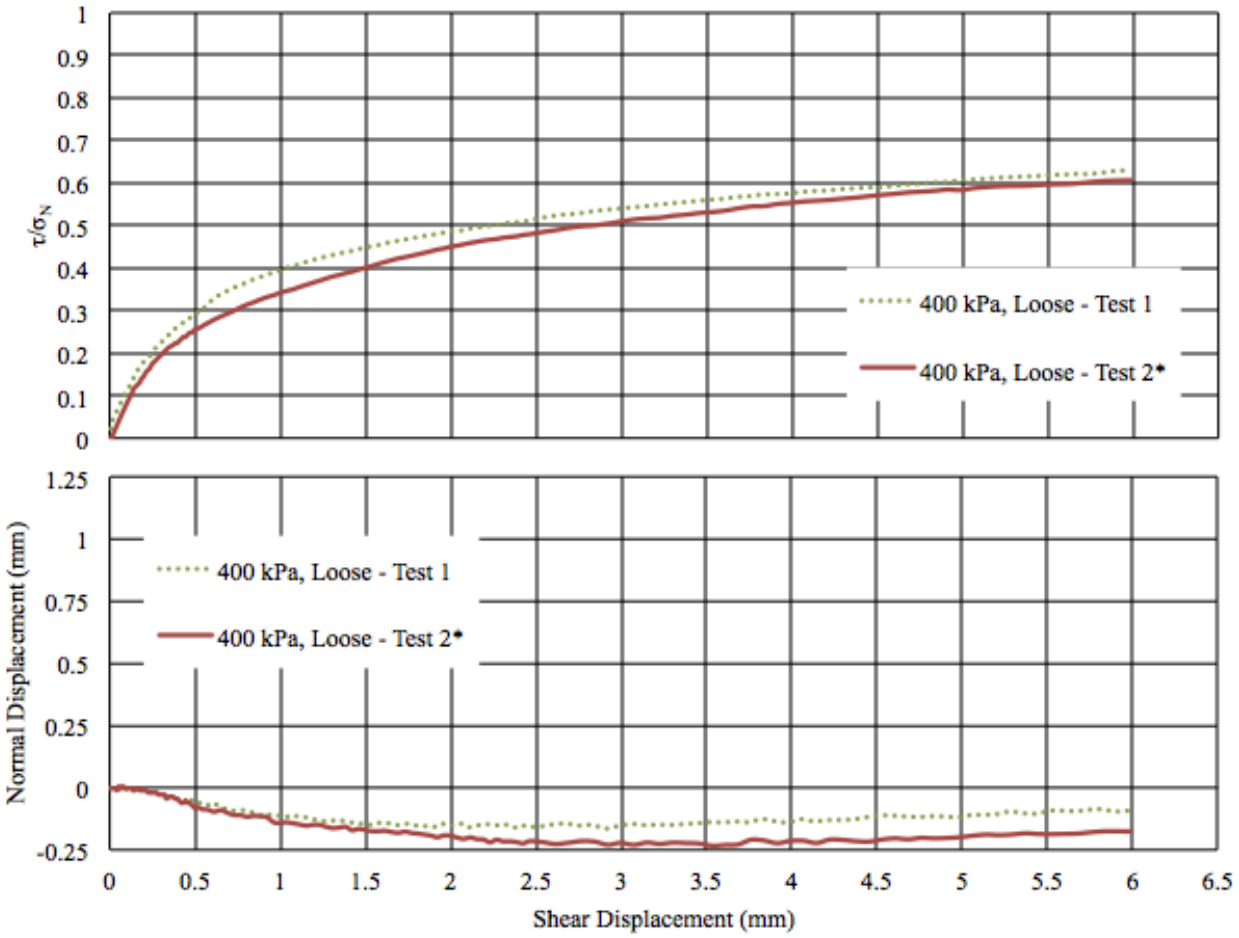

Note: * indicates the test used for statistical modeling.

Normalized Shear Stress and Normal Displacement versus Shear Displacement for #1 Dry Glass Sand, 400 kPa, Loose Specimens

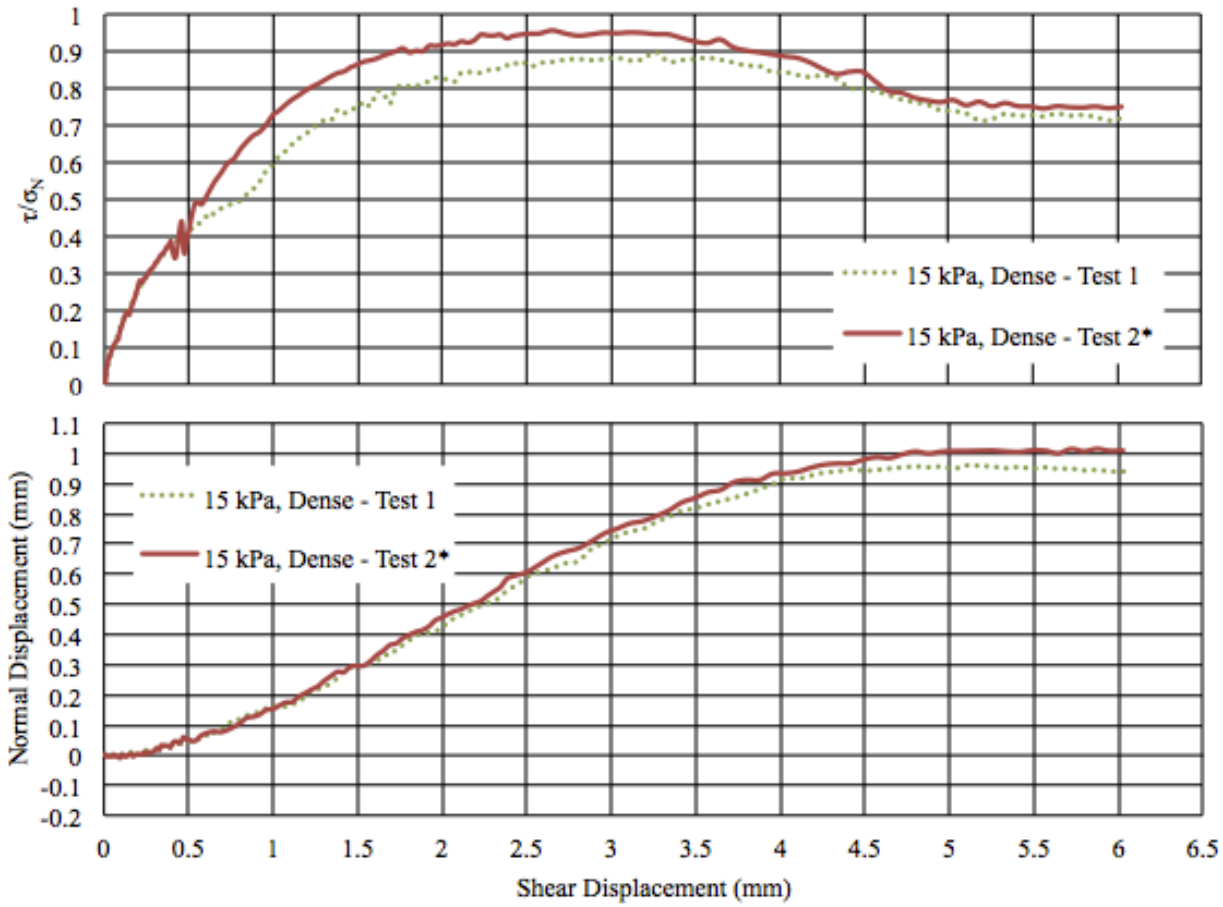

Note: * indicates the test used for statistical modeling.

Normalized Shear Stress and Normal Displacement versus Shear Displacement for GS#40 Columbia Sand, 15 kPa, Dense Specimens

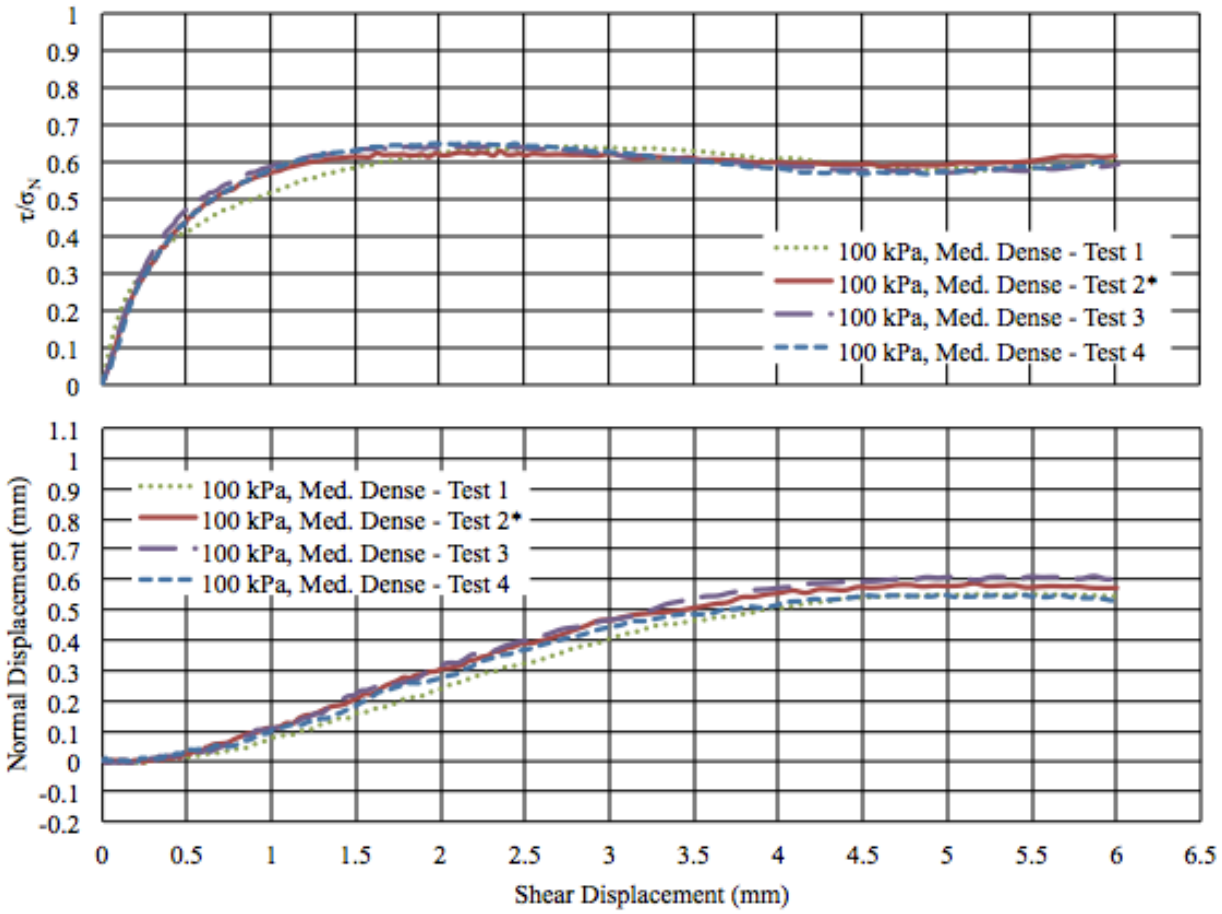

Note: * indicates the test used for statistical modeling.

Normalized Shear Stress and Normal Displacement versus Shear Displacement for GS#40 Columbia Sand, 100 kPa, Medium-Dense Specimens

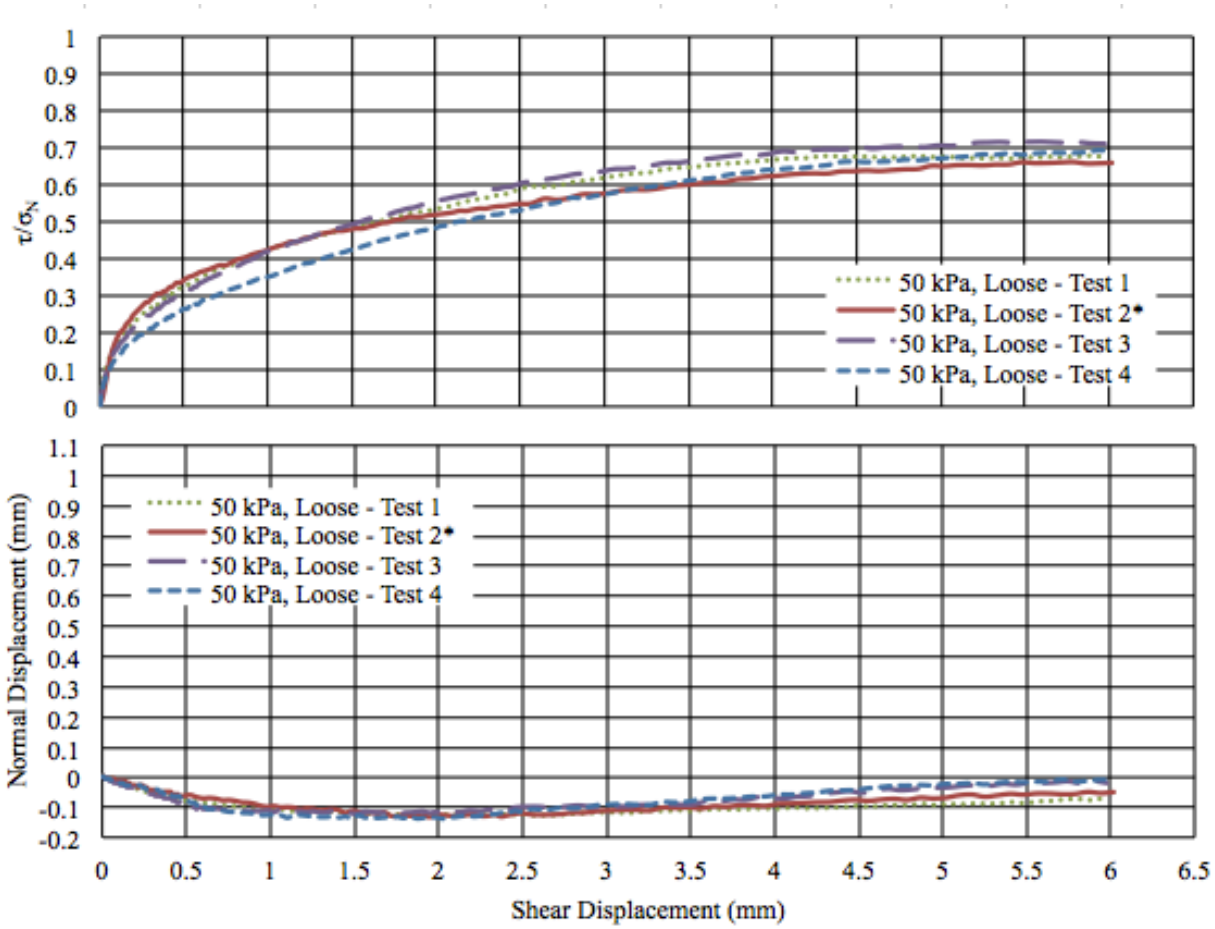

Note: * indicates the test used for statistical modeling.

Normalized Shear Stress and Normal Displacement versus Shear Displacement for GS#40 Columbia Sand, 50 kPa, Loose Specimens

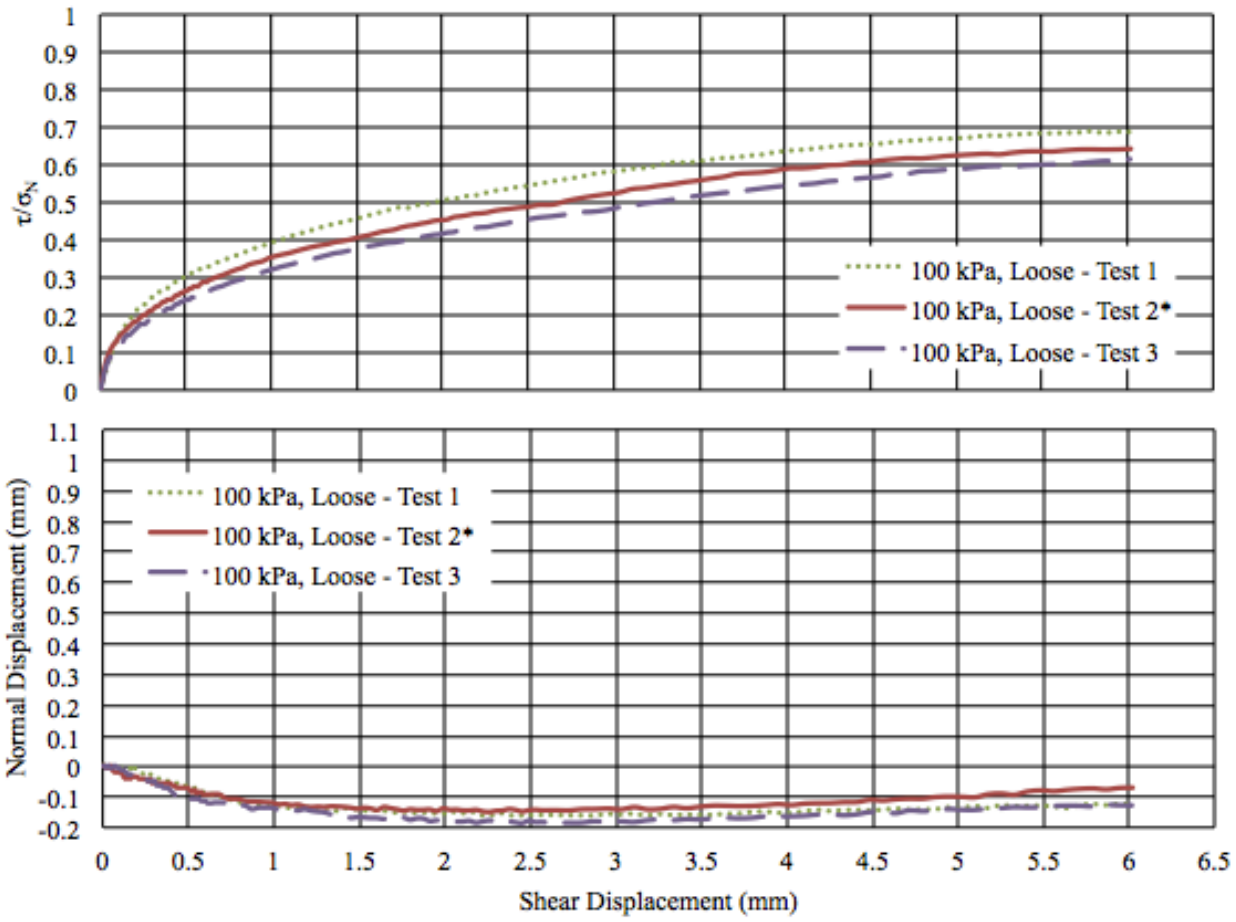

Note: * indicates the test used for statistical modeling.

Normalized Shear Stress and Normal Displacement versus Shear Displacement for GS#40 Columbia Sand, 100 kPa, Loose Specimens

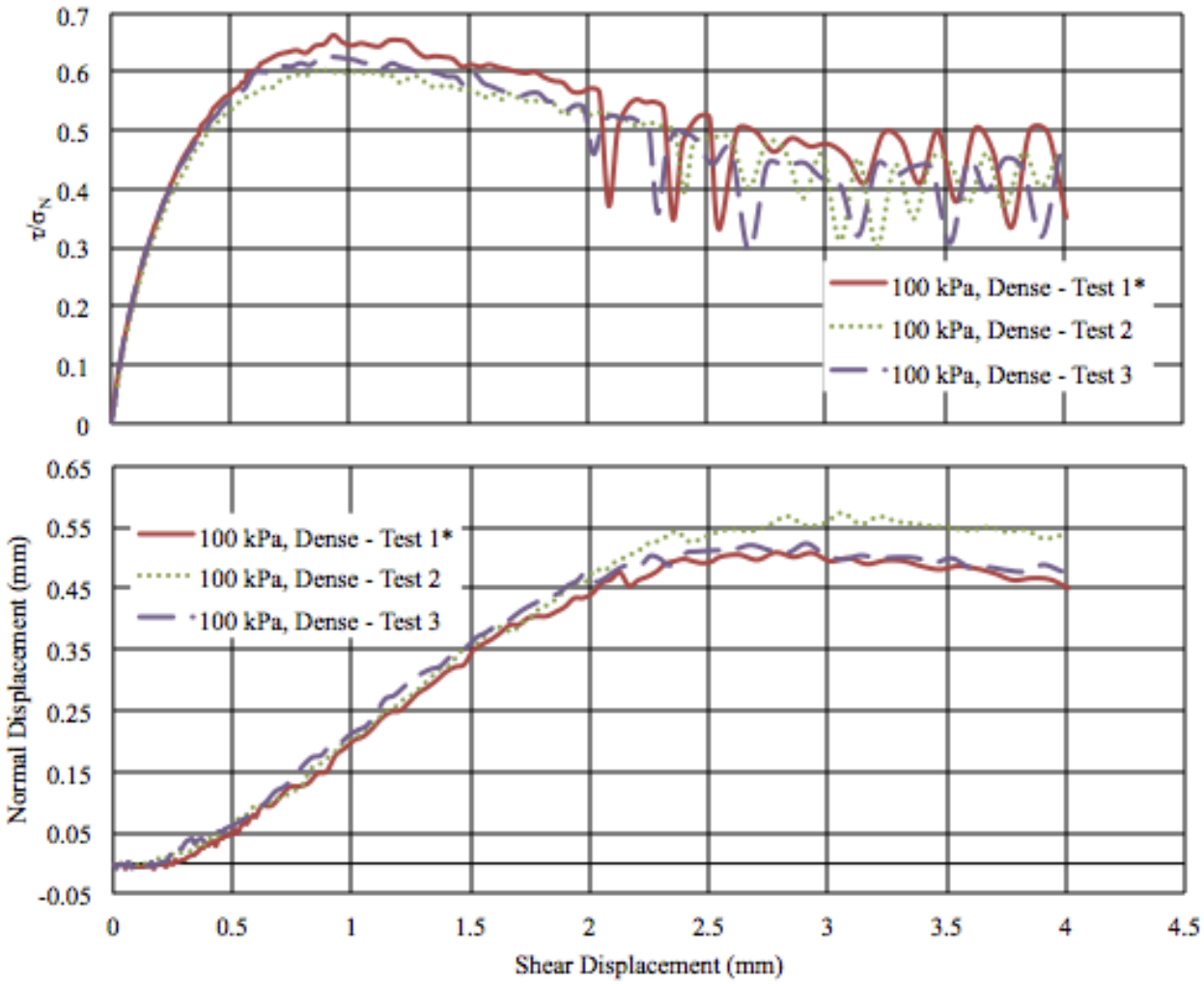

Note: * indicates the test used for statistical modeling.

Normalized Shear Stress and Normal Displacement versus Shear Displacement for Glass Beads, 100 kPa, Dense Specimens

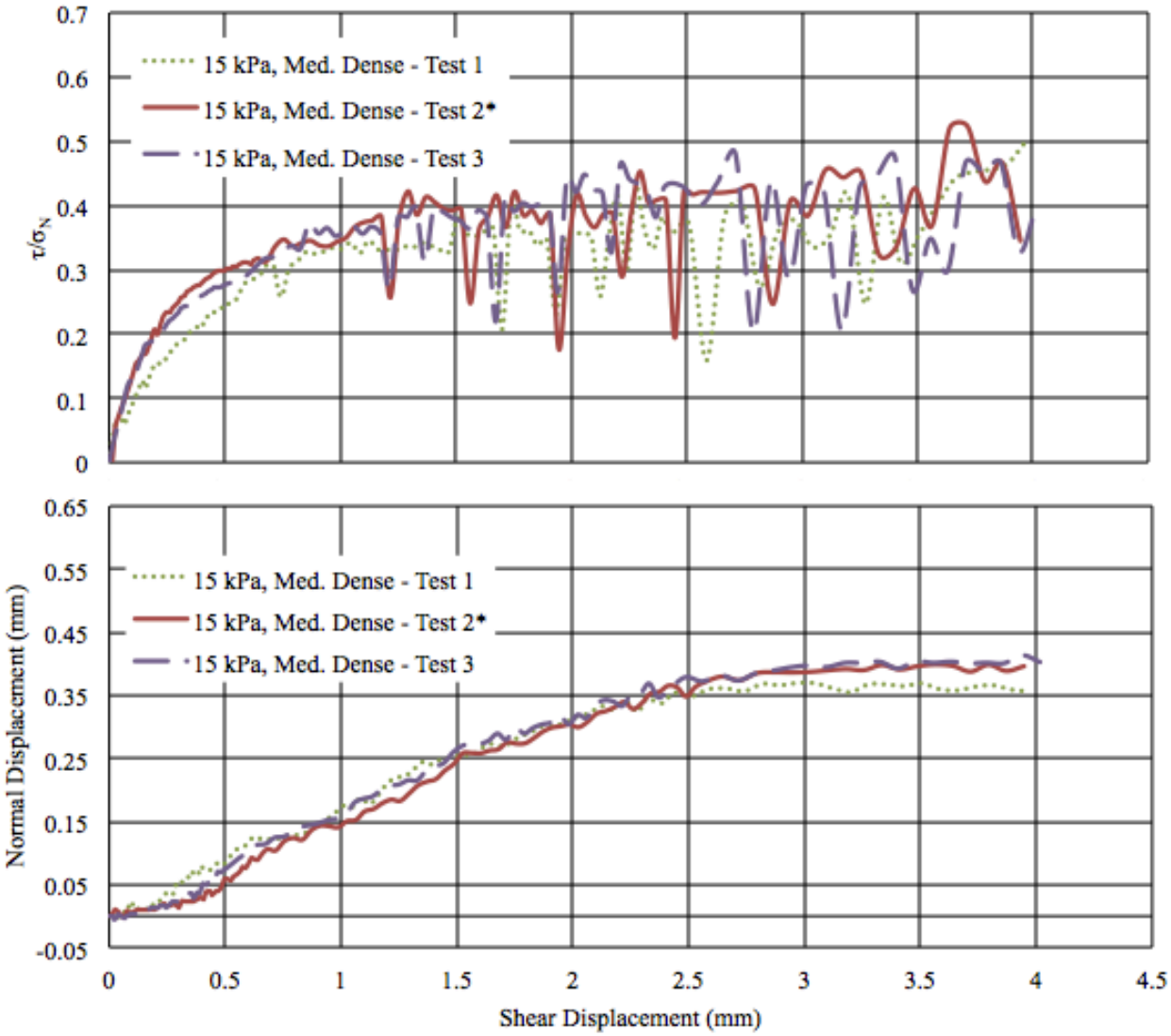

Note: * indicates the test used for statistical modeling.

Normalized Shear Stress and Normal Displacement versus Shear Displacement for Glass Beads, 15 kPa, Medium-Dense Specimens

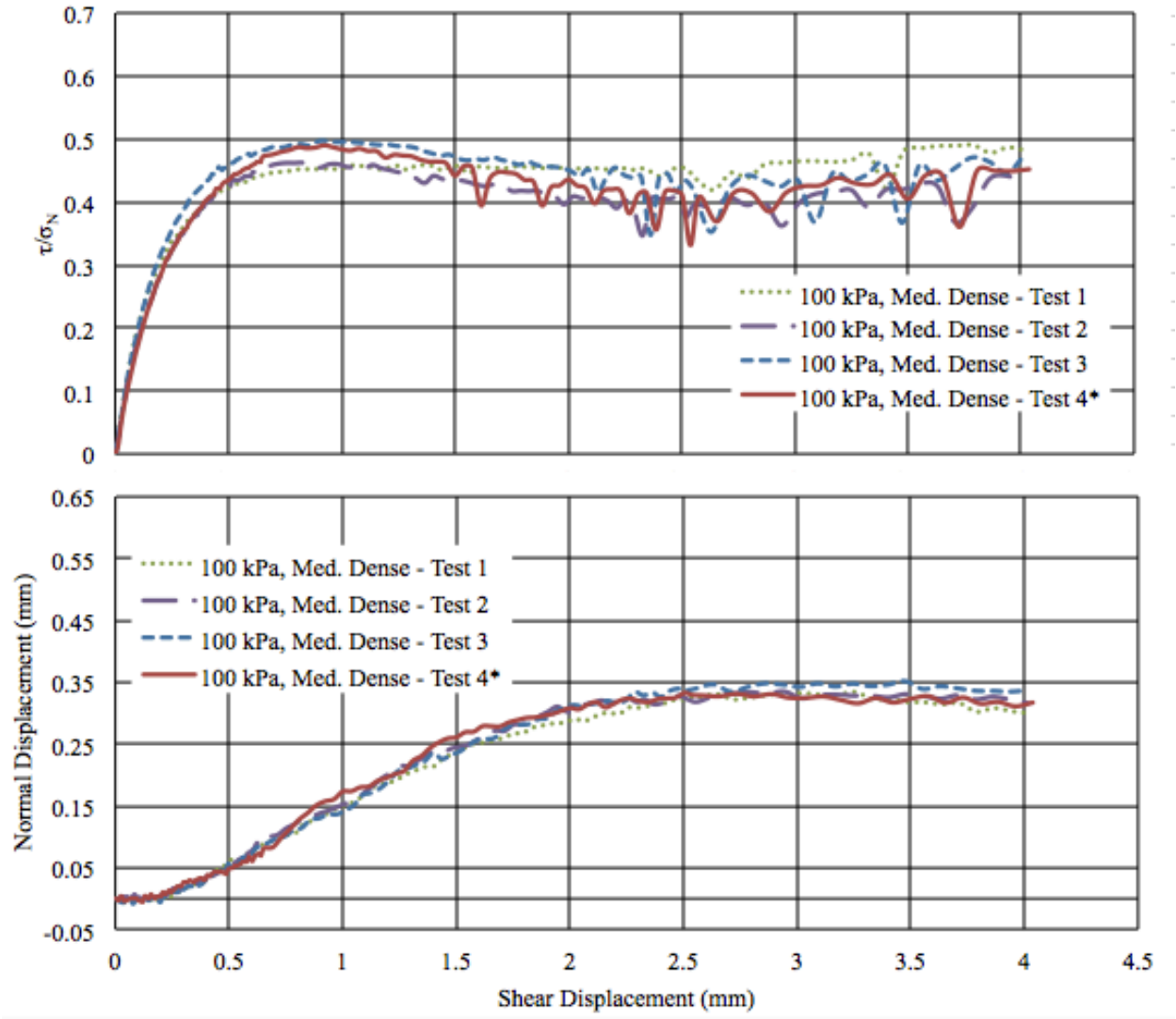

Note: * indicates the test used for statistical modeling.

Normalized Shear Stress and Normal Displacement versus Shear Displacement for Glass Beads, 100 kPa, Medium-Dense Specimens

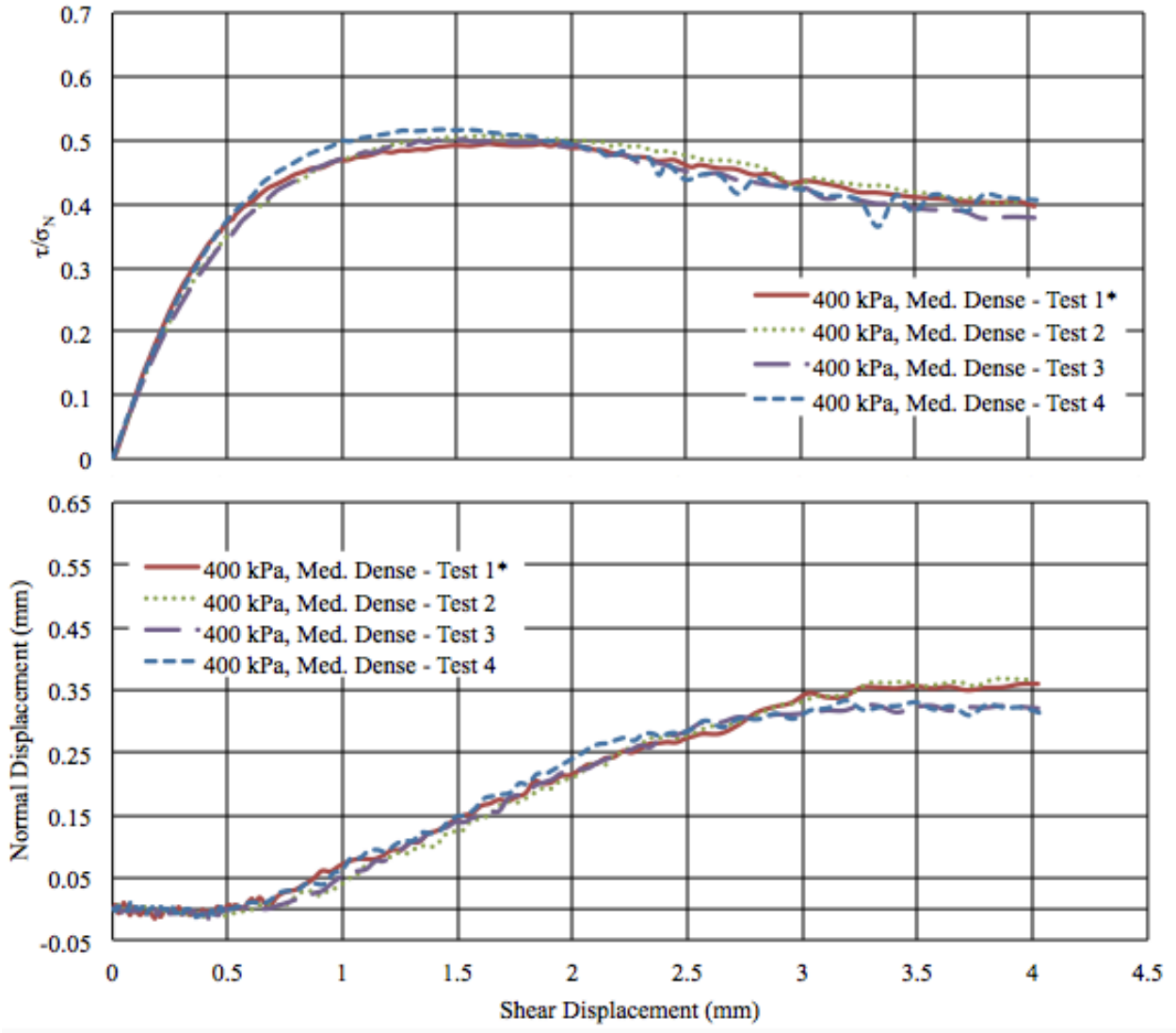

Note: * indicates the test used for statistical modeling.

Normalized Shear Stress and Normal Displacement versus Shear Displacement for Glass Beads, 400 kPa, Medium-Dense Specimens

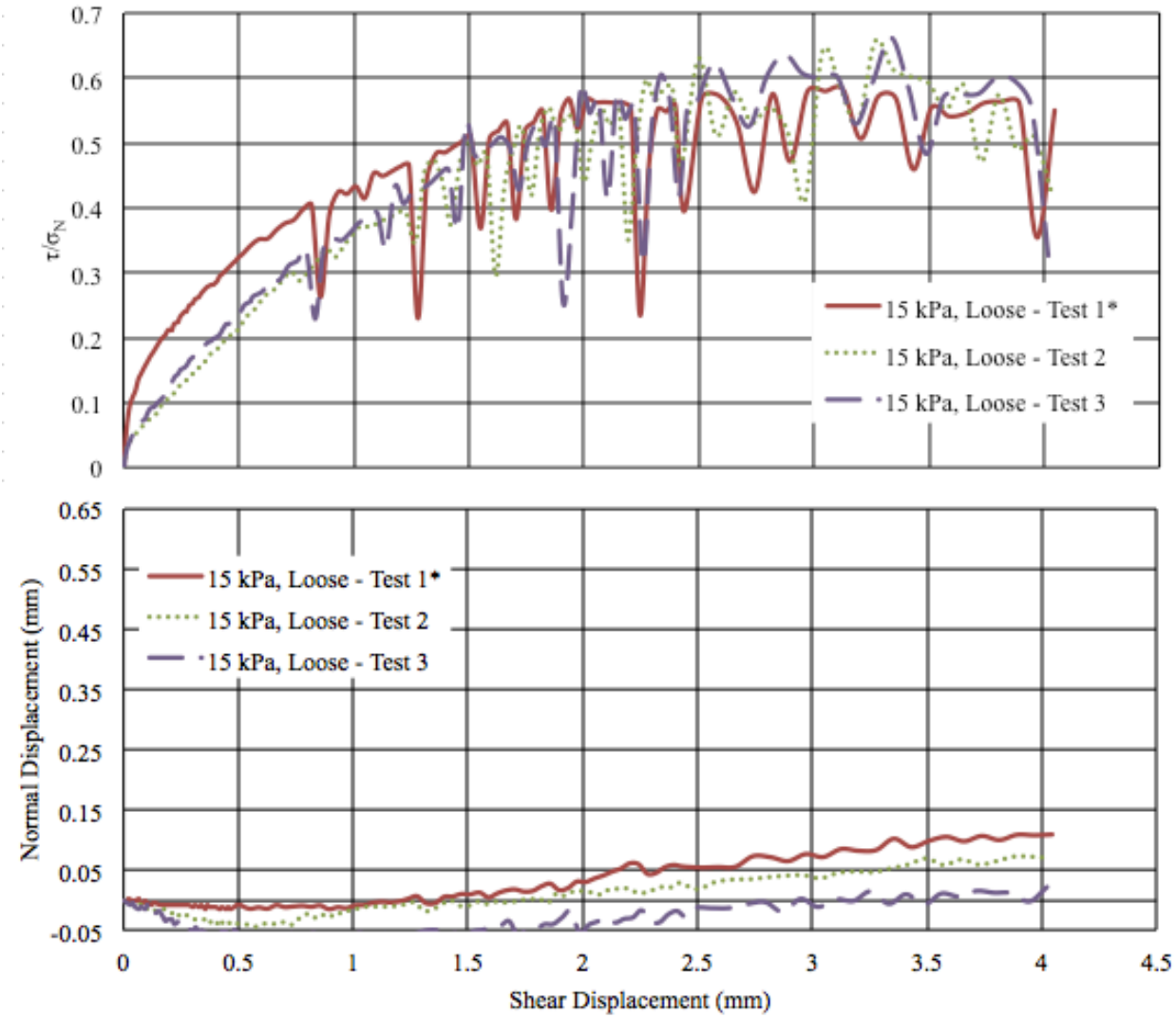

Note: * indicates the test used for statistical modeling.

Normalized Shear Stress and Normal Displacement versus Shear Displacement for Glass Beads, 15 kPa, Loose Specimens

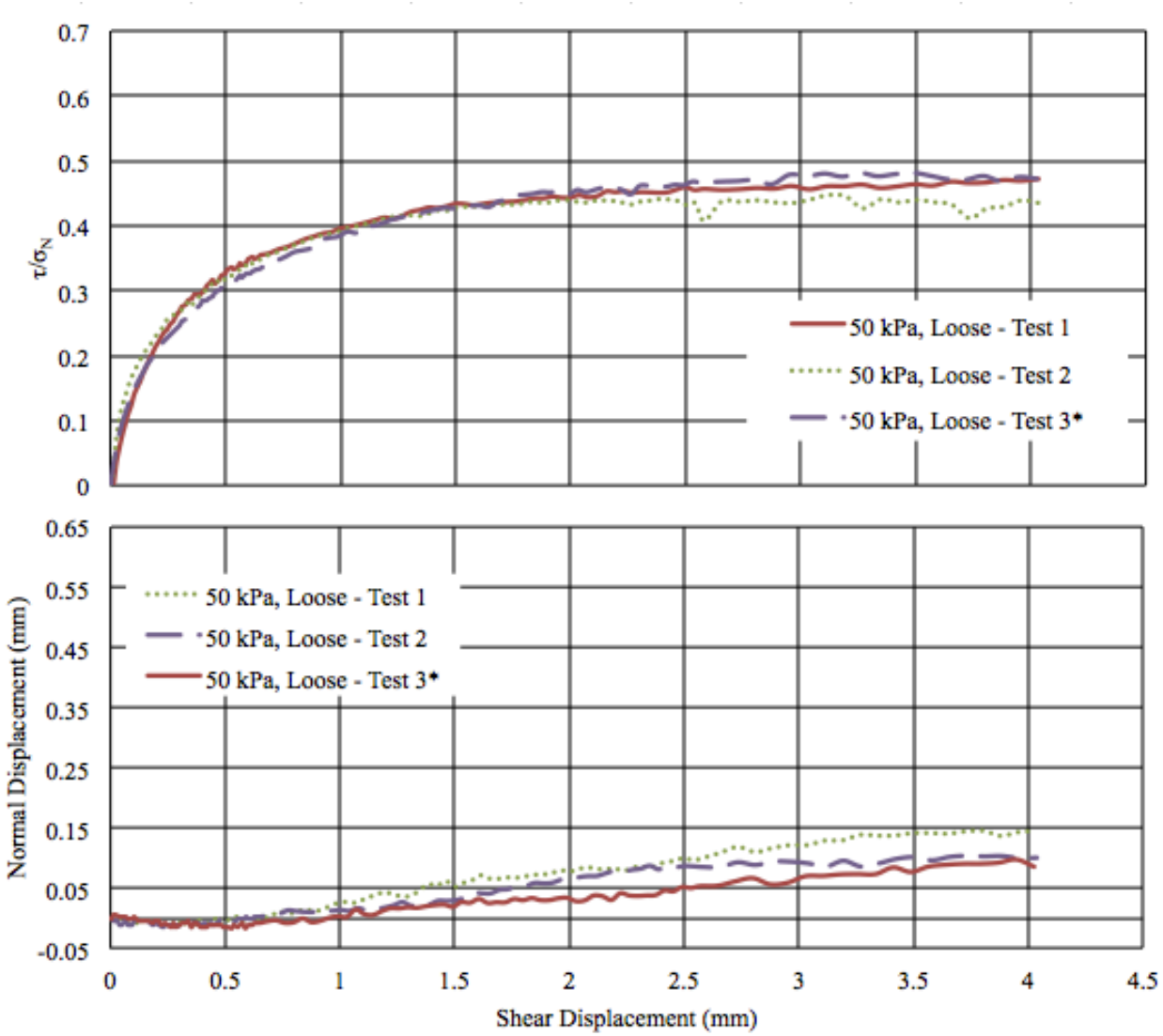

Note: * indicates the test used for statistical modeling.

Normalized Shear Stress and Normal Displacement versus Shear Displacement for Glass Beads, 50 kPa, Loose Specimens

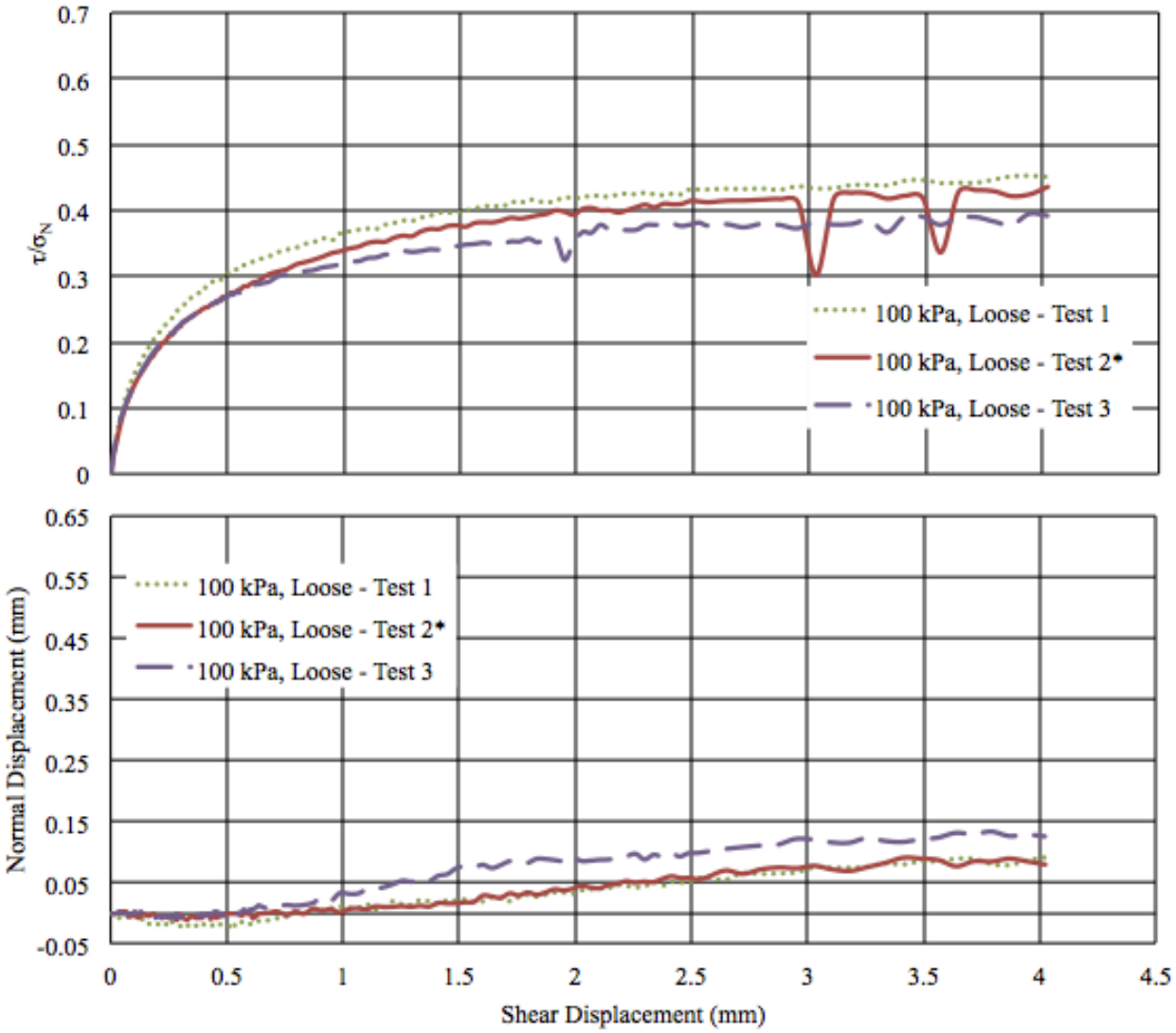

Note: * indicates the test used for statistical modeling.

Normalized Shear Stress and Normal Displacement versus Shear Displacement for Glass Beads, 100 kPa, Loose Specimens

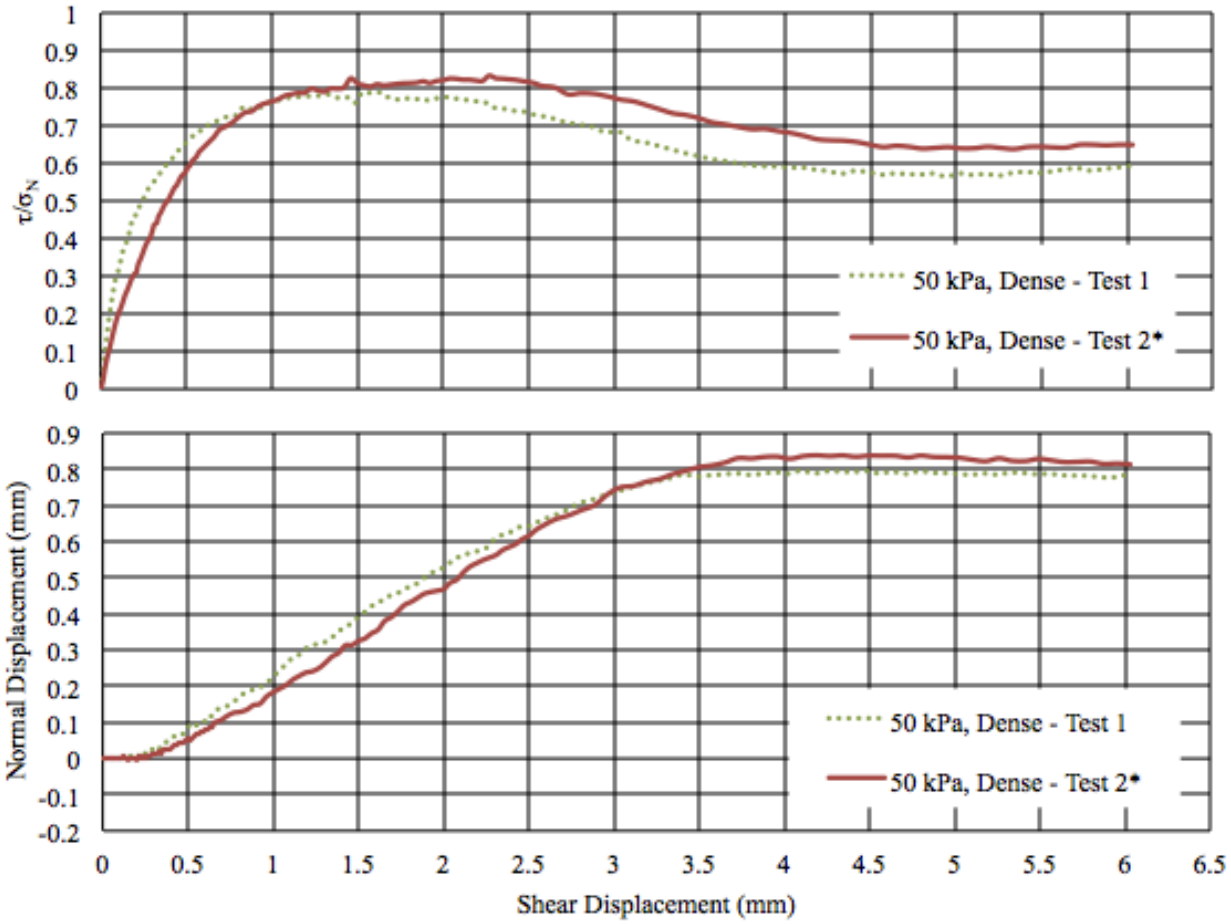

Note: * indicates the test used for statistical modeling.

Normalized Shear Stress and Normal Displacement versus Shear Displacement for F-35 Ottawa Sand, 50 kPa, Dense Specimens

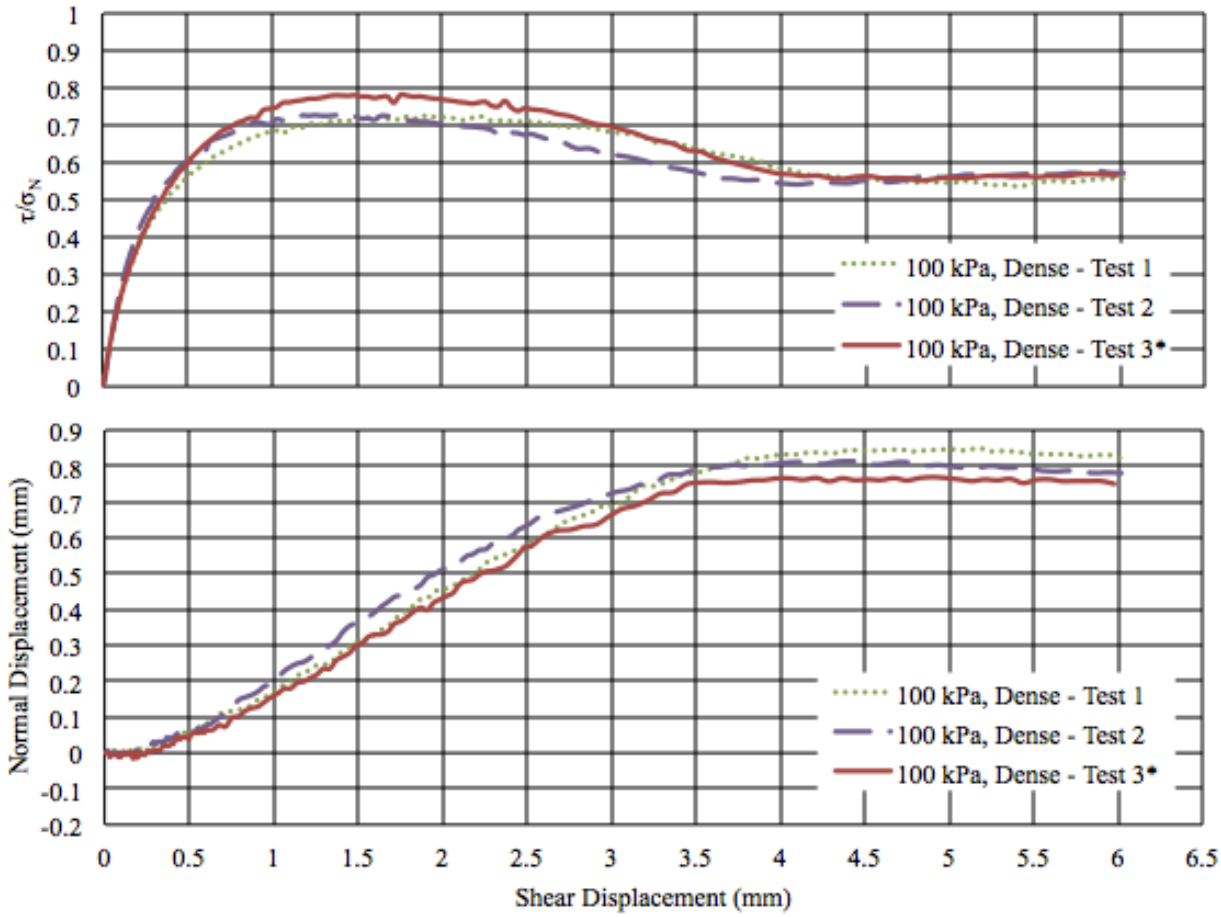

Note: * indicates the test used for statistical modeling.

Normalized Shear Stress and Normal Displacement versus Shear Displacement for F-35 Ottawa Sand, 100 kPa, Dense Specimens

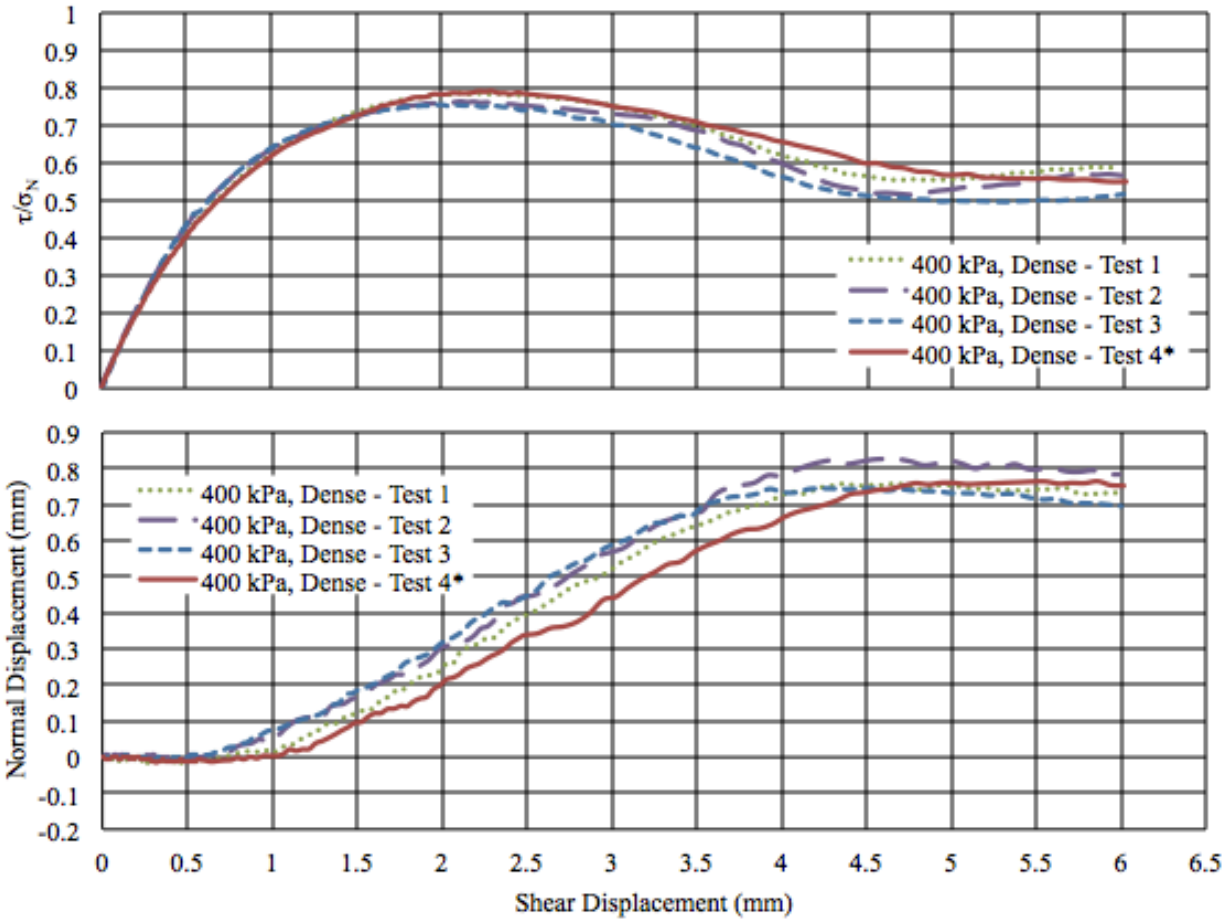

Note: * indicates the test used for statistical modeling.

Normalized Shear Stress and Normal Displacement versus Shear Displacement for F-35 Ottawa Sand, 400 kPa, Dense Specimens

VITA

Karen Lee was born in Oak Ridge, TN to the parents Kiento and Steve Lanter. She grew up in Clinton, TN, attended Clinton Elementary and Middle School, and then graduated from Clinton High School in 2011 fourth in the class. After graduation, she found her passion at the University of Tennessee, Knoxville in Civil Engineering and gained valuable experience by working internships each summer. She also enjoyed undergraduate research each semester. Finishing at the top of her class, she attained her Bachelor of Science degree with geotechnical and structural concentrations and received academic achievement awards. Continuing studies in Geotechnical Engineering with the University of Tennessee, Knoxville, she accepted a graduate teaching assistantship with the Engineering Fundamentals Division and started her graduate study. Karen graduated with her Master of Science degree in Civil Engineering May 2017.